MECHANICAL PROPERTIES, MICROSTRUCTURE, AND ELECTRICAL RESISTIVITY OF ECAE PROCESSED OFHC COPPER FOR HIGH STRENGTH AND HIGH CONDUCTIVITY APPLICATIONS

A Thesis

by

JASON COLE SPRINGS

Submitted to the Office of Graduate and Professional Studies of
Texas A&M University
in partial fulfillment of the requirements for the degree of

MASTER OF SCIENCE

Chair of Committee,	Karl Theodore Hartwig
Co-Chair of Committee,	Bruce Tai
Committee Member	Terry Creasy
Head of Department,	Andreas A. Polycarpou

December 2017

Major Subject: Mechanical Engineering

ABSTRACT

In recent years, superconductors have become a topic of great interest in the scientific and industrial communities due to their ability to carry large currents with zero resistivity. Most superconducting wires have a surrounding matrix material, commonly made of copper, which provides mechanical stability as well as an electrical shut and thermal sink/link. This matrix is vital to the correct and continuous operation of superconductors, and thus must have the correct mechanical and physical properties. Specifically, the matrix material strength and conductivity must be as high as possible. Perhaps the best way to enhance a pure metal's strength without significantly reducing conductivity is through work hardening. By severe plastic deformation (SPD) an ultrafined grained (UFG) material that improved mechanical properties with a minimal increase to resistivity.

In this study, oxygen free high conductivity (OFHC) copper was processed by equal channel angular extrusion (ECAE) and then tested for strength, hardness, microstructure, and residual resistivity. Some of the effects of post processing heat treatment and rolling were studied. The objective of this study is to determine the best processing procedure to develop OFHC copper for its use in a superconductor, or any high strength high conductivity application.

The ECAE routes studied include 1A, 2A, 4A, 8A, 4B, 8B, 4Bc, 8Bc, 16Bc, 4C, 8C, 4E, 8E, and 16E. Tests on these samples included tensile tests, hardness tests, differential scanning calorimetry (DSC) analysis, microscopy, and residual resistivity.

Significant results show a maximum as-worked strength of ~440 MPa for ECAE and ~495 MPa for ECAE plus rolled samples. Hardness and strength saturate after four ECAE passes, with only incremental changes in strength for eight and 16 passes. Heat treatments show that recrystallization temperatures have an inverse relationship to applied strain. Route Bc was shown to give the smallest average as-worked and recrystallized grain size at ~415nm and ~1.4μm respectively. Residual resistivity testing resulted in decreasing values with respect to strength. Grain size and strength are shown to have a linear relationship, as well as those of residual resistivity ratio with both strength and grain size. Lastly, it was determined that a lower number of ECAE passes results in the best ratio of strength to resistivity.

DEDICATION

To my advisor

Dr. Ted Hartwig

To my parents and sisters

Danny, Gail, Staci, Lauren, Kristyn, and Megan

To my friends

Matt, Bradford, and Andrew

And finally, to my fiancé

Callie Rankin

CONTRIBUTORS AND FUNDING SOURCES

Contributors

This work was supervised by a thesis committee consisting of Professors Hartwig and Tsai of the Department of Mechanical Engineering, and Professor Creasy of the Department of Materials Science and Engineering.

All work for the thesis was completed by the student, in collaboration with Zachary Levin of the Department of Mechanical Engineering and Abhinav Srivastava of the Department of Materials Science and Engineering.

There are no outside funding contributions to acknowledge related to the research and compilation of this document.

NOMENCLATURE

SPD	Severe Plastic Deformation
UFG	Ultrafine Grained
ECAE	Equal Channel Angular Extrusion
ECAP	Equal Channel Angular Pressing
OFHC	Oxygen Free High Conductivity
IACS	International Annealed Copper Standard
SEM	Scanning Electron Microscopy
EDM	Electrical Discharge Machining
RRR	Residual Resistivity Ratio (R273K/R4.2K)

TABLE OF CONTENTS

LIST OF FIGURES

LIST OF TABLES

1. INTRODUCTION

1.1 Motivation

The superconducting phenomenon is defined when a material has zero electrical resistance, and the magnetic flux fields are expelled from the surface. There are two main types of superconductors, Type I and Type II. In Type I superconductors there is only a single critical field, where in Type II superconductors there are two critical fields, where critical fields are the highest magnetic field under which a material can remain superconducting at a given temperature. When below the critical field, the electrons that flow through the material behave as a superfluid, meaning they flow with zero energy dissipation. This is due to the electrons forming Cooper pairs, which have an energy gap that is larger than the thermal energy formed from the material lattice. The importance of Type II superconductors comes from their ability to carry extremely large currents. Superconductors are most commonly exploited to generate large magnetic fields that would otherwise be impossible with conventional conductors. One of the most common examples is in Magnetic Resonance Imaging (MRI) machines. Particle accelerators use superconducting wires by the mile in strong magnets that can finely adjust particle beams.

When fabricating superconducting wires there are two main materials needed: the superconducting component and the surrounding matrix. The superconducting component are most often distributed into filaments, which carry the large current with zero resistance, while the surrounding matrix provides structural support keeping

neighboring filaments from contacting each other as well as suppling emergency high thermal conductivity in the case of an unexpected temperate rise. The matrix material needs to have the capability to conduct the large current away from the expensive and fragile filaments if superconducting failure occurs. Therefore, the matrix is used as an electrical shunt and thermal transport pathway to keep the conducting filaments below the superconductor transition temperature during normal operation. In addition to having a high conductivity, the matrix must provide mechanical stability. When producing Type II superconducting wires, the superconducting materials composed commonly of niobium (Nb) and tin (Sn) or niobium-titanium (NbTi) embedded in a matrix are often drawn down in successive increments to their final size. If the matrix is significantly weaker than the superconductor material, the deformation of the composite can be unequal, and non-uniform cross sections of the superconductor filaments can be formed. If the matrix material is closer in strength to the superconductor precursor components, more uniform deformation occurs. With uniform deformation, the superconductor materials are less likely to have unequal cross sections, and in the case of Nb_3Sn, are equally displaced so that during the final heat treatment, a uniform distribution of filaments is formed.

When considering the requirements of the needed matrix material, copper is used commonly for its high electrical conductivity, relatively low cost, and availability. In particular, oxygen free high conductivity (OFHC) copper, which has less than 0.001% oxygen, is used for its superior conductivity characteristics at low temperatures. However, copper has a lower strength than most Type II superconducting filaments,

which can cause significant problems. To improve the strength of the copper in the matrix a number of processing steps could be taken including cold working, solid solution hardening, and precipitation hardening. However, these techniques also increase the resistivity of the copper significantly. The technique that improves strength the most, while only losing a fraction of initial conductivity is work hardening. Equal channel angular extrusion (ECAE) is one such work hardening method that provides superior grain refinement and the capability to apply strains of over 16 while keeping the original sample dimensions.

The objectives of the proposed research are to maximize the strength to resistivity ratio of OFHC copper by evaluating the effect of various ECAE processing routes, as well as being able to control recrystallized grain size after the severe plastic deformation extrusion. The strength, microstructure, and electrical resistivity will be evaluated by preforming mechanical and physical tests, as well as microstructure analysis. Tests include Vickers hardness, Brinell hardness, tensile tests, electrical resistivity measurements, and differential scanning calorimetry (DSC) tests. These tests will give information regarding grain size and shape, yield and tensile strength, hardness, recrystallization temperature, and resistivity.

1.2 Materials

The study of mechanical and physical properties for various materials processed though ECAE have been conducted over the past few decades. Both ferrous and nonferrous metals have been extensively researched with regards to work hardening by ECAE. One of the more common materials processed by ECAE and the focus of this

paper is copper. Copper has excellent thermal and electrical conductivity, resistance to corrosion, good strength and fatigue resistance, superb malleability and formability, and is non-magnetic. Copper was theorized to first be used by ancient Egyptians in as early as 5000-8000 B.C. Around 3000B.C. copper was first alloyed with tin to create bronze, ushering in the Bronze Age [1,2]. The use of copper saw a large increase during the industrial revolution, where copper smelters became a common sight throughout Great Britain. Today, almost every industry and household uses copper extensively, in either electronic components, power transmission, telecommunication, wiring, or many other areas. In fact, in 2016, reported copper consumption worldwide exceeded 1.7 million metric tons [3].

1.3 Equal Channel Angular Extrusion (ECAE)

Characterization and responses of plastically deformed materials have been a topic of great interest in the academic and industrial community due to its ability to alter and improve material structure and properties [4]. The unique properties of bulk nanostructured and ultrafine grained (UFG) materials, which include increased strength and ductility, gave rise to a growing desire for severe plastic deformation (SPD) processes that can achieve submicron grained structures [4,5,6]. The exceptional increase in strength and ductility of nanostructured materials over the more traditional coarse-grained materials mainly come from the large decrease in grain size, and corresponding increase in grain boundaries, which inhibit dislocation motion [7]. Initially, forging techniques such as cold rolling or drawing were used to refine materials, but these techniques couldn’t stand up to the rigorous requirements of industry

and academia [8]. These initial forging processes resulted in altered original dimensions, inefficient grain size refinement, and a limited amount of strain that can be imparted [9]. In the early 1970's the Soviet Union developed a new way of producing SPD while addressing the aforementioned problems with early forging techniques [10]. This technique is equal channel angular extrusion (ECAE) [4].

Equal channel angular extrusion is a process that refines the microstructure by subjecting a thin layer of material to simple shear [4,8,11]. It uses two channels of equal cross section and a well lubricated work piece to force the small section of material at the intersection of the channels to flow though simple shear. Figure 1 presents an illustration of the process. The intersection angle of the channels is given by ϕ and determines the strain intensity. By using a long enough billet the entire area, except the end regions of the bar are subjected to uniform plastic deformation [4,9]. A big advantage of ECAE is the ability to do multiple extrusions on the same billet. Since the exit dimensions are the same as the initial ones, multiple passes can be conducted to accrue extremely large strains after a relatively small number of extrusion passes while keeping the original sample size. ECAE also has an excellent ability to subdivide original grain structures into multiple sub-grains, something not as common with traditional forging techniques.

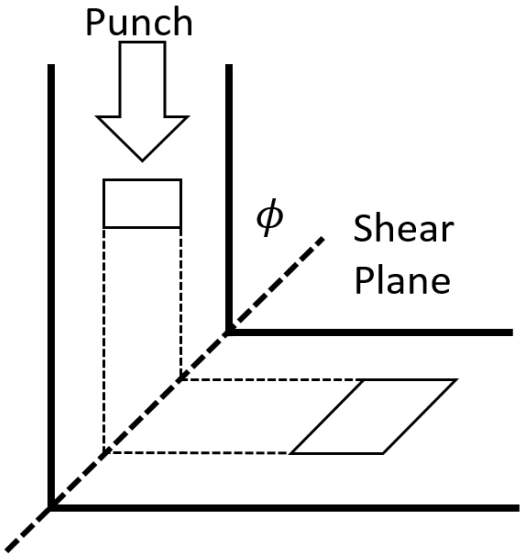

Figure 1: Schematic overview of the ECAE process where material is subjected to simple shear when deforming through a die that contains two intersecting channels

You can relate the total applied strain to the number of incremental passes that you subject sample too. The total strain intensity (ϵ_n) after N number of passes is:

$$\epsilon_n = N\Delta\epsilon_i \tag{1}$$

Where $\Delta\epsilon_i$ is the incremental strain intensity deriving from the die angle ϕ and

$$\Delta\epsilon_i = \frac{2}{\sqrt{3}} cotan(\phi) \tag{2}$$

A conventional die having $\phi = 90°$, gives an equivalent true plastic strain of 1.16 per pass. This means that with only eight passes through a 90° ECAE tool, a total strain intensity of 9.28 and an equivalent reduction in area of 99.99% is achieved. In addition to being able to pass a bar through multiple times, the orientation of the bar between passes can be changed, resulting in different textures, properties, and material

microstructure [10]. This change in work piece orientation during ECAE gives rise to different ECAE routes.

As illustrated in Figure 2, route A keeps the work piece (bar) orientation the same for all passes. In route B, also called route B_A, the bar is rotated by 90° on even numbered passes and by 270° on odd numbered passes. Route C keeps the same bar orientation through all passes at a rotation of 180° between passes. The bar in route E is rotated 180° for all even numbered passes, and by 90° or 270° for the odd numbered passes. Finally, route Bc, also called route C', is where the bar is rotated by 90° for all passes.

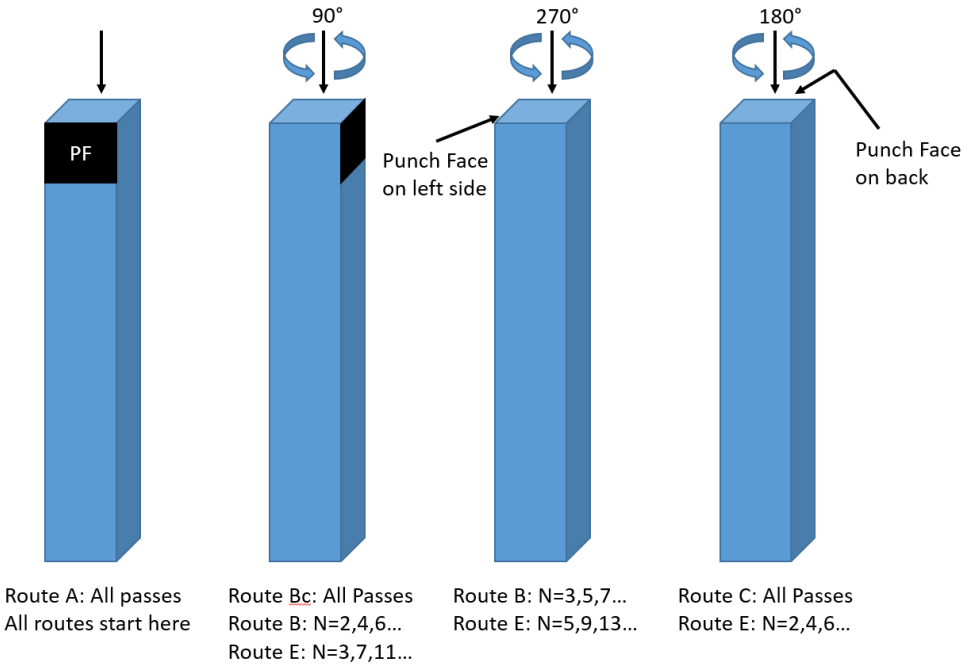

Figure 2: Bar orientation for ECAE routes A, B, C, E, and Bc

For route A because the work piece orientation is the same for all passes, the change in material element shape with each pass is compounded. This creates an elongated lamellar microstructure within the material. For route B, the elements are elongated into a filamentary structure. Route C gives back and forth shearing, while both route Bc and E give back and forth cross shearing. Studies have shown that as the number of passes of ECAE increases, grain refinement correspondingly increases although a near saturation is eventually reached after four passes. Additionally, material element aspect ratios decrease from routes A to B to C and then to both Bc and E [9,12].

When looking at the orientation for ECAE processed bars, a few important distinctions about the different bar planes and directions need to be clarified. The three primary planes studied in ECAE processed bars are the longitudinal plane (XZ), the flow plane (YZ), and the transverse plane (YX), which are illustrated in Figure 3. For the duration of this paper, this coordinate system will not change, and any referenced planes and directions will not change.

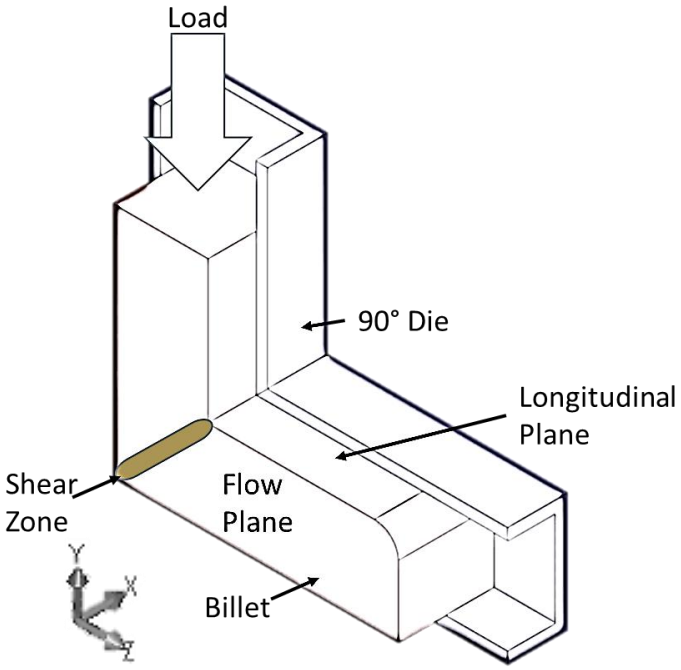

Figure 3: Description of primary directions and planes for ECAE processing

The effects of ECAE on the microstructure of processed materials are significant and notable. Initially, the starting annealed materials generally have very few dislocations and a large ability for the few dislocations to move. After just the first ECAE pass, the high amount of applied strain corresponds to a huge jump in the density of dislocations present within the material. These dislocations arrange themselves into low energy structures to diminish internal energy [9]. With successive passes though an ECAE tool, sub-grains form within the original grains, and more and more dislocations are added within the sub-grains. Due to increasing misorientation of the dislocations, high angle grain boundaries are formed, and grain refinement increases [9,13,14].

Often times after fully working a material via ECAE and achieving submicron grained structures, further processing can be conducted to further refine the microstructure or alter texture. Subsequent heat treatments can be applied to recrystallize the material to relieve internal stress and recrystallize and stabilize the microstructure [15,16,17,18]. By further rolling materials after ECAE, the strength can be further increased due to the flattening of grains and subdivision of some larger gains in the transverse direction [17]. In regards to recrystallization, grain stabilization is an important issue that is often looked over. By relieving some of the strain energy through short-range diffusion made possible by elevated temperatures, the strained UFG microstructure is replaced by more equiaxed recrystallized grains [19].

1.4 Equal Channel Angular Pressing (ECAP)

ECAE, while often used synonymously with ECAP, follows the exact same procedure and routes but is not as ideal in terms of shear deformation. While we define ECAE as having a near perfect sharp outer corner angle on the die, ECAP we define as having a rounded outer corner angle (and possibly rounded inner corner angle) resulting in less than ideal shear deformation [20,21]. In fact, Iwahashi et al [22] reports that the total strain intensity equation changes to reflect the non-ideal outer corner and becomes:

$$\epsilon_n = \frac{N}{\sqrt{3}}\left(\left(2 * \cot\left(\frac{\phi + \Psi}{2}\right)\right) + \left(\Psi * cosec\left(\frac{\phi + \Psi}{2}\right)\right)\right) \quad (3)$$

In this equation the die angle is still defined as ϕ and the number of passes is N, but the outer corner angle is designated as Ψ. This also assumes there is no friction in the

die, which is often not the case. In a different study, Adedokun [20] reports the total strain intensity to be:

$$\epsilon_n = \frac{N}{\sqrt{3}}\left(2 * \cot\left(\frac{\phi + \Psi}{2}\right) + \Psi\right) \quad (4)$$

Both equations result in a strain intensity less than that of the ideal factor reported by Segal [4]. Another consequence of rounded die corners is non-uniform strain across the work piece.

1.5 Literature Review

The microstructural evolution of copper during the ECAE process is the most studied area of research in recent studies. Torre et al [23] and Etter et al [24] both conducted studies on OFHC copper processed by route Bc with varying numbers of passes. Both reported grain sizes of 200-400nm after eight passes, with Torre et al [23] reaching a grain size of below 400 nm after just a single pass. Etter et al [25] in a different article verified the 400nm grain size again running ECAE on route Bc to eight passes. Etter et al [25] also found grain aspect ratios were not completely equiaxed as one might expect for route Bc, generally falling in the region of 0.5 for both grains and subgrains, while Torre et al [23], reported aspect ratios close to one indicating the expected equiaxed grains. Both studies were done for 8-pass route Bc on commercially pure copper. A study done by Haouaoui in 2005 [26], also reported aspect ratios of close to one for routes Bc and C after four passes. Additionally, Haouaoui reported aspect rations for route A, with ratios that grow after the first pass as expected.

Torre et al [27], conducted a comprehensive study evaluating the grain size and grain boundary misorientation angle of ECAE processed copper for route Bc though the use of transmission electron microscopes (TEM), x-ray diffraction (XRD), and electron backscatter diffraction (EBSD). EBSD results show grain size decreasing from an initial mean of 20μm to 1200nm for the first pass and then fluctuating at around 600nm for passes two to 16. However, the subgrain size for passes one to 16 stayed constant with a value of ~250nm for all passes, with aspect ratios also being constant at around one. The misorientation angle indicates that as more passes and more strain is accumulated in the crystal lattice, the original low angle grain boundaries transform into high angle grain boundaries [27].

Some studies have been done on post processing rolling and the effects that it has on the microstructure of pure Cu. Mishin et al [17], characterized the effects of rolling in ECAE processed Cu as producing pronounced textures. They reported that grains observed in the rolling plane were elongated and subdivided in the transverse direction. The microstructure of the ECAE plus rolled samples was also much more homogenous than that of purely rolled samples.

The stress-strain relationship of ECAE processed copper is perhaps the second most studied area of research, with values of tensile strength, yield strength, elongation to failure, and elastic modulus reported. In Torre et al's [23] comprehensive study of route Bc, tensile and yield strength, as well as elongation, were reported for 1, 2, 4, 8, 12, and 16 passes. The results of their study indicate that the maximum ultimate tensile strength (UTS) is reached after four passes with a value of 455 MPa, after which the

UTS decreases slightly for additional passes with the yield strength following the same trend. This decrease in strength was theorized to be due to dynamic recovery leading to annihilation of dislocations within the microstructure, lowering the overall dislocation density.

The largest increase in strength is between the unprocessed and 1st pass, followed by the 1st to 2nd pass. The total elongation to failure is at a maximum before any processing is done and reaches to a minimum at four passes as expected. The elongation to failure then rises with the 8, 12, and 16 passes. In another study done by Xu et al [28], the UTS was found to be approximately 445 MPa, very similar to Torre, but after eight passes vs four passes. For their study however, they used a die angle of 110° vs 90°, as well as having a relatively large outer arc angle compared to Torres ideal case. Due to this, the appropriate number of passes to reach an equivalent strain as reported by Torre would be closer to 5-6, indicating that their results were more similar than first appeared.

Torre et al [27], revealed that the Hall-Petch relationship was a good fit for the ECAE processed copper as long as the subgrain size was used in the calculations. Additionally, the contribution of the misorientation angles had a relatively low importance on the strengthening contribution. The work hardening rate of copper decreases as the number of passes and accumulated strain in the lattice increases [23]. This was supported by the larger plastic deformations seen by the higher number passes being due to the work hardening ability being regained from the loss of dislocations via dynamic recovery.

One study done by Gazder et al [29], looked at the effect of post processing rolling on the stress-strain relationship of ECAE Cu. They found that an increase in strength was seen for eight pass route Bc when rolled to 50% reduction in thickness, achieving a UTS of 470MPa. When rolled to a larger reduction of 97.5%, the UTS dropped back down to below its as-worked condition of 427MPa. Again, the reduction of strength for the larger reduction in thickness was attributed to dynamic recovery. Similar results were seen when eight pass route C Cu was rolled in a study by Kusnierz [30]. In another report by Kusnierz et al [31], a definitive increase in shear banding was seen, and resulted in a 50% reduction in elongation during tensile testing.

Another mechanical test done to evaluate the properties of processed materials is hardness testing. More often than not, Vickers hardness is used, and multiple studies obtained comparable results. For example, Buet et al [32], evaluated Vickers hardness for ECAE copper after one pass and obtained values between 125-135. Etter et al [24], obtained hardness values of approximately 145 for an eight pass route Bc sample. It is stated and tested in several papers that the maximum Vickers hardness values for purely cold worked copper would fall in the range of 130-150, which can be achieved in as little as two passes [23,32,33]. Additionally, the hardness values should closely follow the Hall-Petch relationship with grain size, and therefore could be a possible substitute to calculate tensile strength without measuring grain size.

As far as post processing treatments, the most common is recrystallization. Studies not only look at recrystallized grain structure and size, but tensile strength, hardness, and the recrystallization temperature and time as well. Determining the

recrystallization temperature for ECAE processed copper can be done multiple ways. Daly et al [34], observed a decrease in Vickers hardness with increase in annealing temperature, and reported a recrystallization temperature of around 300°C for a one pass Cu sample. Etter et al [24], observed recrystallization at 200°C after only 7.5 minutes for a route Bc eight pass sample with Vickers hardness measurements. Guo et al [35] characterized both four pass and eight pass samples for route Bc and observed a decrease in the time needed for recrystallization at 200°C from four pass to eight pass samples. Additionally, a similar result using differential scanning calorimetry was obtained by Daly et al [34], where the recrystallization temperature decreased with the number of passes and accumulated strain increased.

Other methods of evaluating recrystallization involve examining the microstructure as a function of temperature and time. Etter et al [24], using EBSD techniques, characterized recrystallization by counting grains larger than 0.3μm with a confidence index of 0.05. He found results that matched with prior Vickers hardness measurements. The average recrystallized grain size was reported to be about 2μm. Guo et al [35], using an SEM found that after 3.5 minutes at 200°C, submicron grains measuring about 0.4μm formed fully recrystallized grains measuring an average of 3μm, and not further growth was seen up to seven minutes of annealing time. A study by Suwas et al [19], evaluated the volume fraction and grain size for three pass routes A, BC, and C after annealing at 250°C for three minutes. The volume fraction for recrystallized grains for all three routes was above 93%, and the recrystallized grain size stayed relatively constant between 0.73-0.76 μm for all three cases. Wang et al [36],

theorized that for route Bc on the odd numbered passes, the newly formed shear bands provided a favorable micro-band for recrystallization nucleation mechanisms.

Some recent studies done on ECAE for copper have examined if recrystallization occurs even at low temperatures. Etter et al [24], observed recrystallized grain after applying large strains of approximately eight at room temperature. These recrystallized grains measured 1.5 micron and accounted for approximately 1.5% of the volume. Saunders et al [37], also reported recrystallized grains for severely deformed copper at low temperatures. Mishin et al [17], reported heavy recrystallization for copper processed by ECAE and additionally rolled to 83% reduction in thickness. These samples experienced recrystallization when stored at room temperature. This is due to the change in strain path from simple shear to rolling deformation producing an unstable microstructure. This instability comes from shear bands, which provide preferential nucleation sites. However, the microstructure of only ECAE processed copper remained extremely stable and did not undergo any recrystallization at room temperature. Additionally, Akhmadeev et al [38], displayed that as-worked copper processed by ECAE had a stable microstructure up to 150°C.

Comparatively few studies have evaluated the resistivity of copper after being processed solely via ECAE. Zhilyaev et al [33], reported conductivity values of copper processed by ECAE and high-pressure torsion to be 91.6% of the course grained counterpart. Davydenko et al [39], evaluated the resistivity of copper being processed by ECAE followed by direct hydro extrusion, and obtained a conductivity of 96.7% of the International Annealed Copper Standard (IACS) published value. Higuera-Cobos et al

[40], found that even after 16 passes of route Bc, the conductivity of electrolytic tough pitch (ETP) copper only dropped to 95% of the IACS value. This slight drop in conductivity derives for the increased scattering of conducting electron because of an increased number of defects such as grain boundaries, dislocations, and point defects. However, because this decrease is small compared to alloying effects, while still giving a significant increase in strength, it is still the preferred method for strengthening electrical conductor materials.

2. MATERIALS AND METHODS

2.1 Materials

The as-received material used in this study was CDA10100 commercially pure oxygen free high conductivity copper (OFHC). This copper has a minimum of 99.99% composition of pure Cu.

2.2 Processing

2.2.1 Initial Machining and Annealing

Before any processing, the as-received Cu bars were cut into 254mm long sections via a Kalamazoo wellsaw. For this project a total of 15 bars were cut to be processed. Next these bars were annealed at 350±3°C in a Thermolyne MUFL F6010 furnace for one hour in air to ensure that starting conditions were the same. Lastly, the bars were machined down to a 25×25mm cross section using a manual knee A-Trump mill with a four insert face cutter running at 200-300 RPM and a feed speed of 2.54 mm/second.

2.2.2 ECAE

Routes that were tested included routes A, B, C, Bc, and E. Route A included 1, 2, 4, and 8-pass samples while routes Bc and E included 4, 8, and 16-pass samples. Routes B and C both included only four and eight pass samples. The annealed and machined copper bars were coated with Loctite LB 8150 silver grade anti-seize before ECAE processing to reduce friction in the die. Additionally, the press ram that enters the dies was also lubricated with the anti-seize. Next, the bars were extruded at 2.54

mm/second at room temperature. Sensors recorded load, stroke, and time during the entire process, and the temperature of the bar was measured immediately after extrusion as well. Bar dimensions are also recorded, and the bars were stamped with ID numbers to ensure no mix-up occurred. Completed processed bars were stored together at room temperature.

2.2.3 Machining

After each ECAE pass, the bars had to be machined down a small amount to remove flash and ensure they would fit in the die for the following extrusion. This was again accomplished with an A-Trump mill operating with the same condition as listed in above in section 2.2.1. After machining, the bar dimensions were again recorded, and then the bars were ready for the next ECAE pass.

2.2.4 Wire EDM

Small samples were cut from the processed bars using a Mitsubishi MD PRO III wire electrical discharge machining (Wire EDM) unit. A total of five different profiles were cut out of the copper bars for study and further post processing. These included small rectangles for heat treatment and microscopy, thick squares for further rolling treatments, cylinders for resistivity ratio testing, small differential scanning calorimetry samples, and dog-bones for tensile testing. A 25.4mm slice was removed from the ends of routes A, B, C, and E bars and a 50.8mm slice was removed from both ends from route Bc. This was to ensure only fully processed material was tested.

The small rectangles measured 12.7×6.35mm by 3.175mm thick. Multiple sections at a time were cut by first cutting a 6.35mm slice of the bar, and then cutting

multiple samples of the correct height and thickness from the center of the slice. They were cut so the large side of the rectangle, which was used for microscopy and micro-hardness measurements came from the flow plane. The schematic given by Figure 4 gives a visual representation of how the bar was sliced and then divided.

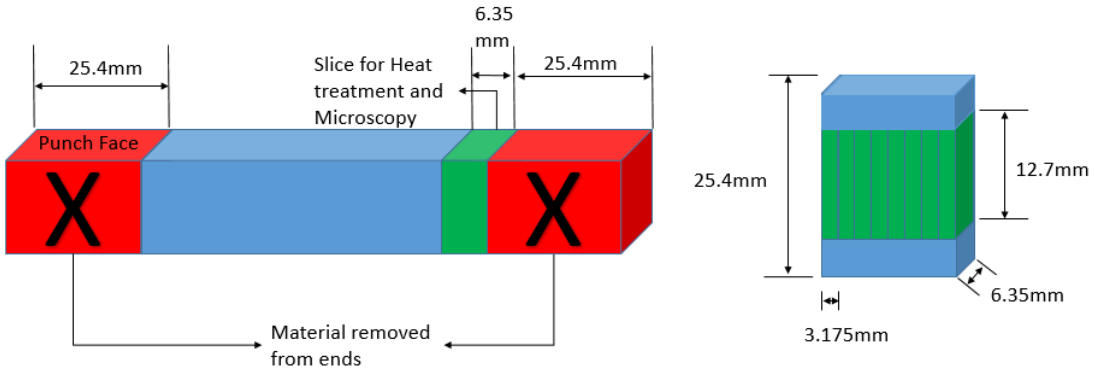

Figure 4: Wire EDM schematic for cutting heat treatment and microscopy samples

The left part of the schematic shows cutting a 6.35mm slice from the bar while discarding the ends, and the right shows sectioning the 6.35mm slice into final 12.7×6.35×3.175mm samples. All processed routes had heat treatment and microscopy profiles cut from the original bar for testing.

Four squares with a 25.4×25.4mm cross section and 12.7mm in thickness were removed for different orientation rolling experiments. Two were cut from the flow plane (XY) to roll with and across the extrusion direction, and two were cut from the transverse plane to roll in the direction of the flow and longitudinal planes. Again, the schematic given by Figure 5 shows a visual representation of material removed for

rolling experiments. Material from the end of the bar was again not used for the reasons mention above.

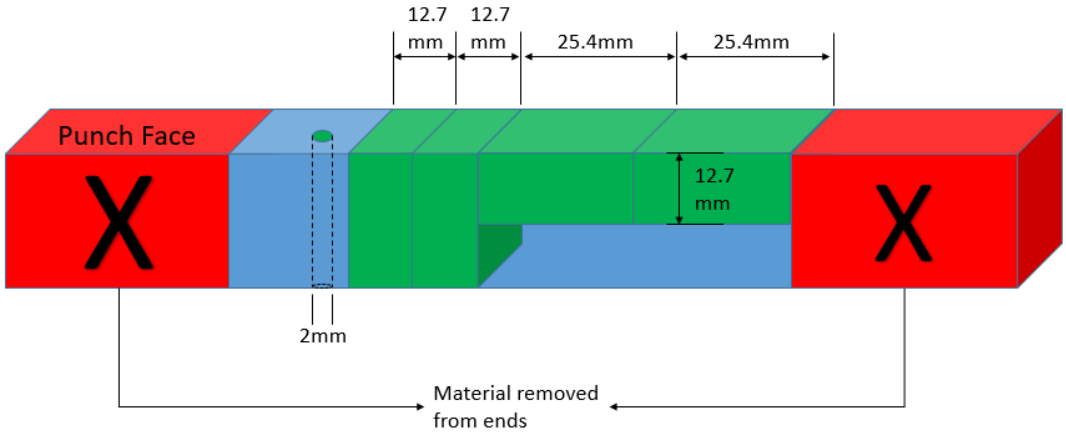

Figure 5: Wire EDM schematic for rolling and resistivity samples

The cylinders for resistivity testing measured 2mm in diameter and were 25.4mm long. They were cut from the punch face to the bottom of the bar, and can be seen in Figure 5 on the left side. These cylinders were cut from all processed bars.

The dog-bone sample for tensile testing measured 26mm long, with 7mm tabs and a 3mm and 8mm gauge width and length respectively. The radii of the dog bone measured 1.97mm for all fillets. There were two 1.59mm holes drilled in the center of each tab for pinning during tensile testing. The tensile samples were sliced to be 1.27mm thick. Figure 6 shows a drawing view of the dog-bone tensile sample.

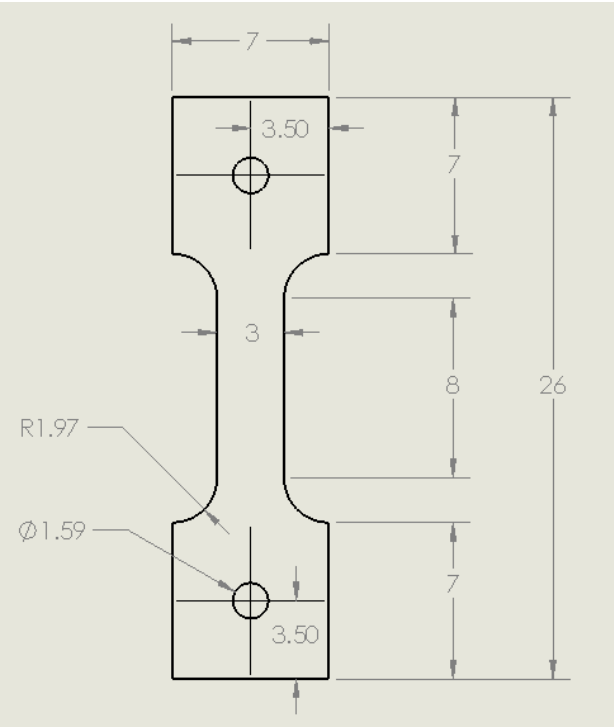

Figure 6: 26mm dog-bone tensile sample EDM schematic (All measurements shown are in mm)

2.2.5 Rolling

The as-received, 2A, 4A, 4Bc, and 4E square samples cut from the longitudinal plane (XZ) were rolled along the extrusion direction (Z) to 10, 30, 69, and 90% of their initial height using a Fenn Combination 2-high rolling mill with approximately 100mm diameter rollers. The squares are rolled by a reduction of 2% of the initial gauge height every pass though the mill and cooled in water every other pass. For the 4A sample, two squares are cut from the longitudinal plane: one is rolled with the extrusion direction (Z), while the other is rolled across the extrusion direction (X). The other two squares were

rolled on the transverse plane (YX) toward either the flow plane (X), or the longitudinal plane (Y).

After a 10% reduction in height, a dog-bone tensile profile was removed from the edge. The additional rolling was preformed until a 30% reduction in height was obtained, where again a dog-bone profile was cut from the edge. This process was repeated for the 69% and the 90% samples.

2.2.6 Heat Treatment

The 12.7×6.35×3.175mm samples were heat treated in a sand bath at various temperature for 15 minutes, then immediately quenched in water. The sand bath was heated via an electrical heating coil and pressurized air was pumped in to the bottom where the coil was located which fluidly circulated the heated sand. The operating pressure was anywhere between 60-90 kPa depending on temperature. The selected heat treatment temperatures for recrystallization runs were 23, 100, 150, 175, 185, 200, 215, 225, 240, 250, 275, 300, 400, and 500°C (±5°C). Only selected bars were chosen for the entire range of temperature. These bars were 1A, 2A, 4A, 8A, 8B, 8C, 8Bc, and 8E.

All samples were recrystallized after determining recrystallization temperature via procedures above. The one pass sample was recrystallized at 350°C, the two pass sample at 275°C, the four pass samples at 250°C, and the eight and 16 samples at 225°C.

2.2.7 Mechanical and Electrolytic Polishing

Mechanical and electrolytic polishing was done on the 12.7×6.35×3.175mm samples for both heat treated and as-worked conditions. The procedure started using 320 grit sandpaper and distilled water for flushing removed material to plane the surface of

the sample. Finer grits of 400, 600, 800, and finally 1200, all with distilled water for flushing, were used for the base mechanical polish.

To obtain a mirror finish, electrolytic polishing was preformed using an 85% phosphoric (H_3PO_4) solution, distilled water, Hewlett Packard DC power supply, Nuova II stir plate, a copper sheet cathode, and assorted containers. First 82.5mL of the 85% H_3PO_4 was mixed with 17.5mL of distilled water. This was added to a polypropylene container with a magnetic stir rod on the stir plate. The negative terminal was connected to the copper sheet (cathode), while the positive terminal was connected to the 12.7×6.35×3.175mm sample (anode) and both were placed in the phosphoric acid solution. The stir speed was set to three, and the setup located in a fume hood.

First, a voltage sweep curve was done by successively increasing the applied voltage by 0.1V and recording the corresponding current draw to determine the voltage range for polishing. This curve can be found in Appendix A. After finding a preferred voltage of 2V, polishing was done at room temperature, with a stir speed of three, for 10-15 minutes. After the appropriate time had passed, the power supply was turned off, and the sample rinsed in distilled water. Next, the sample was cleaned in methanol in an ultrasonic cleaner for at least five minutes. Lastly, the samples were gently wiped off with Kimtech wipes.

2.3 Characterization

2.3.1 Rockwell and Brinell Hardness

Between each pass of ECAE treatment, Rockwell and Brinell hardness values were taken from both the flow and longitudinal plane. Rockwell B-scale hardness values

were taken using a Wilson Rockwell Series B2000 hardness tester with a 1/16” hardened steel ball tip. Three measurements were taken, and the averages and standard deviations determined. Additionally, Brinell hardness indents were applied with a Detroit Testing Machine Model P.H. 2, and the indent measured with a Sun-Tec model SBS-20 microscope. The indent diameter was then compared to a Brinell indent/hardness correlation chart to determine hardness value. Again, three measurements were taken, and the averages and standard deviations are determined.

2.3.2 Vickers Hardness

Vickers hardness measurements were taken on both the as-received and heat treated 12.7×6.35×3.175mm samples. These samples were polished to a mirror shine via mechanical and electrolytic polishing before testing. Using a Micro Vickers Hardness Tester Phase II machine with a diamond tip indenter, a square diamond shape indentation applied to the sample under a load of 300gf and the cross section of the tips measured. By measuring the distances, the Vickers hardness value was calculated and subsequently recorded. At least ten measurements per sample were taken to obtain a more accurate average and standard deviation.

2.3.3 Differential Scanning Calorimetry (DSC)

In order to determine the recrystallization temperature of the ECAE processed bars, DSC analysis are performed on route 1A, 2A, 4A and 8A samples, weighing 60-75mg each. DSC Q2000 equipment was used to perform the test at a heating rate of 10°C/min in a nitrogen atmosphere. The scanning temperature ranged from 30°C to 300°C.

2.3.4 Tensile Testing

The 26mm dog-bone samples were tensile tested with an MTS tensile tester powered via an MTS hydraulic unit. Tests were conducted at room temperature with an 11kN Interface 1010AF load cell. Additionally an Epsilon Miniature Model 3442-008M-020-LHT extensometer was used to measure the engineering strain during testing. MTS Station Manager and MTS Test Suite Multipurpose Elite were used to setup and run the programs to conduct the tensile tests.

For testing, the samples gauge length was measured and the tabs were labeled with sharpie insuring no mix-ups could occur. Then the samples were loaded into the MTS clamps and the top tab pinned to the clamp though the drilled hole. Then the lower clamp was adjusted in order to pin the bottom through hole in the second clamp. Before tightening the clamps, a load of 20N was applied to ensure the sample did not slip during testing. While the sample is under tension, the clamps were tightened appropriately to ensure no slippage occurs. Next, the sample was unloaded and a clip-on extensometer mounted on the gauge length of the sample. The extensometer was aligned, then software opened and tests ran. Figure 7 displays what the MTS tensile tester setup was with and without the sample, as well as with the extensometer.

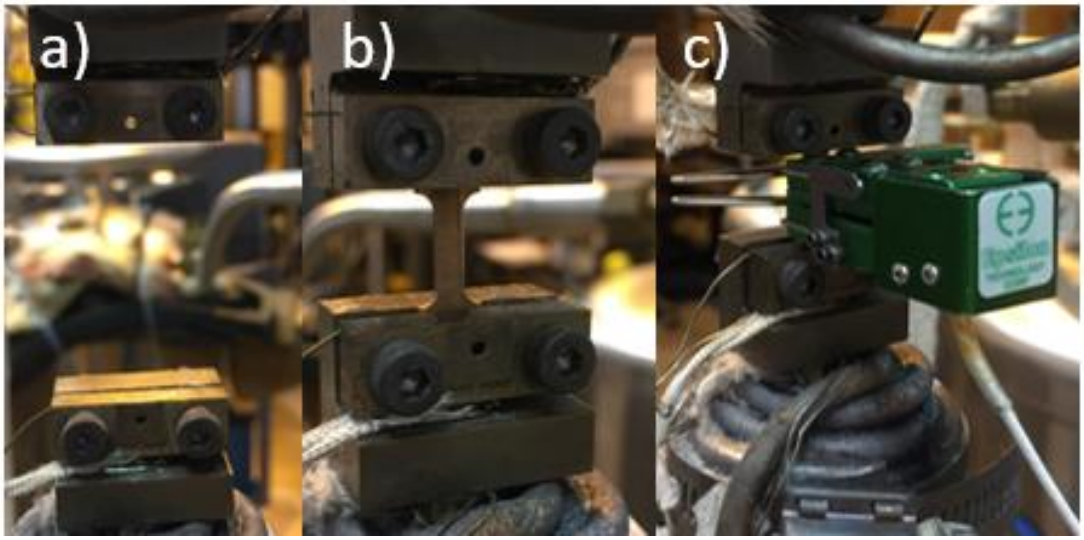

Figure 7: Tensile testing setup- a) MTS clamps without sample, b) MTS clamps with sample and pins (not visible), c) MTS clamps with sample, pins, and extensometer, ready for testing

The first test run was a modulus check to make sure all components of the tester were working properly and no slippage of the sample was occurring. The modulus checked used a ramping force of 10N/sec to a maximum of 100N, and then decreased by 10N/sec back to zero. The tensile test was run next, and used a strain rate of 0.01mm/s for the entire test. The test was run until the sample broke, and afterwards, the program was stopped, the extensometer and sample removed, and the data files saved. Three tensile tests were performed for each case being studied and the average strength of the three is what is reported later in the study. For the case of the annealed and recrystallized samples, the extensometer had to be reset so it did not go over its operating range. This was done by pausing the tests and quickly resetting the extensometer to zero extension. Then the test was resumed and the data paired together during analysis.

2.3.5 Microstructure

Using a FEI Quanta 600 FE-SEM, the polished 12.7×6.35×3.175mm samples were examined to determine microstructure. Each sample was marked prior to imaging and aligned similarly so that the flow plane was imaged for every sample. The SEM was generally ran at 13kV, but was changed if the situation required it for better resolution images. The working distance was 10mm, and both secondary electron and backscattered electrons detectors used. Magnification for worked materials usually ranged between 20k to 40k, while the as-received material had a magnification of 200-500. The magnification for heat treated samples fell in-between these two depending on the level of recrystallization and recrystallization grain size.

Using ImageJ, an image processing program, the grain size was measured and recorded. This was accomplished by measuring the scale bar on the SEM images and creating a relationship to the given measurement from ImageJ. Then by measuring the longest straight distance across a clearly visible grain, and then measuring the distance perpendicular to the first line, and taking the average of these two numbers as the recorded grain size. Additionally, one can record the grain aspect ratio by dividing the first measurement by the second measurement. Repeating this procedure for at least 50 grains, and then taking the average of all calculated numbers, the average grain size and aspect ratio can be calculated for that specific sample.

2.3.6 Residual Resistivity Ratio (RRR)

In order to determine the RRR for the 2mm cylinder samples, the four point probe measurement method was used. Current was passed from one end of the sample to

the other, and two voltage taps with one end insulated and the other a knife-edge was used to measure the voltage drop across the sample. An Agilent E3633A DC power supply was used to supply the constant current required, while a Keithley 181 Nano-voltmeter was used to measure the voltage drop. In order to test more than one sample at a time a six throw two pole switch was used to quickly change between voltage taps and measure the voltage drop. A current reversal switch was also used in order to cancel the effects of thermal emf's. The samples were tested at room temperature (298K), ice water (273K), in liquid nitrogen (77K), and under liquid helium (4.2K). Figure 8 shows a wiring diagram for this setup.

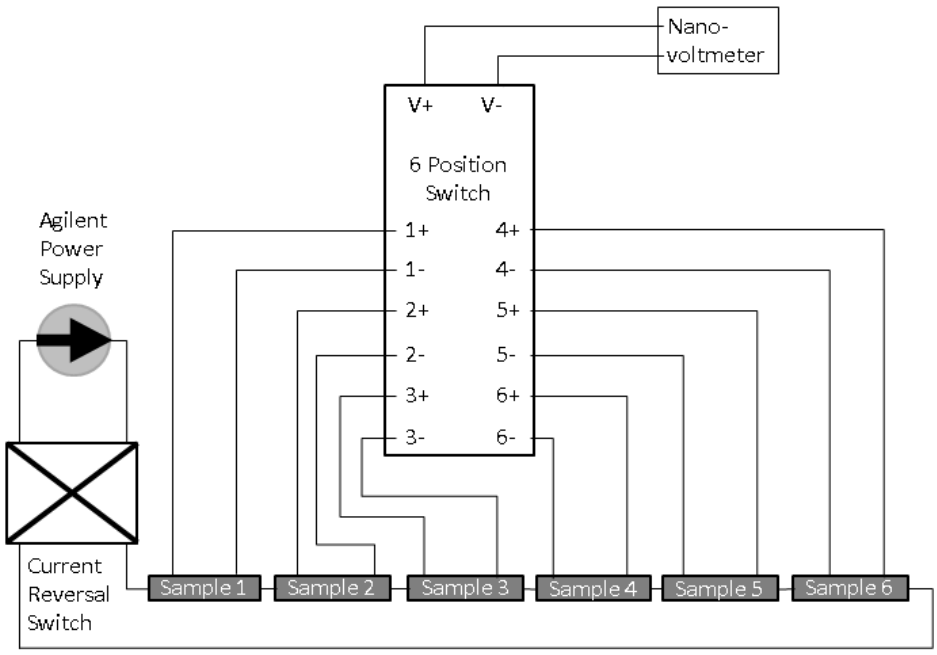

Figure 8: Wiring diagram for residual resistivity ratio measurements

To connect the samples together in series, a 9mm coupler was made out of a 3mm inner diameter stainless steel thin-walled tube with 1-72 holed drilled and tapped on either ends 1mm from the edge. 1-72 flat-headed screws were used to pin the individual sample cylinders together in series. The knife-edge voltage taps were made of a copper-beryllium clip that had one end insulated and the other end twisted to form a knife-edge. The copper-beryllium clips were then soldered to the 34 gauge enamel coated magnet wires running to the six position switch. The current reversal switch was soldered to the power supply 20 gauge insulated wire, and to the first and last coupler in the series via 28 gauge enamel coated magnet wire. The series setup was placed in a 0.3m long 12.7mm diameter thin walled copper-nickel tube, which was then attached to a 1m length of tube via a brass coupler. This tube ended in an aluminum box which contained the six position switch, current reversal switch, and leads for the nano-voltmeter and power supply. The tube was sealed with calk at the top in the box to prevent air from flowing down the tube and forming ice during testing with liquid nitrogen and helium. Figure 9 gives an image of the important parts of the setup.

Figure 9: a) RRR couplers and samples aligned in series, b) Samples encased in heat shrink to prevent grounding to nickel-copper tube, c) 0.3m nickel-copper tube holding samples in series, d) Entire setup ready to be tested and placed in dewars

Readings for six samples were then taken at room temperature, for both a forward and reverse current of one amp. Then the six samples were slowly immersed in a liquid helium dewar and allowed to cool until boiling stopped, and readings were taken again. The samples were them immersed in a liquid nitrogen dewar and followed the same procedure. Lastly, the samples were placed in ice water for at least five minutes to warm to temperature, and then readings were taken again. After the ice bath treatments the 0.3m section was removed and the six samples replaced with new samples and the tests run again. Care was taken to ensure the setup had warmed back to room temperature and dried before testing began again.

3. RESULTS

3.1 Extrusion Press Load

Press loads for all examined routes were recorded and selected examples of eight pass route B and 16-pass route Bc are found in Figure 10. Press load values for the initial pass, where the starting microstructure is assumed to be the same, should be very similar, with slight differences due to local friction effects within the die. As seen in Figure 10, the first pass is indeed similar for both routes. It has a local and global maximum of around 350kN which then steadily decreases to 250-275kN. Successive passes increase the press load significantly from the baseline, reaching a maximum force at 7-8 passes. Again, this is true for both cases of eight pass route B and 16-pass route Bc. After eight passes the press load begins a gradual decrease for successive passes up to 16 passes. The decrease in total stroke length comes from the machining of the billet between each pass to ensure it will fit in the die. Small deviations in press loads are possible results from friction forces when extruding. The other routes see a similar trend and additional press load curves are found in Appendix A.

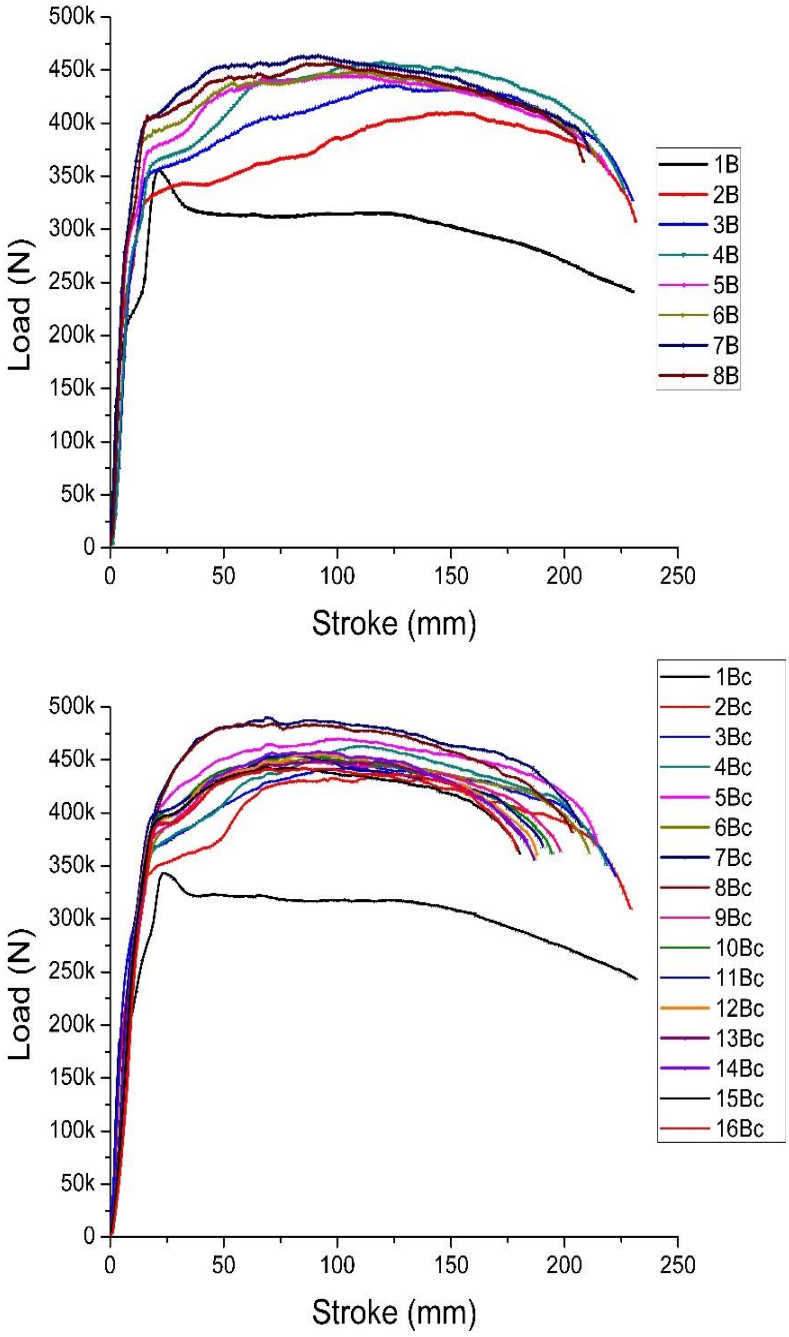

Figure 10: Top-Press load vs pass for route B, Bottom-Press load vs pass for route Bc

3.2 Brinell Hardness for Longitudinal and Flow Planes

Between each extrusion pass, hardness values recorded from both the longitudinal plane and the flow plane revealed an interesting occurrence in all bars. In almost every route studied, the flow plane consistently produced a higher hardness value than the longitudinal plane. Figure 11 illustrates this trend for routes 8A and 8E. The initial hardness of the annealed copper is around 73HBW. This number sharply increases to above 100 for every route after a single pass. After 3-4 passes, the hardness tends to level off and hold constant anywhere between values of 120BHW and 140BHW depending on the route and orientation. Error for the hardness values is initially very small for the unprocessed and 1st pass samples, but grows to be a maximum of about 4% for the fully worked samples. Additional graphs of the remaining routes are found in Appendix A.

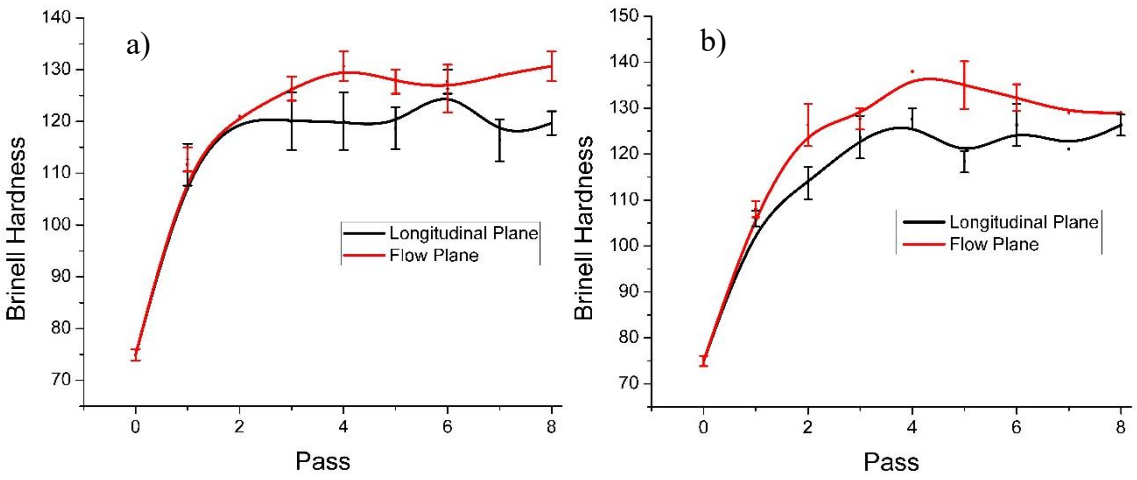

Figure 11: a) Longitudinal and flow plane Brinell hardness for bar 8A, b) Longitudinal and flow plane Brinell hardness for bar 8E

3.3 Vickers Hardness

Vickers hardness tests were completed for all processed routes, as well as the as-received material. Average hardness results for each sample as well as the corresponding error for each sample are shown by Table 1. The starting material had the lowest hardness as expected coming in at $54VH_{300}$, and after one pass the hardness doubled to 126 VH_{300}. After additional passes, the increase in hardness slowed dramatically, reaching a plateau. The maximum hardness values were seen by routes 4B, 8C and 8E with values of $145VH_{300}$. Error, calculated as one standard deviation, follows the same trend as with the Brinell hardness with unprocessed and first pass samples being lower at 1% to almost 4% for the worked samples.

Table 1: Vickers hardness results for as-received and processed materials

	Vickers Hardness VH_{300}	**Error VH_{300}**
As-Received	54	1
1A	126	2
2A	132	5
4A	137	2
8A	140	2
4B	145	4
8B	142	2
4C	141	3
8C	145	5
4E	143	2
8E	145	2
16E	141	3
4Bc	144	2
8Bc	141	4
16Bc	136	2

3.4 Recrystallization Temperature

Based on Vickers hardness results after heat treatment, a recrystallization curve for routes 1-8A and all 8-pass samples was generated. Figure 12 illustrates how the recrystallization temperature, defined as the bottom knee of the curve, is approximately 225°C for route 8E. The curve starts out constant with a hardness value of $145VH_{300}$ with no heat treatment. Heat treatments up to 150°C have little to no significant impact on the hardness value. However, after 150°C there is a sharp drop in the hardness where it then begins to level out around 200-215°C. By 225°C the hardness value has leveled out and the sample is claimed to be fully recrystallized. After 225°C, the hardness has a very slight decrease with increasing treatment temperature. For the most part the error in the Vickers hardness is less than 3%. This is not the case in the steep part of the curve where rapid recrystallization is occurring. In this section, the standard deviation is recorded to be upwards of 15% in some cases.

The recrystallization temperature for other eight pass samples is also approximated to be 225°C. This is clearly shown in Figure 13, which is a compiled plot of all eight pass recrystallization curves. All of the curves follow the same trend of reasonably constant hardness up to 150°C, with some slight increases due to recovery, and then a rapid decrease after 150°C that plateaus and levels out at 225°C. The exception to this trend is for route 8Bc, which has a decrease in hardness beginning at 150°C but still has the same plateau region at 225°C. All of the curves begin with hardness values between 140-$145VH_{300}$ and end with hardness values between 65-$75VH_{300}$ at the 300°C treatment temperature.

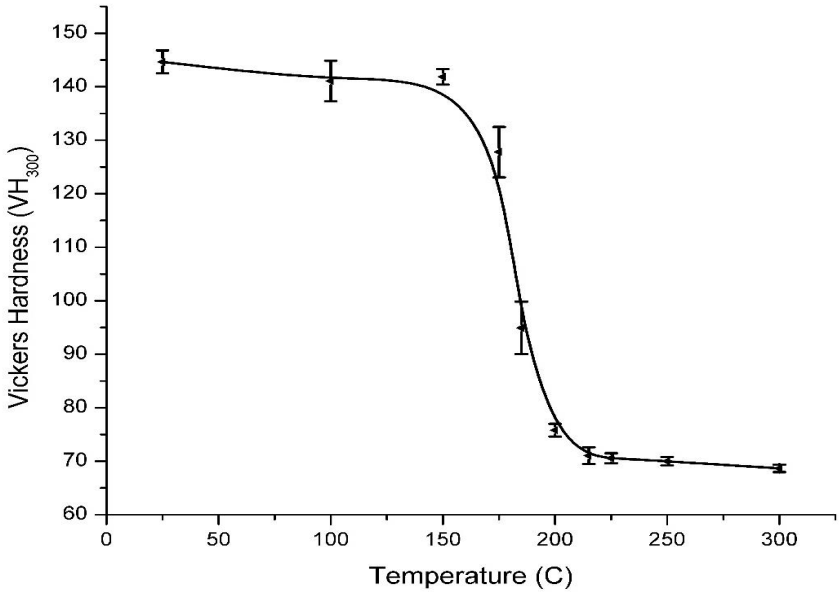

Figure 12: Vickers hardness vs heat treatment temperature for ECAE route 8E

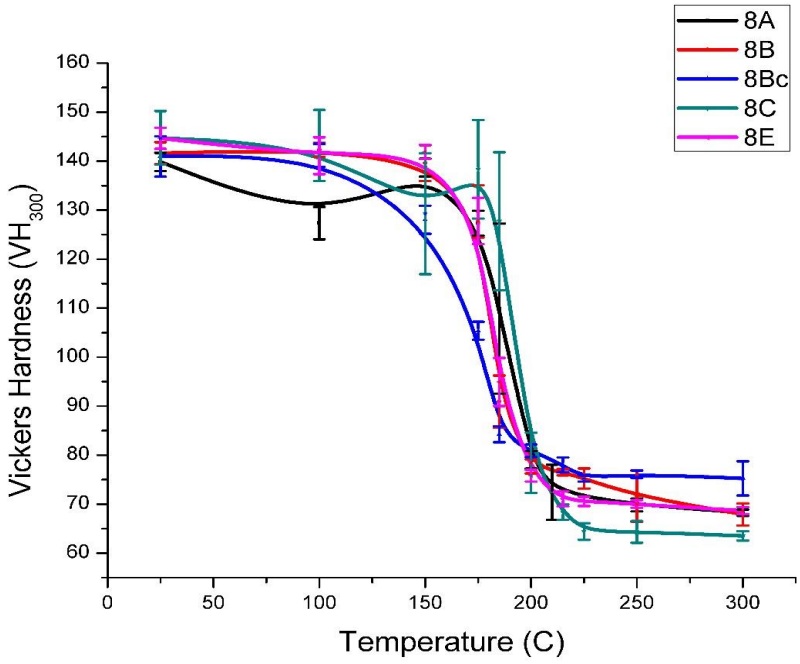

Figure 13: Recrystallization curves for ECAE routes 8A, 8B, 8Bc, 8C, and 8E

The hardness values all start approximatly the same, but after full recrystallization route Bc has a difinitivly higher hardness ending at $75VH_{300.}$ Routes B, A, and E all have the same recrystallized hardness at $68VH_{300}$, with Route C having the lowest recrystallized hadrness at $63.5VH_{300.}$ Error within all the eight pass routes follows the same trend as seen before with up to 15% strandard deviation during rapid recrystalization, and 3-4% everywhere else.

The recrystallization temperature decreases with increasing amounts of applied strain. This is evident in Figure 14, which compares the recrystallization curve of routes 1A, 2A, 4A, and 8A. The larger applied strain of the eight pass route leads to a recrystallization temperature of 225°C as previously stated. The 4A, 2A, and 1A routes have higher recrystallization temperatures of approximately 250°C, 275°C, and 350°C respectively.

In addition to conducting recrystallization runs using Vickers hardness, DSC tests were also conducted to determine recrystallization temperature. The results for these samples match with the results, within a 10°C range, from the Vickers hardness data. Figure 15 shows the spike in heat flow, indicating recrystallization at 225°C for the 8A sample. This is exactly what was determined by the Vickers hardness data seen previously. Additionally, the spike in the 4A sample happens at 240°C only 10°C away from the approximated value of 250°C from the hardness results. Additional DSC curves are found in Appendix A.

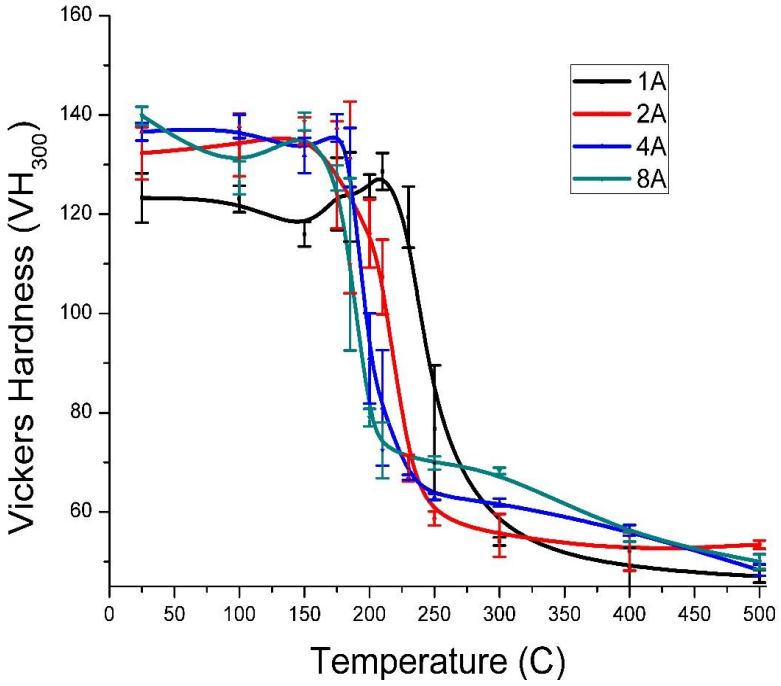

Figure 14: Recrystallization curves for routes 1A, 2A, 4A and 8A

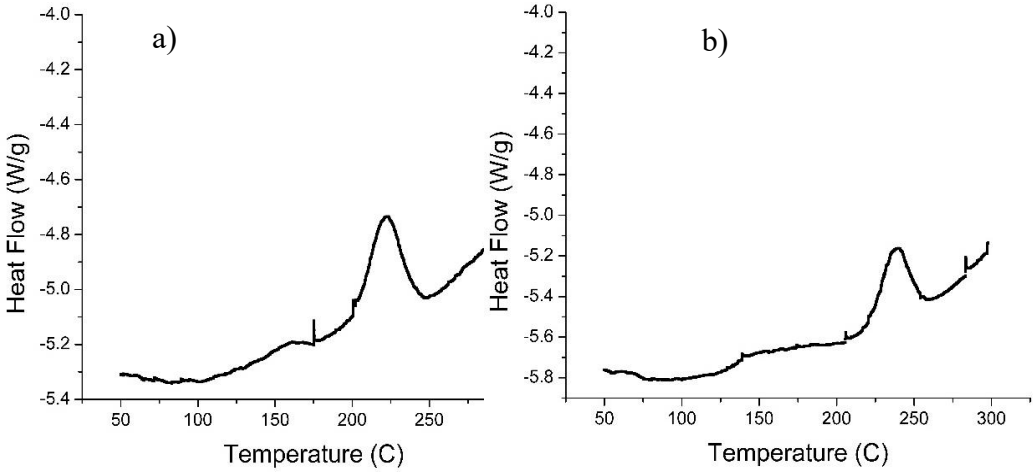

Figure 15: a) DSC temperature vs heat flow for route 8A, b) DSC temperature vs heat flow for route 4A

3.5 Residual Resistivity Ratio

Resistivity ratios were determined for all samples, and the results are listed in Table 2. The as-received material had the highest residual resistivity ratio (R273K/R4.2K) at 91.02, while route 16Bc had the smallest ratio at 19.2. The most common trend is that as the level of plastic strain increases the residual resistivity ratio decreases. Following similar trends of data seen earlier, the largest change in RRR comes from the first few passes. However, samples see differences when compared to other routes with the same level of applied strain. For example, route Bc has the smallest ratio for each of the three levels of applied strain, while route C has the highest value of RRR at similar strains. Routes A, B, and E fall in-between these two for both levels of applied strain. The values of the resistivity ratio for the 77K/4.2K and 273K/77K cases follow closely to the more accurate measurements of the RRR at 273K/4.2K.

Table 2: Resistivity ratios (RR) and residual resistivity ratios (RRR) for all samples

	RR (77K/4.2K)	RR (273K/77K)	RRR (273K/4.2K)
AR	11.22	8.11	91.02
1A	7.40	6.96	51.57
2A	6.05	6.01	36.42
4A	4.94	6.23	30.78
8A	4.32	5.71	24.66
4Bc	4.14	5.92	24.52
8Bc	3.64	5.51	20.06
16Bc	3.48	5.53	19.20
4E	4.79	6.27	30.01
8E	4.28	6.37	27.26
16E	4.09	5.64	23.10
4B	4.39	6.04	26.49
8B	3.85	5.99	23.02
4C	5.10	6.12	31.23
8C	4.53	6.60	29.88

3.6 Engineering Stress vs Strain

3.6.1 ECAE Processed

Engineering stress strain curves were generated for all processed routes, which give values for tensile strength, yield strength, and elongation to failure. These curves are chosen representatives for each case, with averages being presented later. As expected, the as-received annealed sample has the lowest strength and greatest ductility, while increasing the amount of applied strain increases strength and decreases ductility to a degree. Figure 16 gives a visual representation of the as-received, 1A, 2A, 4A, and 8A samples.

As seen, the as-received material has an ultimate tensile strength (UTS) of approximately 250MPa, and after one pass the UTS increases to just under 350MPa. After an additional pass UTS increases to 380MPa, and all additional passes produce diminishing returns with the UTS for 4A and 8A samples being 397MPa and 404MPA respectively. When comparing different routes to each other while keeping the amount of applied strain equal, minute differences in the stress-strain relationships are seen.

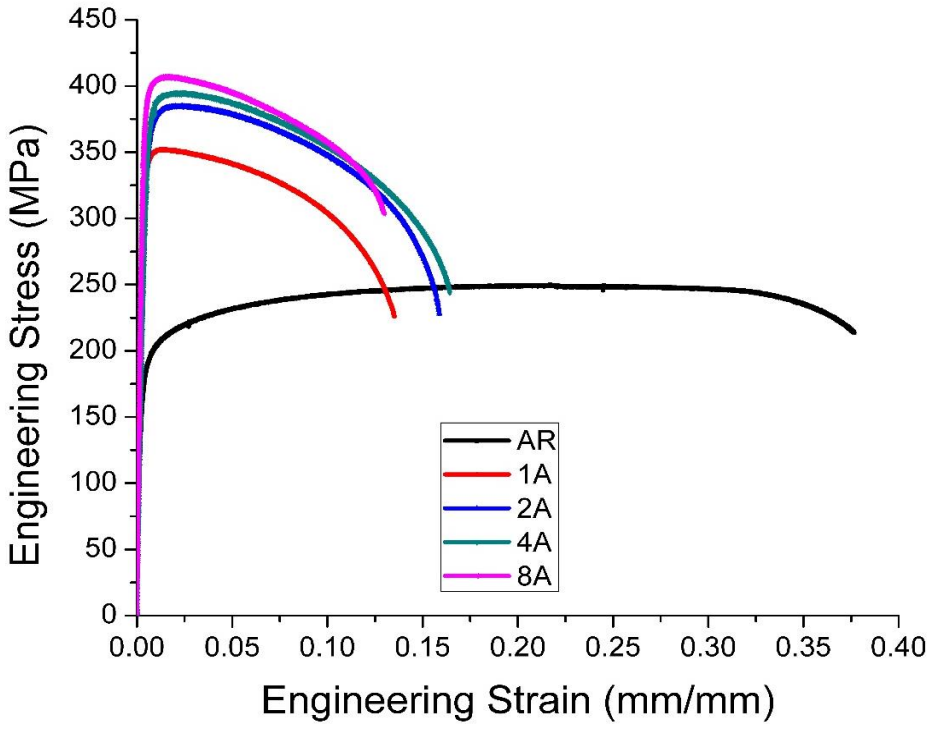

Figure 16: Engineering stress-strain curves for samples as-received (AR), 1A, 2A, 4A, and 8A

Figure 17 demonstrates the differences between the four pass routes. Route B has the highest UTS followed by route E, Bc, C, and ending with route A with average UTS

values of 442MPa, 438MPa, 421MPa, 411MPa, and 397MPa respectively. The elongation to failure of the different routes follows a different pattern. Route E has the highest strain to failure, while route C has the lowest strain to failure. Routes A, B, and Bc all have approximately the same strain to failure.

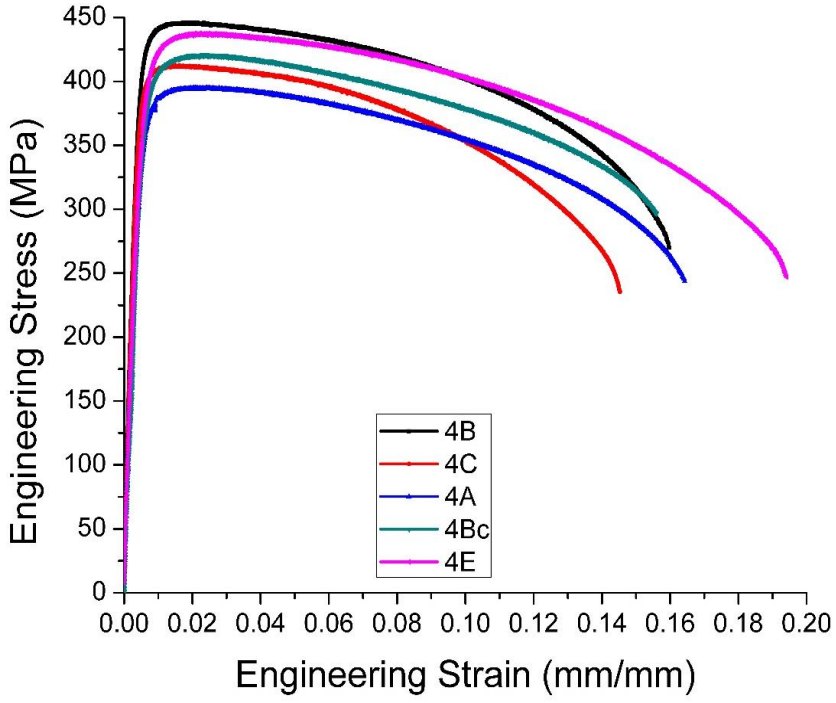

Figure 17: Engineering stress-strain curves for four pass routes (A, B, Bc, C, E)

Figure 18 shows the stress strain relationship for the same five routes discussed above but for eight passes rather than four. The results are slightly different than that of the four pass routes. For example, Route Bc now has the highest UTS followed by route B, E, C and ending again with route A. Only route Bc saw a significant increase in

average UTS from 421MPa at four passes to 437MPa at eight passes. Route E actually saw a decrease in average UTS from four pass to eight pass going from 438MPa to 427MPa. Routes A, B, and C all had similar UTS values between four and eight passes.

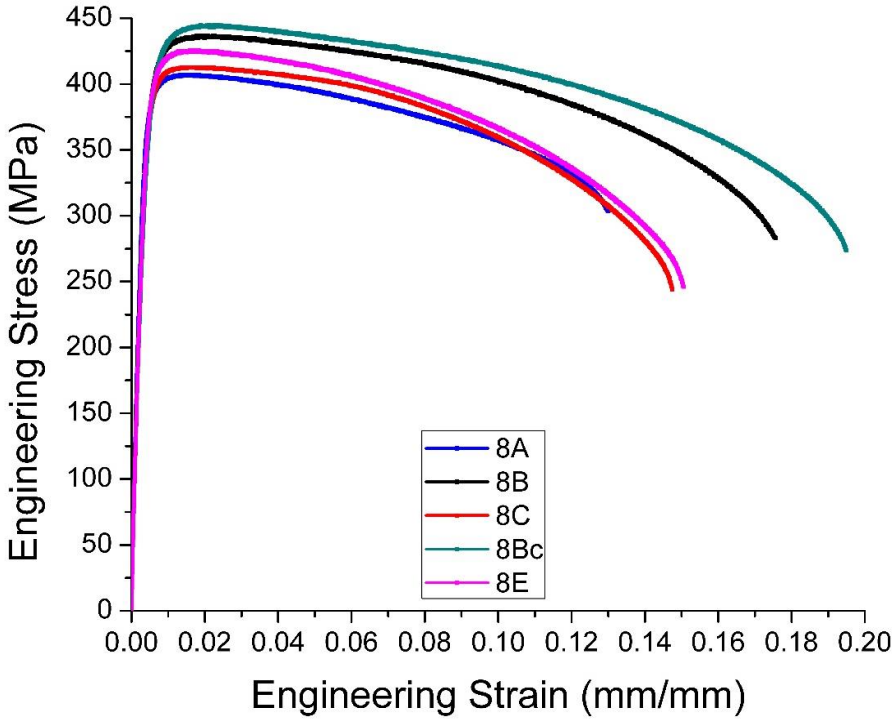

Figure 18: Engineering stress-strain curves for eight pass routes (A, B, Bc, C, E)

Figure 19 shows the stress strain relationship for the two 16-pass samples tested. Route Bc had the higher UTS, with an average of 438 Mpa, staying equal to that of the eight pass sample. Route E interestingly decreased in average UTS again from the eight pass sample coming in at 413MPa. Both showed similar ductility values as compared to the eight pass samples. Table 3 gives an overview of average UTS, yield strength, and

elongation to failure for all processed samples. Error is calculated as the standard deviation of the three tensile test performed.

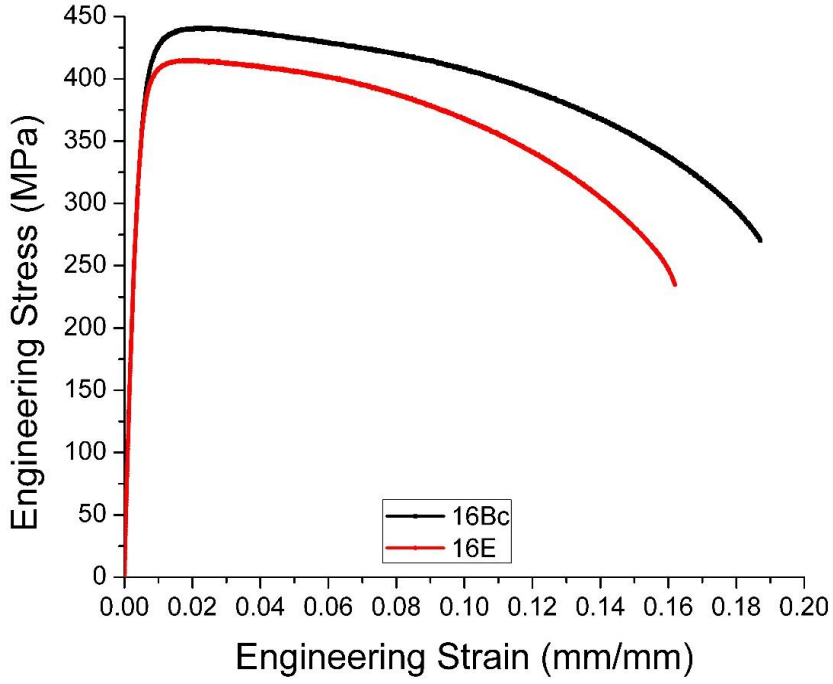

Figure 19: Engineering stress-strain curve for route 16BC and 16E

Table 3: Average ultimate tensile strength, yield strength, and elongation to failure for all processed samples

	Yield Strength (MPa)	Tensile Strength (MPa)	Strain to Failure
AR	181 ± 2	248 ± 2	0.38 ± .02
1A	323 ± 5	349 ± 4	0.14 ± .01
2A	364 ± 1	383 ± 4	0.14 ± .03
4A	372 ± 1	397 ± 2	0.16 ± .01
4B	399 ± 4	442 ± 4	0.16 ± .01
4C	382 ± 4	411 ± 2	0.15 ±.02
4E	402 ± 1	438 ± 2	0.19 ± .01
4Bc	383 ± 17	421 ± 6	0.16 ± .02
8A	371 ± 7	404 ± 4	0.12 ± .01
8B	373 ± 4	437 ± 1	0.18 ± .02
8C	369 ± 7	411 ± 6	0.15 ± .01
8Bc	373 ± 3	437 ± 6	0.20 ± .01
8E	382 ± 2	427 ± 1	0.15 ± .01
16Bc	357 ± 3	438 ± 3	0.18 ± .01
16E	358 ± 7	413 ± 3	0.16 ± .01

3.6.2 ECAE Processed + Rolling

Selected samples were rolled along the extrusion direction after processing to evaluate the influence on their stress-strain properties. Samples rolled included 2A, 4A, 4Bc, and 4E. Additionally, the 4A sample was rolled in the direction across the extrusion direction as well as two directions in the transverse plane. All samples were rolled to 10%, 30%, 69%, and 90% reduction in thickness.

Figure 20 compares the results of rolling after ECAE for the as-received, 2A, 4Bc, and 4E samples. As seen for the three ECAE processed samples the 10% reduction in thickness results in an increase in strength for the 4Bc sample but a decrease in

strength for the 2A, and 4E sample. The 30% reduction in thickness for processed samples results in a decrease in strength from the as-worked condition, and is in fact the lowest strength of all rolled cases. The 69% reduction in thickness results in the highest strength for all processed samples, with route 4Bc almost reaching a UTS of 500 MPa. The 90% reduction in thickness in the processed samples resulted in a lower strength than that of the 69% reduction, but generally was higher than that of the as-worked material condition. For the as-received material, as the amount of rolling increases, the UTS is correspondingly increased.

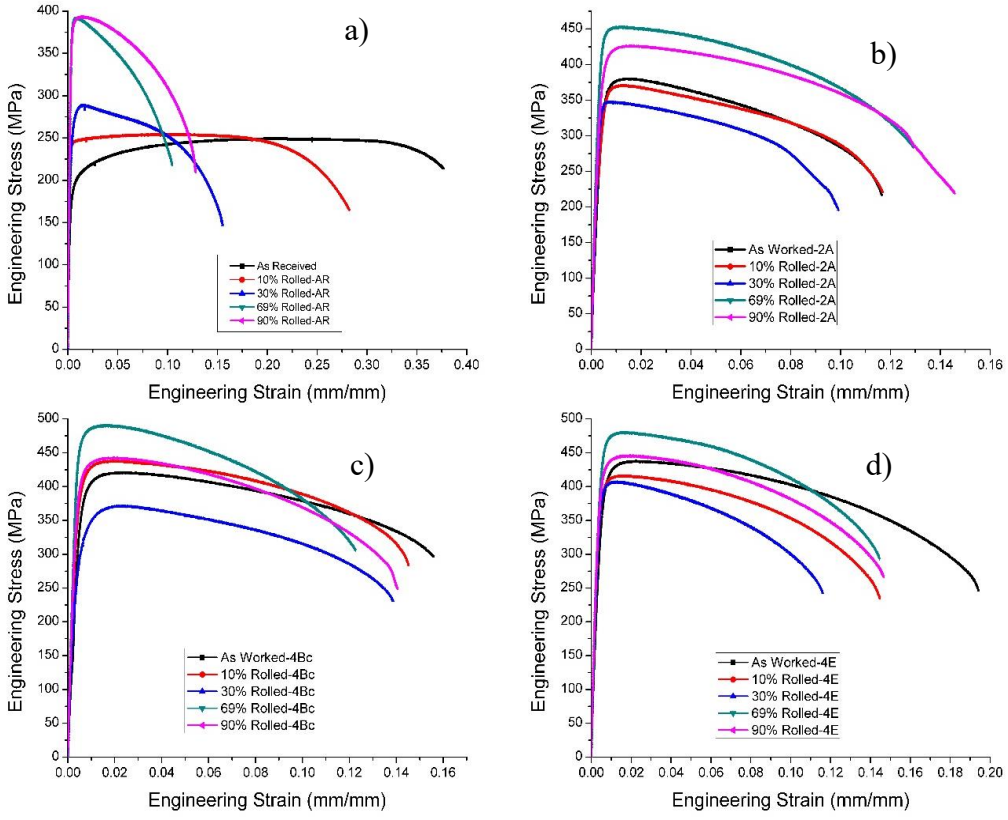

Figure 20: a) ECAE + rolling stress-strain curves for as-received, b) 2A, c) 4Bc, d) 4E

Table 4 gives averages for UTS, yield strength, and strain to failure for as-received, 2A, 4Bc, and 4E samples. Error is again calculated as the standard deviation between the three separate tests for each sample. Errors in the UTS were significantly greater for 30% reduction in thickness samples when compared to the rest of the rolled samples. Errors for the yield strength were higher for not only the 30% but also the 10% and 69% reduction in thickness cases.

Table 4: Average ultimate tensile strength, yield strength, and elongation to failure for rolled as-received, 2A, 4A, and 4E samples

	Yield Strength (MPa)	Tensile Strength (MPa)	Strain to Failure
AR	181 ± 2	248 ± 2	0.38 ± .02
AR-R10	246 ± 6	256 ± 2	0.28 ± .01
AR-R30	261 ± 22	290 ± 1	0.16 ± .01
AR-R69	377 ± 5	393 ± 1	0.11 ± .01
AR-R90	375 ± 9	388 ± 9	0.12 ± .01
2A	364 ± 1	383 ± 4	0.14 ± .03
2A-R10	345 ± 23	371 ± 8	0.18 ± .01
2A-R30	356 ± 22	361 ± 20	0.09 ± .01
2A-R69	419 ± 21	454 ± 3	0.13 ± .01
2A-R90	403 ± 5	426 ± 5	0.14 ± .01
4Bc	383 ± 17	421 ± 6	0.16 ± .02
4Bc-R10	360 ± 25	430 ± 12	0.14 ± .01
4Bc-R30	299 ± 64	378 ± 42	0.14 ± .02
4Bc-R69	431 ± 23	492 ± 1	0.13 ± .01
4Bc-R90	411 ± 5	443 ± 5	0.14 ± .01
4E	402 ± 1	438 ± 2	0.19 ± .01
4E-R10	N/A	409 ± 9	N/A
4E-R30	383 ± 9	411 ± 4	0.12 ± .01
4E-R69	402 ± 35	474 ± 9	0.14 ± .01
4E-R90	414 ± 11	449 ± 8	0.14 ± .01

Route 4A was rolled in four different directions; with extrusion (WE), across extrusion (AE), transversely in the Y direction (BT), and transversely in the X direction (SS). The results of the directional rolling are seen in Figure 21. Similar to the other routes when rolled along the extrusion direction (WE), the 10% and 30% reduction in thickness resulted in a decrease in strength, while the 69% reduction resulted in the highest UTS with an average value of 468MPa. The 90% case again was lower than the 69% but higher than the as-worked. For the sample rolled across the extrusion direction (AE), the 10% case had a significant increase over the as-worked condition. The 30% resulted in a drop in the UTS bringing it back down to approximately as-worked condition. The 69% reduction again resulted in the highest UTS with an average value of 449MPa. The 90% reduction resulted in a UTS that was similar again to the as-worked condition. The sample cut from the transverse plane and rolled in the Y direction (BT) followed a similar pattern as when rolling with the extrusion direction where 10% and 30% reduction results in a lower strength, 69% resulted in the highest strength at 441MPa and 90% resulted between 69% case and the as-worked condition. The last sample had the best results, with all rolling percentages resulting in increases in strength vs the as-worked condition, and the 69% reduction resulting with UTS of almost 500MPa. Figure 21 compares the results of the directional 4A rolling experiments. Additionally, Table 5 gives averages for UTS, yield strength, and strain to failure for 4A rolled samples.

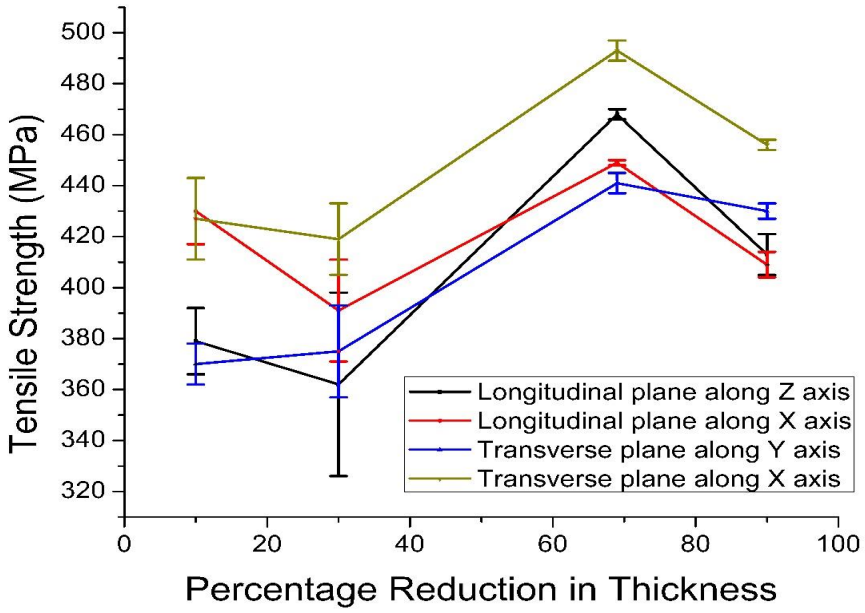

Figure 21: Tensile strength vs percentage reduction in thickness for route 4A

Table 5: Average ultimate tensile strength, yield strength, and elongation to failure for rolled 4A samples

	Yield Strength (MPa)	Tensile Strength (MPa)	Strain to Failure
4A	372 ± 1	397 ± 2	0.16 ± .01
4A-WE-R10	333 ± 23	379 ± 13	0.13 ± .01
4A-WE-R30	359 ± 26	378 ± 27	0.14 ± .01
4A-WE-R69	423 ± 19	468 ± 2	0.13 ± .01
4A-WE-R90	355 ± 7	413 ± 8	0.15 ± .01
4A-AE-R10	390 ± 22	430 ± 13	0.12 ± .01
4A-AE-R30	357 ± 19	391 ± 20	0.14 ± .01
4A-AE-R69	400 ± 10	449 ± 1	0.11 ± 01
4A-AE-R90	335 ± 4	409 ± 5	0.16 ± .01
4A-SS-R10	401 ± 20	427 ± 16	0.13 ± .01
4A-SS-R30	340 ± 35	419 ± 14	0.15 ± .01
4A-SS-R69	454 ± 11	493 ± 4	0.10 ± .01
4A-SS-R90	398 ± 6	456 ± 2	0.13 ± .01
4A-BT-R10	334 ± 12	370 ± 8	0.12 ± .01
4A-BT-R30	334 ± 7	375 ± 18	0.14 ± .01
4A-BT-R69	403 ± 7	441 ± 4	0.13 ± .01
4A-BT-R90	371 ± 21	430 ± 3	0.15 ± .01

3.6.3 ECAE Processed + Recrystallization

Engineering stress-strain curves were generated for partially recrystallized and fully recrystallized route 4A. Heat treatments included temperatures of 150°C, 175°C, 185°C, 200°C, 210°C, 230°C, and 250°C. Figure 22 illustrates the results from the tensile tests for the various heat treatment temperatures. The 150°C and 175°C treatment show a small decrease compared to the as-worked sample giving a UTS of right around 380MPa. The 185°C treatment results in a similar drop in UTS resulting in a value of 367 MPa, and increases the strain to failure by a small margin. The 200°C treatment

results in an extremely large drop in UTS and a corresponding increase in strain to failure. The UTS for the 200°C sample is 289 MPa. The 210°C treatment results in a much smaller drop in UTS, with a value of 276MPa, and increases the strain to failure. The 230°C and 250°C treatments both result in approximately the same UTS of 245 MPa and 243MPa respectively, but the 250°C treatment has a slightly larger strain to failure.

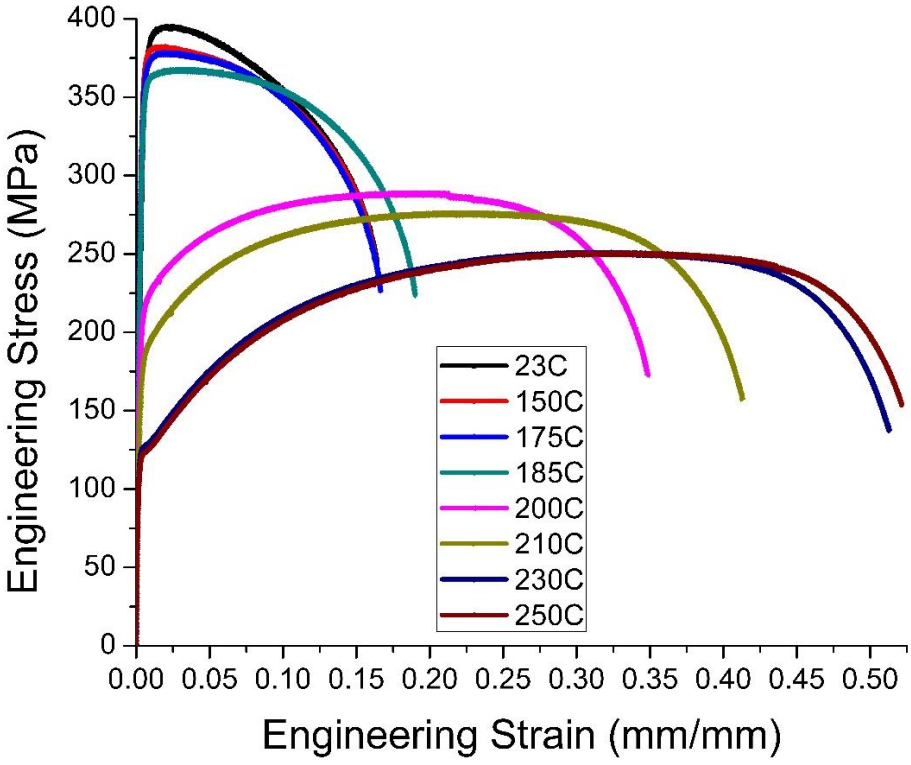

Figure 22: Stress strain curve for heat-treated 4A samples

3.7 Microstructure

3.7.1 As-Worked

Following the procedure listed in above sections, SEM images were taken of all as-worked and recrystallized samples to evaluate microstructure. The starting microstructure of the as-received CDA 101 copper is shown in Figure 23 with an average grain size of 29.5μm.

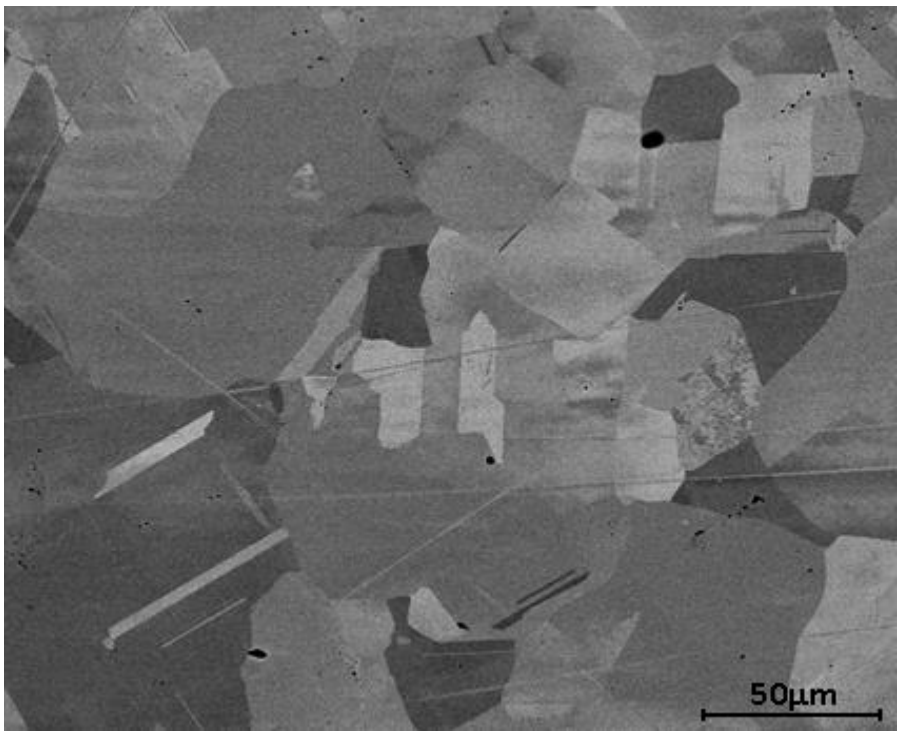

Figure 23: BSE image of as-received annealed OFHC Cu microstructure at 500x magnification

Immediately after one pass, the grain size drastically decreases to an average of 980nm. Successive passes through the ECAE die results in smaller average grain sizes

with diminishing returns. Depending on the route, the grain size either continues to decrease by a diminishing factor with each additional pass, or it levels out. However, route E actually sees a slight increase in grain size for the heavily deformed eight and 16 pass cases. A comparison of microstructures for the 1A, 2A, 4A, and 8A samples is shown in Figure 24 to illustrate the evolution of the microstructure. Table 6 presents all sample conditions and their corresponding grain sizes.

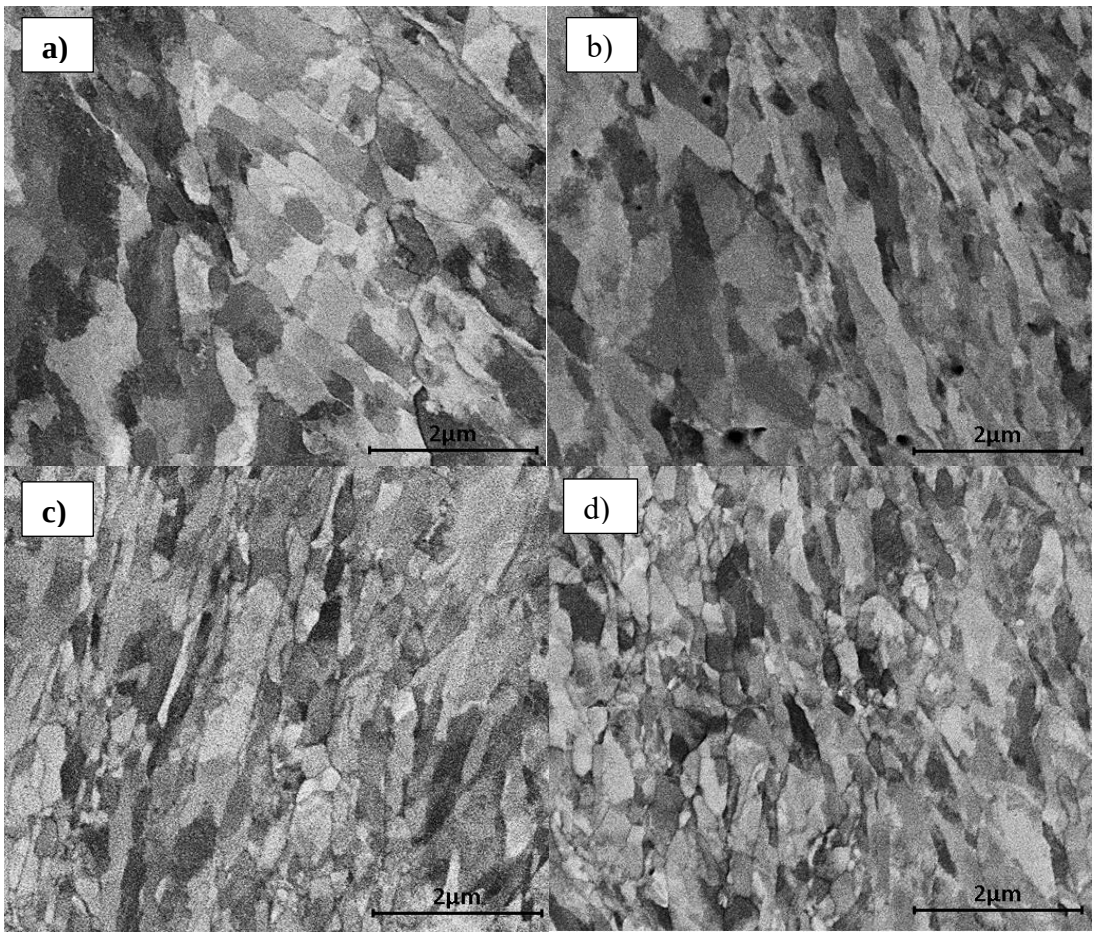

Figure 24: BSE images of 1A (a), 2A (b), 4A (c), and 8A (d) microstructure at 20000x magnification

Table 6: Route, applied strain, average grain size, standard deviation, and 95% confidence intervals of grain size for all samples

	Applied Strain	Grain Size (micron)	Standard Error (micron)	95% Confidence Interval (micron)
AR	0	29.5	3.15	[23.2,35.8]
1A	1.16	0.978	0.043	[0.893,1.06]
2A	2.32	0.751	0.039	[0.675,0.828]
4A	4.64	0.578	0.043	[0.493,0.663]
4B	4.64	0.493	0.031	[0.432,0.555]
4Bc	4.64	0.412	0.027	[0.359,0.467]
4C	4.64	0.501	0.034	[0.434,0.569]
4E	4.64	0.473	0.028	[0.419,0.528]
8A	9.28	0.512	0.028	[0.458,0.566]
8B	9.28	0.416	0.024	[0.368,0.464]
8Bc	9.28	0.415	0.026	[0.364,0.466]
8C	9.28	0.505	0.028	[0.438,0.545]
8E	9.28	0.527	0.027	[0.474,0.580]
16Bc	18.56	0.415	0.027	[0.362,0.468]
16E	18.56	0.534	0.028	[0.479,0.591]

As seen in Table 6, route A has a continually decreasing grain size as the amount of applied strain increases. This follows closely with the tested tensile strength for route A. Route B has a definite decrease in grain size from four pass to eight pass. This is contradictory to the results from the tensile tests. Route Bc had very small change between 4, 8, and 16 pass which is consistent with the tensile test data. Route C also had a constant grain size for both four and eight pass samples. Lastly, route E had an increasing grain size from four to 16 passes, which was also seen by the tensile tests. The standard error for worked samples except for the single pass sample was below 10% of the average value. Additional images of worked microstructures can be found in Appendix A.

Comparing the means of each of the separate routes, average grain size by a one-way analysis using Tukeys HSD test with an alpha value of 0.05 results in non-significant differences for almost all worked samples. The only means that differ significantly at the 0.05 level are the 1A and 2A cases with the rest of the routes. Appendix B has the one-way analysis report from JMP, a statistical software, for the worked samples.

3.7.2 Recrystallized

Grain size measurements were also taken after recrystallization for all worked samples. Additional images were taken of partly recrystallized 4A and 8Bc samples to further verify recrystallization temperature. Figure 25 displays the development of the recrystallized grains as heat treatment temperature was increased for route 8Bc. This supports the findings that the recrystallization temperature is 225°C as described in prior sections.

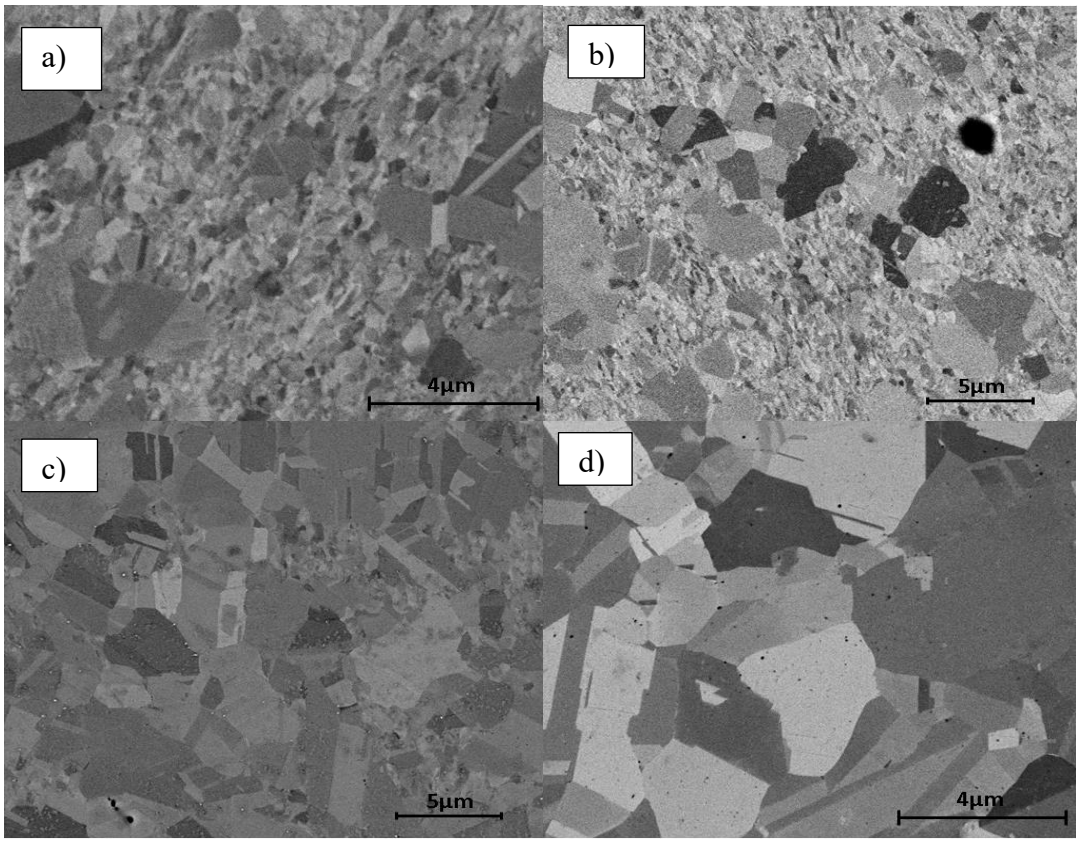

Figure 25: Microstructure of partly recrystallized and fully recrystallized route 8Bc samples at 150°C (a), 175°C (b), 185°C (c), and 225°C (d)

Figure 26 gives an example of fully recrystallized worked material, while Table 7 provides a summary of grain size, standard error, and 95% confidence intervals. Additional microscopy images for the rest of the samples can be found in Appendix A.

As indicted by Table 7, as the amount of applied strain increases, the recrystallized grain size correspondingly decreases. The one exception is route C, which has a slight increase in recrystallized grain size from four passes to eight passes. Route Bc has the smallest recrystallized grain size of all samples with route E following close behind. All recrystallized samples have standard errors of below 10%.

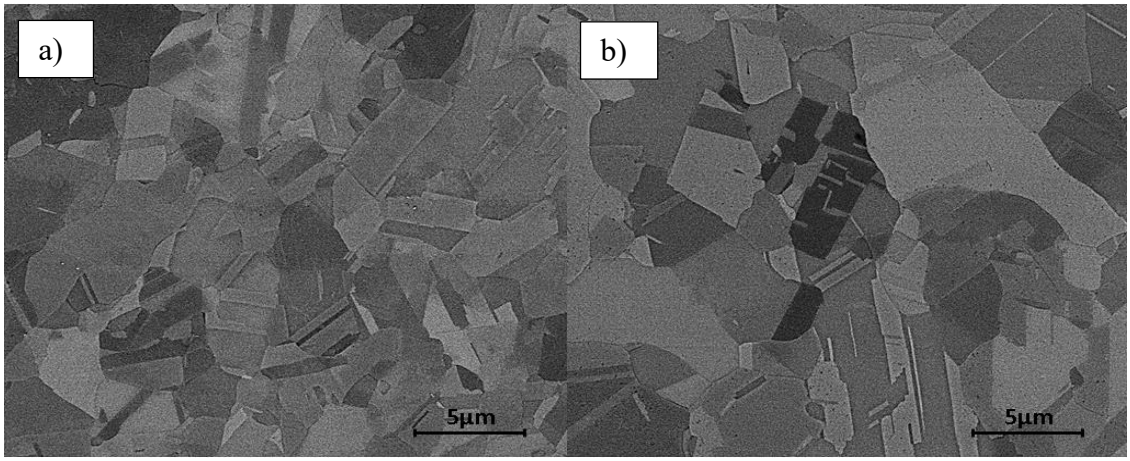

Figure 26: Fully recrystallized sample for route 4C (a) and route 4E (b)

Table 7: Route, applied strain, average grain size, standard deviation, and 95% confidence intervals of grain size for all recrystallized samples

	Applied Strain	Grain Size (micron)	Standard Error (micron)	95% Confidence Interval (micron)
1A	1.16	6.26	0.191	[5.88,6.63]
2A	2.32	4.44	0.197	[4.06,4.83]
4A	4.64	2.22	0.170	[1.89,2.56]
4B	4.64	2.48	0.179	[2.13,2.83]
4Bc	4.64	1.95	0.145	[1.66,2.24]
4C	4.64	1.93	0.145	[1.64,2.23]
4E	4.64	2.14	0.179	[1.80,2.47]
8A	9.28	1.79	0.123	[1.54,2.03]
8B	9.28	1.87	0.152	[1.57,2.17]
8Bc	9.28	1.40	0.115	[1.17,1.63]
8C	9.28	2.18	0.141	[1.90,2.45]
8E	9.28	1.66	0.138	[1.39,1.93]
16Bc	18.56	1.32	0.135	[1.06,1.59]
16E	18.56	1.51	0.132	[1.25,1.77]

Again, the means of the different average recrystallized grain sizes for each material sample were compared using Turkey's HSD test with an alpha level of 0.05. The HSD test results in some sample means being statistically different from others. Mainly samples 8Bc and 16Bc result in smaller grain sizes when compared to 1A, 2A, 4A, 4B, 4E, and 8C. However, at the 0.05 level of confidence, the remaining routes cannot be considered statistically different, even with their dissimilar average recrystallized grain size. Appendix B has the one-way analysis report from JMP for the recrystallized samples.

3.8 Correlations

3.8.1 Strength and Vickers Hardness

When plotting hardness data vs strength, the general trend is as hardness increases, strength also increases. This is evident from Figure 27 which gives a side by side view of both yield and tensile strength vs hardness for all processed routes. As seen in prior graphs and tables, the hardness values range for 125 to 150 for worked samples while strength falls between 320MPa to 450MPa. The yield strength vs hardness does have a slightly larger scatter when compared to the tensile strength vs hardness. The largest scatter falls to the right of the graphs when strength is high.

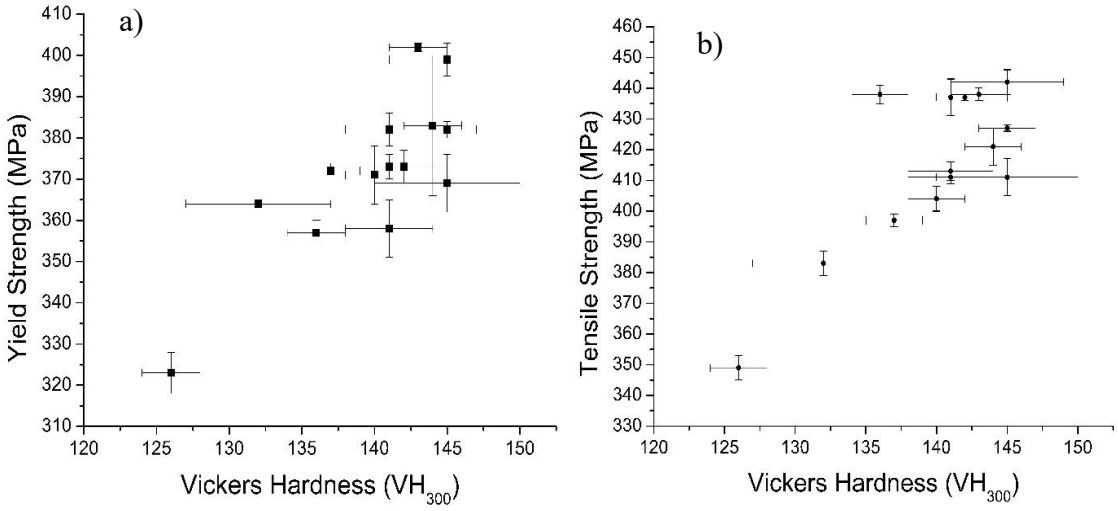

Figure 27: a) Yield strength vs Vickers hardness for all processed samples b) tensile strength vs Vickers hardness for all processed samples

3.8.2 Strength and Grain Size

Looking at the relationship between grain size and strength gives a far more linear relationship as shown by Figure 28 and Figure 29. When plotting the yield and tensile strength vs the inverse square root of the average grain size R^2 values of over 0.9 are generated for both plots. Again the yield strength plot has more variability when compared to the tensile strength. Inverse grain sizes range for $0.005nm^{-0.5}$ to $0.05nm^{-0.5}$ and strengths vary between 180 to 450MPa. It should be noted that for both graphs, the linear fit is heavily influenced by the higher grain size values, mainly the as-received sample.

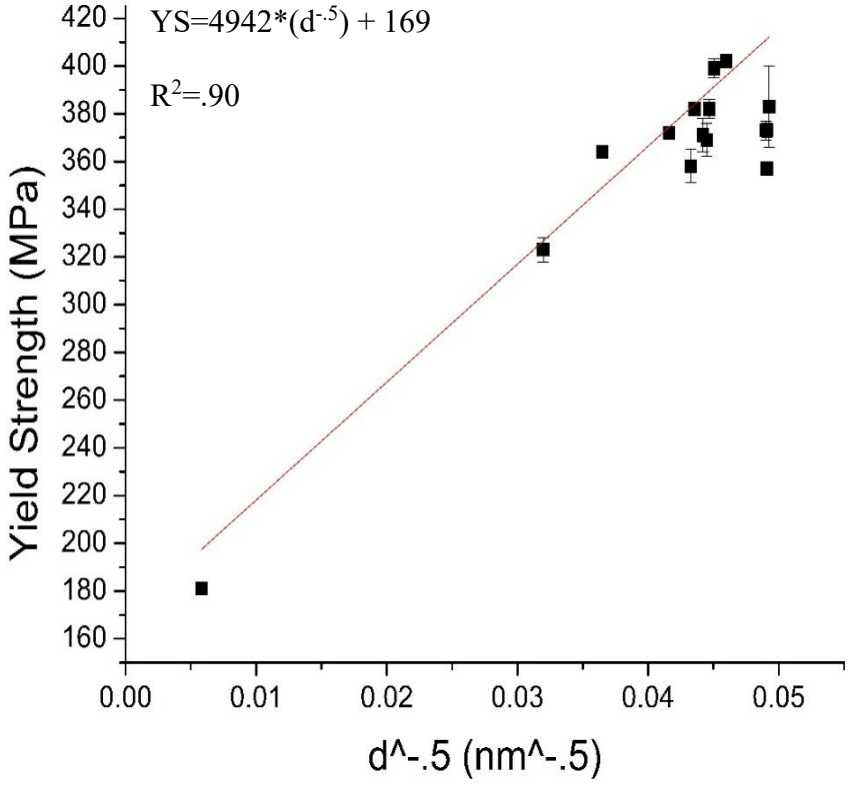

Figure 28: Linear fit for yield strength vs inverse square root of the grain size

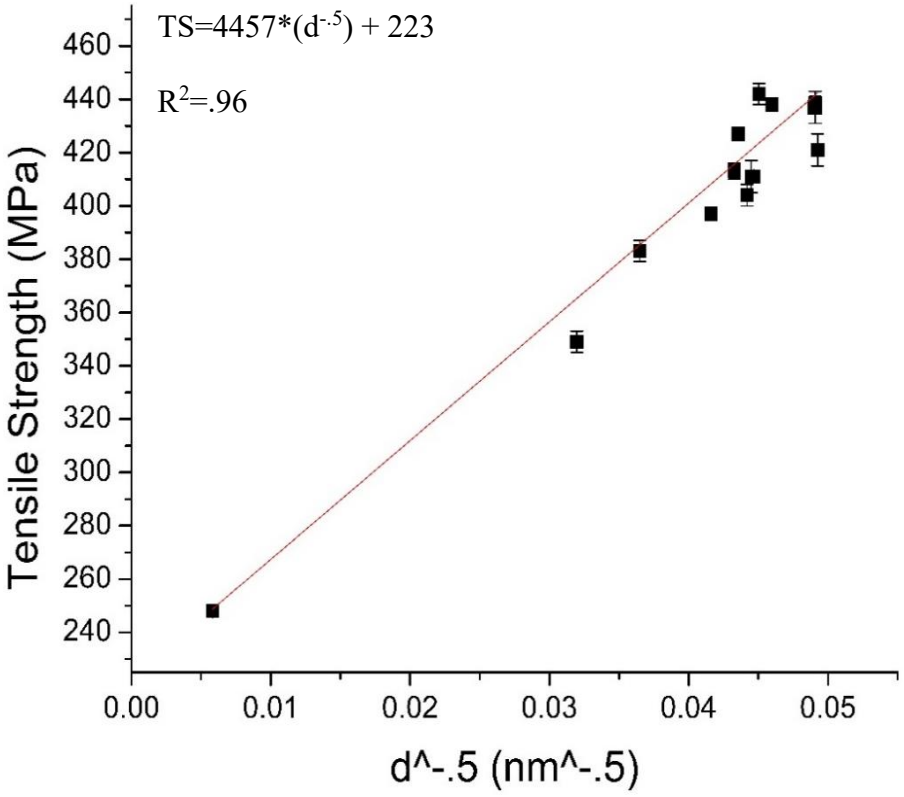

Figure 29: Linear fit for tensile strength vs inverse square root of the grain size

3.8.3 RRR, Strength, and Grain Size

In finding the best processing method to create the strongest copper that still has a high conductivity, finding the relationship between strength and conductivity is paramount. Therefore, tensile strength values have been plotted against both the 273K/4.2K residual resistivity ratios and the 77K/4.2K resistivity ratios. As seen by Figure 30, as strength increases residual resistivity decreases, corresponding to a decrease in conductivity. Again, the spread is larger for samples with higher strength. The resulting relationship is linear, again with R^2 values being over 0.93. There are

practically no differences between the two trials, with similar R^2 values and trends. Similarly, the linear fit is highly influenced by the low strength as-received material.

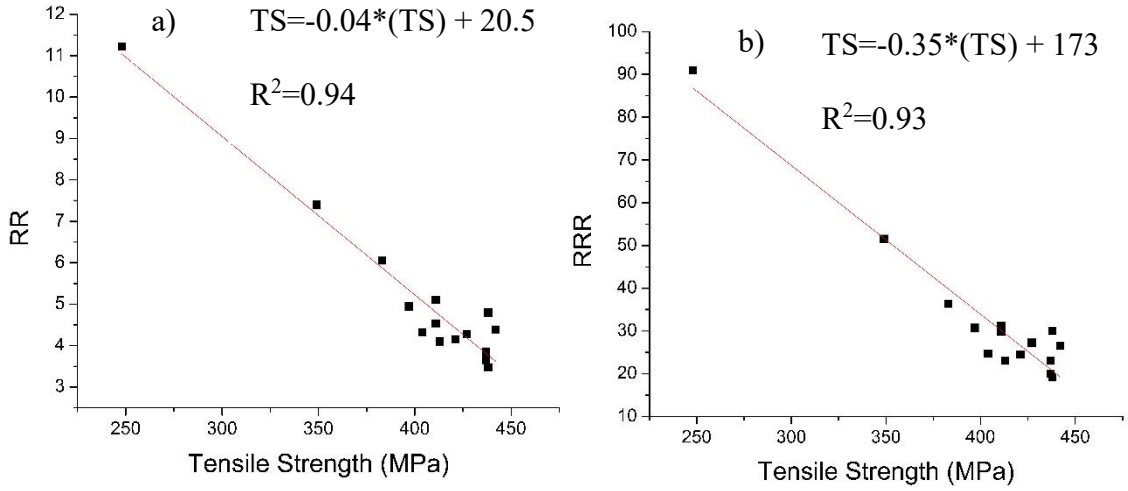

Figure 30: a) Resistivity ratio (77K/4.2K) vs tensile strength b) residual resistivity ratio (273K/4.2K) vs tensile strength

Another correlation that has importance is the resistivity ratios relationship to grain size. Grain size is one of the main dictators of strength and hardness for the processed material. Figure 31 shows the relationship between the inverse square grain size and the resistivity ratio for 77K/4.2K and 273K/4.2K. Again, the relationship is linear with R^2 values equal to 0.96 for both cases. The larger inverse square root values have smaller resistivity ratios.

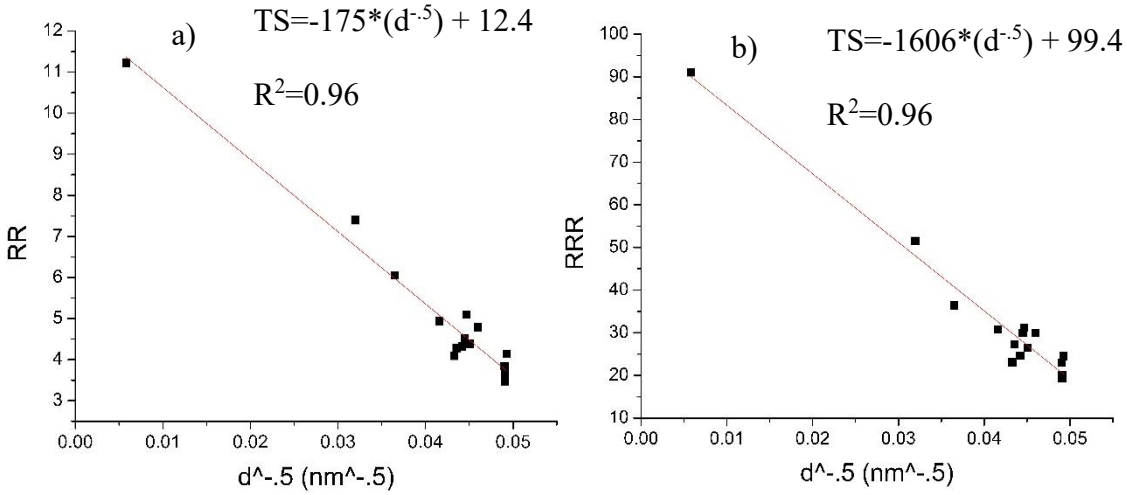

Figure 31: a) Resistivity ratio (77K/4.2K) vs inverse square root grain size b) residual resistivity ratio (273K/4.2K) vs inverse square root grain size

4. DISCUSSION

Hardness and strength are dependent on the ability of the copper to plastically deform, which is defined as a large movement of dislocations. Dislocations are inhibited by the differing orientations of grains in the Cu matrix, as well as the disorder of the grain boundaries, meaning that a smaller average grain size, the harder and stronger the Cu becomes. In addition, because dislocation interactions generally inhibit motion, a higher dislocation density increases strength and hardness. This is a well know phenomenon that occurs as you work harden a material. The grain size progression after processing was indeed measured and results are as expected.

The largest grain size seen by the as-received material had the lowest strength and hardness. The next largest grain size was seen by the one pass sample which had the second lowest strength and hardness. The same decrease in grain size and increase in hardness and strength was seen for the 2A and 4A samples. These values can be found in Table 1, Table 3, and Table 6. The general relationship is that the decreasing grain size corresponds to an increase in strength. The grain size and strength has a Hall-Petch type relationship as seen in Figure 28 and Figure 29. However, some of the other four pass samples had differences we speculate due to the texturing effect created by the different routes. For example, four pass route E had a much higher strength, with a larger grain size. Route E also had an interesting result in that it actually had larger grains and was weaker for the eight and 16 pass samples. This could be due to dynamic recovery of the material brought on by the large stored energy in the lattice, or possibly producing a

more pronounced texture alteration. Route Bc had increasing strengths from four to eight to 16 passes, but had a constant grain size. This could mean that the dislocation density that increased, but it is more probable that the material obtained a favourable texture. Route C had practically no difference in grain size and strength from the four to eight pass samples. Lastly, route B had another interesting result. While the grain size from the four to eight pass decreased, the strength actually fell by a small amount ~5 MPa. The four pass route B sample had a surprisingly large tensile strength of 442 MPa, one that was not expected, and did not match with its grain size. Again, while it is possible dislocation density or pronounced texture could be the cause, more testing is recommended to validate the strengths reported here. Additionally, differences between the routes could be due to the varying texture in the microstructure. Route A produces a very laminar grain structure, while route B has a more filamentary structure. Route C produces equiaxed grains on even numbered passes. Routes Bc and E both have quite equiaxed grain structures after ECAE processing. Hardness values for all the 4, 8, and 16 pass samples were similar with a large enough standard deviation that making a meaningful comparison between the routes is not possible.

Recrystallization temperatures were found to decrease as the amount of applied strain increased as expected. The differences in recrystallization come from the differing amounts of stored energy within the crystal lattice. For samples with larger amounts of applied strain there is a larger amount of strain energy, therefore the required energy input to recrystallize the material is less. This is evident from Figure 14, which shows the hardness curve vs annealing temperature for four separate levels of applied strain.

While the recrystallization temperature stays approximately the same for routes with the same level of applied strain, the ending hardness values and microstructure differ some. Route Bc has the smallest recrystallized grain size and corresponding hardness for reasons previously mentioned. Route C has the lowest recrystallized hardness, with routes A, B, and E having approximately the same recrystallized hardness. The grain size matches this trend, with route C having the largest recrystallized grain size and routes A, B, and E having similar recrystallized grain sizes.

Rolling as a post processing treatment after equal channel angular extrusion was shown to dramatically increase UTS as compared to the as-worked condition. In fact, the strongest 4A sample rolled to 69% reduction in thickness in the transverse plane along the X direction has an increase of 24% in UTS over the pure ECAE processed condition. It is possible that a UTS of well over 500 MPa could be accomplished by transverse or longitudinal rolling in the other ECAE processed samples. While the 69% reduction in thickness resulted in the largest strengths, the 10, 30, and 90% reduction in thickness all resulted in lower or equal strengths when compared to pure ECAE processing. This decrease in strength could possibly be due to a few different reasons. One is that due to rolling producing a very pronounced texture within the material, the low levels of rolling produce a material with “fighting” textures, effectively reducing strength. By rolling to a further reduction in thickness, the rolling texture overwhelms the ECAE produced texture and strength increases again. A second possibility is dynamic recrystallization within the material cause by the addition of rolling deformation. This phenomenon has been reported by other researchers in the past decade, where copper is reported to have

recrystallized at room temperature after rolling deformation [17,29,30,31]. Because rolling produces a non-isotropic grain structure compared to pure ECAE, the microstructure may be less stable and prone to recrystallization at room temperatures. This can also be the case during odd numbered passes as new shear band are formed, providing favourable sites for nucleation. However, if the grains stay equiaxed, the more common triple junction in the microstructure inhibits grain boundary migration, corresponding to a more stable structure. Therefore, the elongation of the grains from rolling deformation may reduce the number of triple junctions and lead to possible dynamic recovery. Grain size measurements after each rolling sequence are recommended in order to validate the claims of dynamic recovery.

The resistivity ratios of the different samples behaves very similarly to strength and hardness in that as applied strain increases, the resistivity increases. This is evident from the smaller and smaller resistivity ratios shown in Table 2. The reasons for the decrease in RRR is the inhibition of electron flow due to the increase in grain boundary and dislocation density. The more numerous grain boundaries and higher dislocation density scatter electrons as they flow through the material, leading to increased resistivity. The correlations illustrated in Figure 30 and Figure 31 clearly show the linear relationship between grain size and strength to RRR.

The resistivity at 77K and 4.2K ca be estimated by assuming a small drop in resistivity at room temperature. The room temperature resistivity of copper is known with large accuracy, and based on previous research we can assume that the maximum gain in resistivity at room temperature is 5% of the IACS value which is 1.71μΩcm.

Therefore samples that have strain greater than four are assumed to have a 5% gain in room temperature resistivity. Samples 1A and 2A are assumed to have a gain of 2% and 3% respectively. Now because we have a constant cross section, and the RRR and room temperature resistivity are known, the resistivity at 77K and 4.2K can be calculated. The results are shown in Table 8.

Table 8: Estimates of resistivity values at 4.2K and 77K

	RRR (273K/77K)	RRR (273K/4.2K)	Resistivity @77K (μΩcm)	Resistivity @4.2K (nΩcm)
AR	8.11	91.0	0.21	18.8
1A	6.96	51.6	0.25	33.8
2A	6.01	36.4	0.29	48.4
4A	6.23	30.8	0.29	58.3
8A	5.71	24.7	0.31	72.8
4Bc	5.92	24.5	0.30	73.2
8Bc	5.51	20.1	0.33	89.5
16Bc	5.53	19.2	0.32	93.5
4E	6.27	30.0	0.29	59.8
8E	6.37	27.3	0.28	65.9
16E	5.64	23.1	0.32	77.7
4B	6.04	26.5	0.30	67.8
8B	5.99	23.0	0.30	78.0
4C	6.12	31.2	0.29	57.5
8C	6.60	29.9	0.27	60.1

One objective of this research was to find the strongest most conductive material processing method. A figure of merit was chosen by multiplying the strength by the RR and RRR value to identify which material has the best performance. This value has been divided by 1000 for simplicities sake, and Table 9 lists the samples with the figure of

merit. Based on these results, it is evident that the as-received material has the highest merit value. This is due to its high RRR value. While strength only increases by about 1.8 times for the best case, the RRR value decreases by 4.75 times in certain cases. However, some situations need a higher strength than that of as-received material as a design consideration, and then the values for the fully processed materials have greater meaning. If this were the case it would be route 4E that would be the chosen candidate as it had the highest figure of merit value for fully worked samples. For the RR ratios, route 4E would be the best case, even including the as-received material. This is because the differences in resistivity are much less evident at 77K meaning that strength plays a heavier role.

Table 9: Figure of merit table for all ECAE processed samples

	Tensile Strength (MPa)	RR (273K/77K)	RRR (273K/4.2K)	Figure of Merit (RR*TS)	Figure of Merit (RRR*TS)
AR	248	8.11	91.0	2.01	22.6
1A	349	6.96	51.6	2.43	18.0
2A	383	6.01	36.4	2.30	13.9
4A	397	6.23	30.8	2.47	12.2
8A	404	5.71	24.7	2.31	10.0
4Bc	421	5.92	24.5	2.49	10.3
8Bc	437	5.51	20.1	2.41	8.80
16Bc	438	5.53	19.2	2.42	8.40
4E	438	6.27	30.0	2.74	13.1
8E	427	6.37	27.3	2.72	11.6
16E	413	5.64	23.1	2.33	9.50
4B	442	6.04	26.5	2.67	11.7
8B	437	5.99	23.0	2.62	10.1
4C	411	6.12	31.2	2.52	12.8
8C	411	6.60	29.9	2.71	12.3

5. SUMMARY, CONCLUSIONS, AND FUTURE WORK

In this study, oxygen free high conductivity (OFHC) copper was processed to varying levels of strain using a severe plastic deformation (SPD) process known as equal channel angular extrusion (ECAE). Material properties such as yield and tensile strength, hardness, electrical resistivity, and microstructure characteristics were evaluated for as-received materials and ECAE routes 1A, 2A, 4A, 8A, 4B, 8B, 4Bc, 8Bc, 16Bc, 4C, 8C, 4E, 8E, and 16E. Additionally, samples were recrystallized to determine recrystallized microstructure and hardness, strength, and in some cases recrystallization temperature . In addition to recrystallization, some selected as-worked materials were rolled to determine the effect of post processing deformation. The main findings of this testing are listed below:

- Hardness and press load reach saturation at 3-4 ECAE passes
- Processing past four passes results in only small incremental increases in strength
- Recrystallization temperature decrease with applied strain
- Vickers hardness is an effective method to measure recrystallization temperature
- Route Bc produced the smallest as-worked and recrystallized grains of studied routes
- Residual resistivity ratios decrease linearly with increasing strength and decreasing grain size

From these findings, we draw these conclusions:

- Post processing rolling has the possibility to achieve tensile strengths above 500MPa
- Processing up to four passes gives the greatest effort to benefit ratio in terms of increased properties and processing requirements
- For producing low resistivity high strength materials, a low number of passes give the best figure of merit when strength and resistivity are equally weighted

Possible future work could include strength and RRR testing of the recrystallized samples to determine if a post processing heat treatment would increase the figure of merit value to possibly above that of the as-received value. It would also enable determination of the resistivity produced from grain boundaries. Because recrystallization should decrease the dislocation density to the level of the annealed starting material, yet keep the grain size much smaller than the annealed value, the fraction of the resistivity that can be attributed to the grain boundaries could be calculated by comparing the recrystallized, as-worked, and annealed material.

Other future work could include RRR testing of the rolled samples to see how much rolling impacted the resistivity. Additional rolling of other ECAE processed samples could possibly lead to strengths exceeding 500MPa, if results follow the same trend as seen in this study. Future characterization should also include determining the dislocation density, as its impact on resistivity may be substantial.

Because superconductors operate at cryogenic temperatures, material properties at this temperature would be very valuable. Therefore mechanical tests such as hardness and tensile tests run at both 77K and 4.2K are suggested, allowing the determination of yield and tensile strength, as well as other properties.

REFERENCES

[1] Dartmouth Toxic Metals Superfund Research Program, "Copper: An Ancient Metal," 2010.

[2] Jeff Doebrich, "Copper—A Metal for the Ages," 2009.

[3] Annie Hwang, Glenn J. Wallace Mark Brininstool, "2014 Minerals Yearbook," 2016.

[4] V.M. Segal, "Material processing by simple shear," *Materials Science and Engineering A*, pp. 157-164, 1995.

[5] Ayan Bhowmik, Somjeet Biswas Satyam Suwas, "Ultra-fine Grain Materials by Severe Plastic Deformation: Application to Steels,"*Microstructure and Texture in Steels*., 2009, pp. 325-344.

[6] V.M. Segal, F.Alford, J. Kardokus, S. S. Ferrasse, "Scale up and application of equal-channel angular extrusion for the electronics and aerospace industries," *Materials Science and Engineering A*, pp. 130-140, 2008.

[7] Robert W. Messler, Rajiv Asthana, Edward P. Furlani, R. E. Smallman, A.H.W. Ngan, Roy J. Crawford, Nigel Mills Michael F. Ashby, *Engineering Materials and Processes*.: Butterworth-Heinemann, 2009.

[8] R.K. Islamgaliev, I.V. Alexandrov R.Z. Valiev, "Bulk nanostructured materials from severe plastic deformation," *Progress in Materials Science*, vol. 45, pp. 103-189, 2000.

[9] Guney Guven Yapici, "Investigation and modeling of processing-microstructure-property relations in ultra-fine grained hexagonal close packed materials under strain path changes," 2007.

[10] V.M. Segal, "Engineering and commercialization of equal channel angular extrusion (ECAE)," *Materials Science and Engineering A*, pp. 269-276, 2004.

[11] K.T. Hartwig, R. Goforth V.M. Segal, "In Situ Composites Processed by Simple Shear," *Materials Science and Engineering A*, pp. 107-115, 1997.

[12] Wenquan Q. Cao, Christopher H.J. Davies, E V. Pereloma Azdiar A. Gazder, "An EBSD investigation of interstitial-free steel subjected to equal channel angular extrusion," 2008.

[13] V.Y. Gertsman, R.Z. Valie, G. Gottstein O.V. Mishin, "Grain boundary distribution and texture in ultra-fine grained copper produced by severe plastic deformation," *Scripta Materialia*, vol. 35, pp. 873-878, 1996.

[14] N. Hansen D. A. Hughes, "High angle boundaries formed by grain subdivision mechanisms," *Acta Metallurgica*, vol. 45, pp. 3871-3886, 1997.

[15] V.M. Segal, F. Alford S. Ferrasse, "Effect of additional processing on texture evolution of Al0.5Cu alloy processed by equal channel angular extrusion (ECAE)," *Materials Science and Engineering A*, vol. 372, pp. 44-55, 2004.

[16] Yuntian Theodore Zhu Michael J. Zehetbauer, *Bulk Nanostructured Materials*.: John Wiley & Sons, 2009.

[17] G. Gottstein O. V. Mishin, "Microstructural aspects of rolling deformation in ultrafine-grained copper," *Philosophical Magazine A*, vol. 78, pp. 373-388, 1998.

[18] Ruslan Z. Valiev Terry Lowe, *Investigations and Applications of Severe Plastic Deformation.*: NATO Science Series, 2000.

[19] Dong-Ik Kim Satyam Suwas, "Annealing texture of ECAE processed Copper ," *Materials Science Forum*, vol. 558, pp. 1353-1358, 2007.

[20] Samuel T. Adedokun, "A Review on Equal Channel Angular Extrusion as a Deformation and Grain Refinement Process," *Journal of Emerging Trends in Engineering and Applied Sciences*, vol. 2, pp. 360-363, 2011.

[21] M. Ebrahimi F. Djavanroodi, "Effect of die parameters and material properties in ECAP with parallel channels," *Materials Science and Engineering A*, vol. 527, pp. 7593-7599, 2010.

[22] Y., Wang, J., Horita, Z., Nemoto, M., and Iwahashi, "Principle of equal-channel angular pressing for the processing of ultra-fine grained materials," *Scripta Materialia*, vol. 35, pp. 143-146, 1996.

[23] R. Lapovok, J. Sandlin, P.F. Thomson, C.H.J. Davies, E.V. Pereloma F. Dalla Torre, "Microstructures and properties of copper processed by equal channel angular extrusion for 1–16 passes," *Acta Materialia*, vol. 52, pp. 4818-4832, 2004.

[24] D. Solas, T. Baudin, R. Penelle A.L. Etter, "Evolution of microstructure and texture during annealing of a copper processed by ECAE," *Materials Science Forum*, vol. 495-497, pp. 845-850, 2005.

[25] T. Baudin, C. Rey, R. Penelle A.L. Etter, "Microstructural and textural characterization of copper processed by ECAE," *Materials Characterization*, vol. 56, pp. 19-25, 2006.

[26] Mohammed Haouaoui, "An investigation of bulk nanocrystalline copper fabricated via severe plastic deformation and nanoparticle consolidation.," 2005.

[27] Azdiar A. Gazder, Cheng F. Gu, Christopher H.J. Davies, E V. Pereloma Florian H. Dalla Torre, "Grain size, misorientation, and texture evolution of copper processed by equal channel angular extrusion and the validity of the Hall-Petch relationship," *Metallurgical and Materials Transactions A* , vol. 38, pp. 1080-1095, 2007.

[28] Jianwei Li, Debin Shan, Bin Guo Jie Xu, "Microstructural evolution and micro/meso-deformation behavior in pure copper processed by equal-channel angular pressing," *Materials Science & Engineering A*, vol. 664, pp. 114-125, 2016.

[29] S S Hazra, C F Gu, W Q Cao, C H J Davies, E V Pereloma A A Gazder, "Mechanical, microstructure and texture properties of interstitial-free steel and copper subjected to equal channel angular extrusion and cold-rolling," *Journal of Physics: Conference Series 240*, 2010.

[30] J. Kusnierz, "Rolling Texture of ECAP Processed Al and Cu," *Solid State Phenomena*, vol. 105, pp. 339-344, 2005.

[31] W. Baliga, J Boguka J. Kusnierz, "Effect of pre-deformation by ECAE pressing on shear banding and texture of cold rolled copper," *Applied Crystallography*, pp. 181-184, 2004.

[32] J.B. Dubois, P. Olier, L. Thilly, F. Lecouturier, P.O. Renault E. Buet, "Microstructure and texture of copper/niobium composites processed by ECAE," *International Journal of Material Forming*, vol. 3, pp. 1071-1074, 2010.

[33] Iaroslava Shakhova, Andrey Belyakov, Rustam Kaibyshev, Terence G. Langdon Alexander P. Zhilyaev, "Wear resistance and electroconductivity in copper processed by severe plastic deformation," *Wear*, vol. 305, pp. 89-99, 2013.

[34] Mouhamed Khitouni, Nabil Njah Rakia Daly, "Microstructural and mechanical properties of copper processed by equal channel angular extrusion," Sfax, 2008.

[35] D. Dolas, A.L. Etter, T. Baudin, R. Penelle Z. Guo, "Microstructural changes in copper processed by Equal Channel Angular Extrusion and static annealing," *Materials Science Forum*, vol. 426-432, pp. 2723-2728, 2003.

[36] S.D. Wu, L. Zuo, C. Esling, Z.G. Wang, G.Y. Li G. Wang, "Microstructure, texture, grain boundaries in recrystallization regions in pure Cu ECAE samples," *Materials Science and Engineering A*, vol. 346, pp. 83-90, 2003.

[37] J. Nutting I. Saunders, "Deformation of metals to high strains using combination of torsion and compression," *Metal Science*, vol. 18, pp. 571-576, 1984.

[38] N.P. Kobelev, P.R. Mulyukov, Ya.M. Soifer, N.A. Akhmadeev, "The effect of heat treatment on the elastic and dissipative properties of copper with the

submicrocrystalline structure," *Acta Metallurgica Materialia*, vol. 41, pp. 1041-1046, 1993.

[39] Victor Spuskanyuk, Victor Varyukhin Oleksandr Davydenkoa, "Production a High-Strength and High-Conductivity Copper Wire by Using Equal-Channel Angular Hydroextrusion Method ," *Materials Science Forum*, vol. 67-699, pp. 909-913, 2010.

[40] J.M. Cabrera O.F. Higuera-Cobos, "Mechanical, microstructural and electrical evolution of commercially pure copper processed by equal channel angular extrusion," *Materials Science & Engineering A*, vol. 571, pp. 103-114, 2013.

APPENDIX A

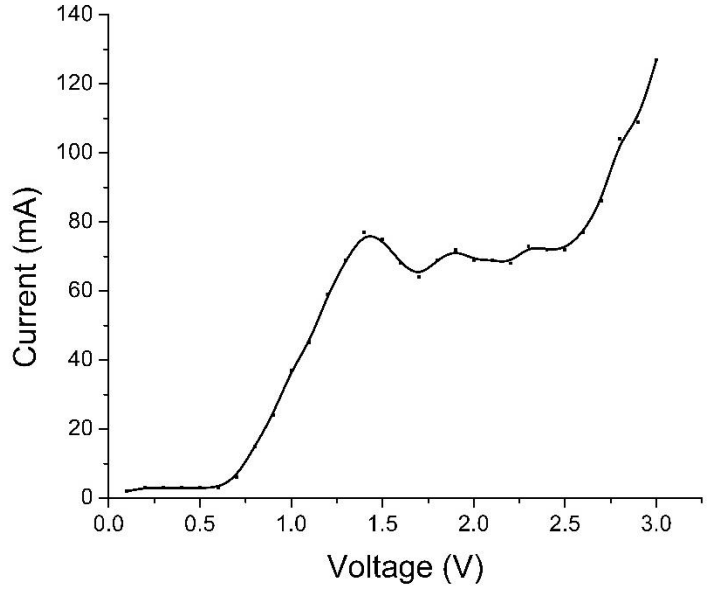

Figure 32: Voltage current sweep for electrolytic polishing

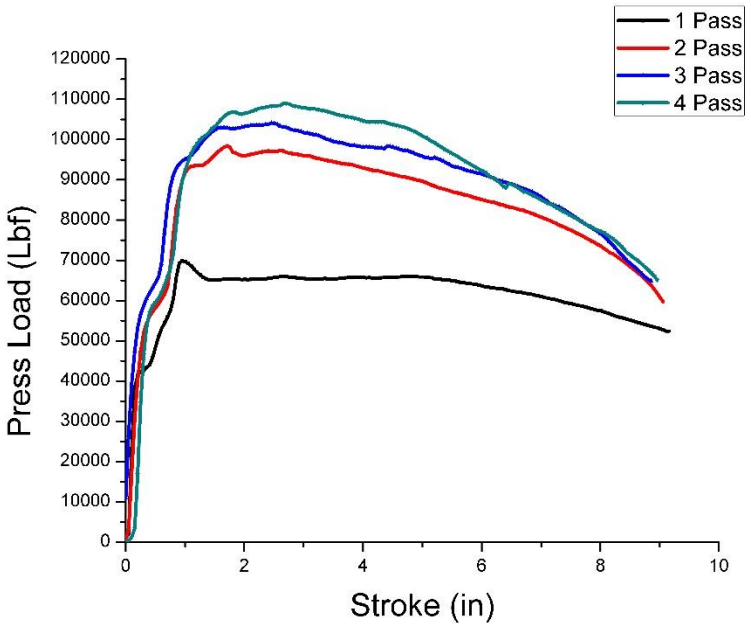

Figure 33: Press load for route 4A

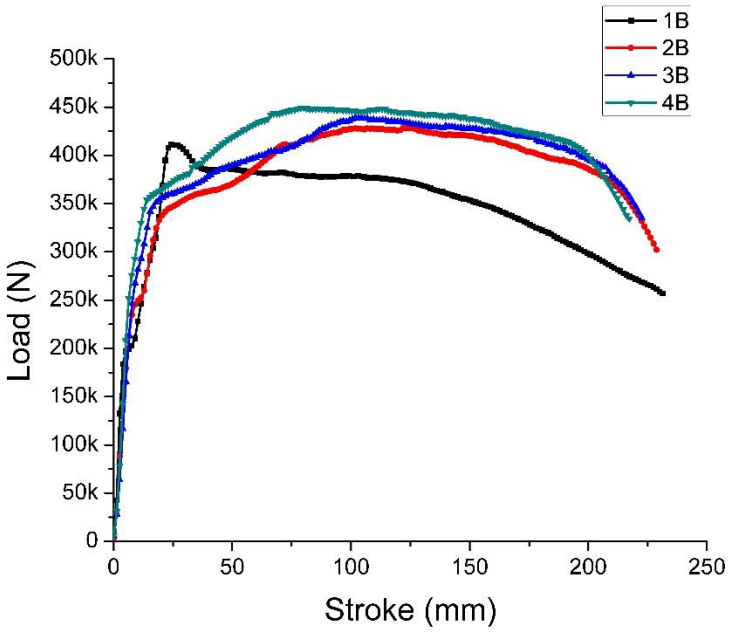

Figure 34: Press load for route 4B

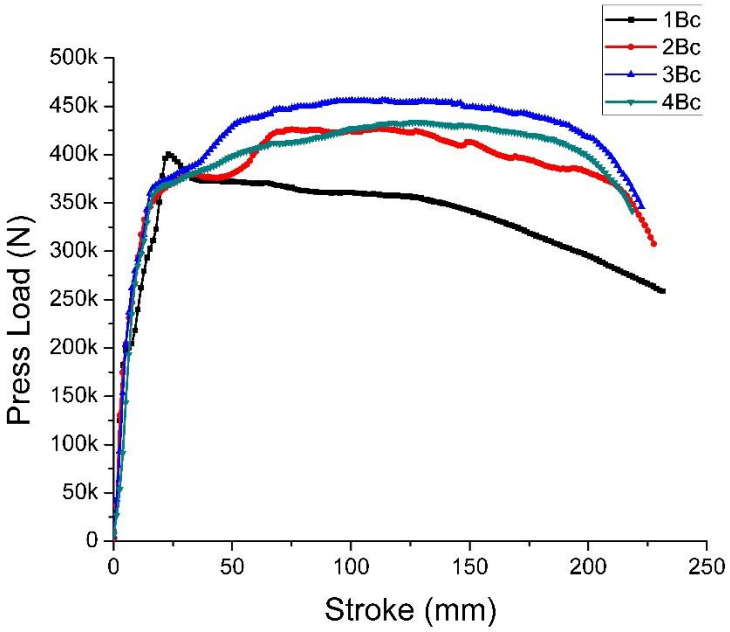

Figure 35: Press load for route 4Bc

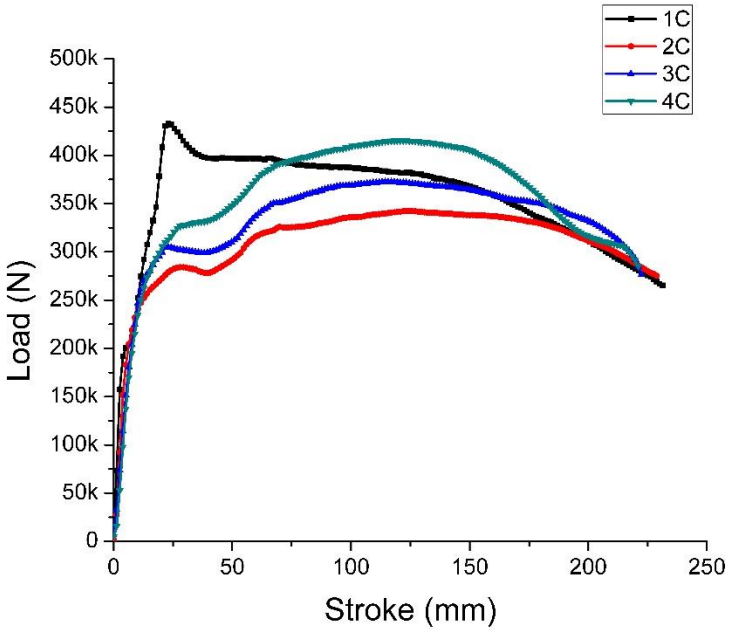

Figure 36: Press load for route 4C

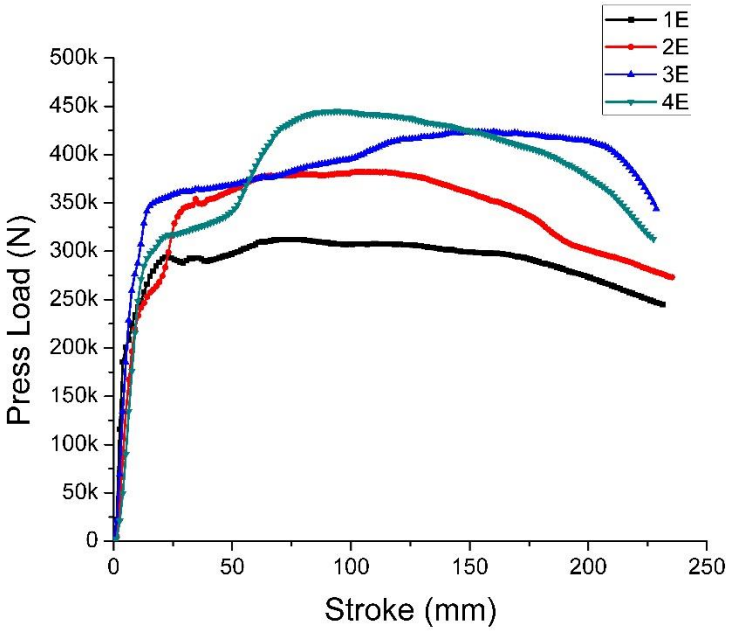

Figure 37: Press load for route 4E

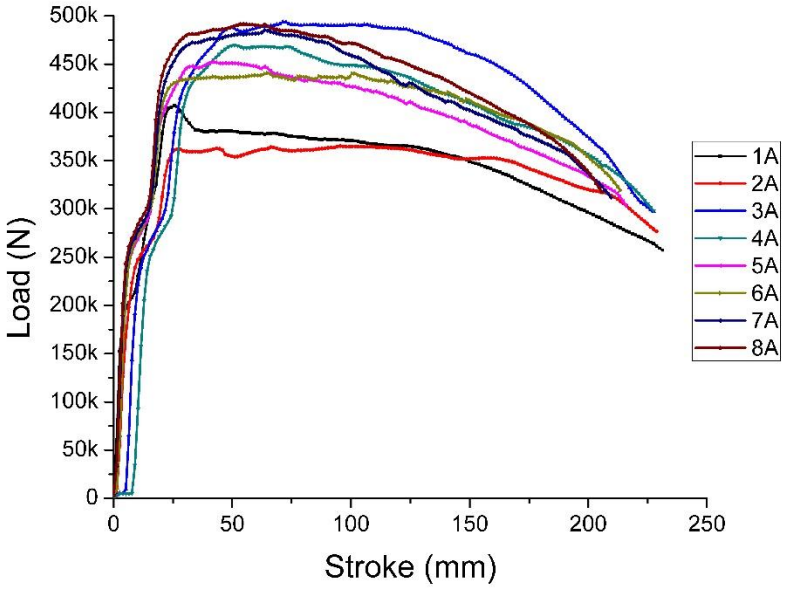

Figure 38: Press load for route 8A

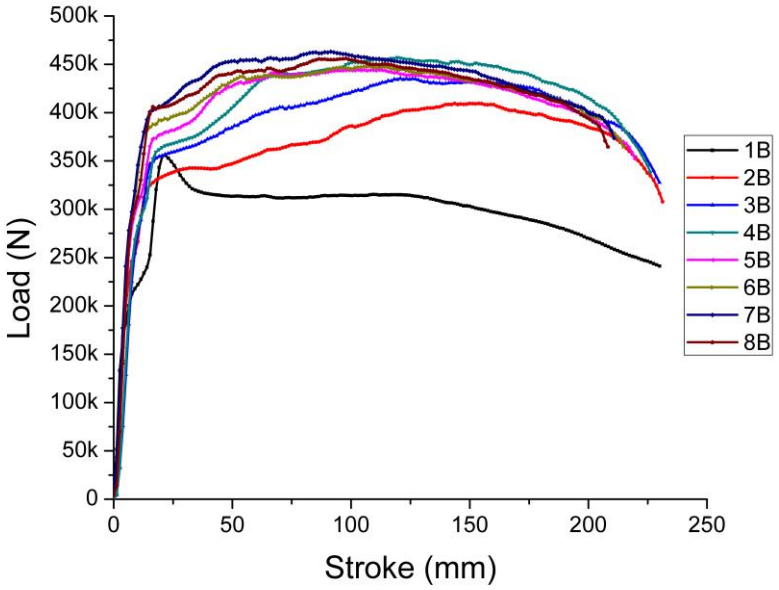

Figure 39: Press Load for route 8B

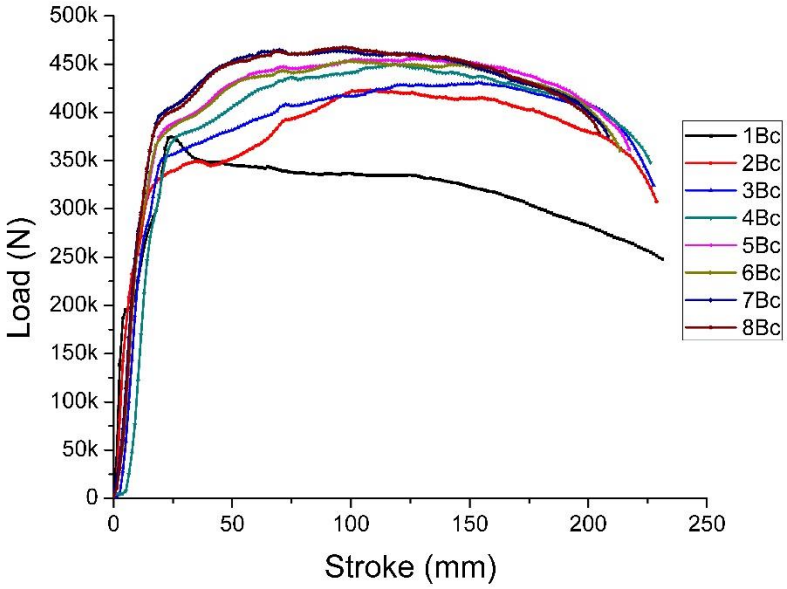

Figure 40: Press load for route 8Bc

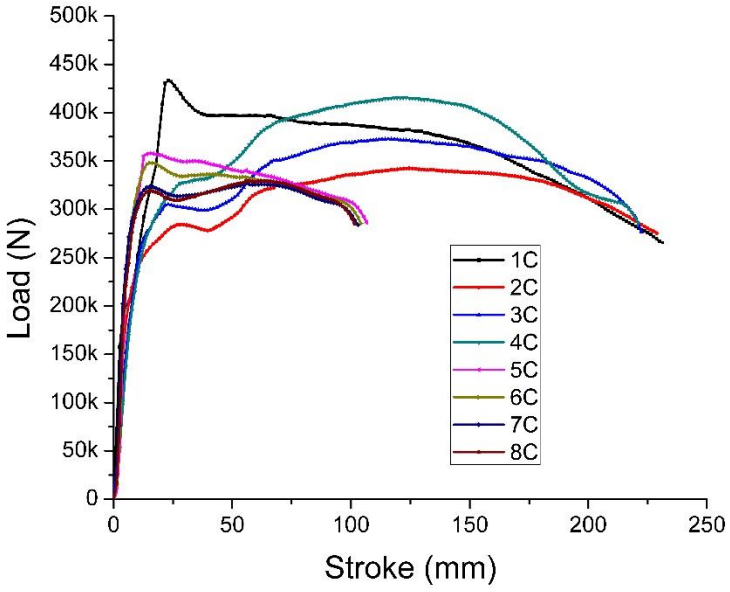

Figure 41: Press load for route 8C

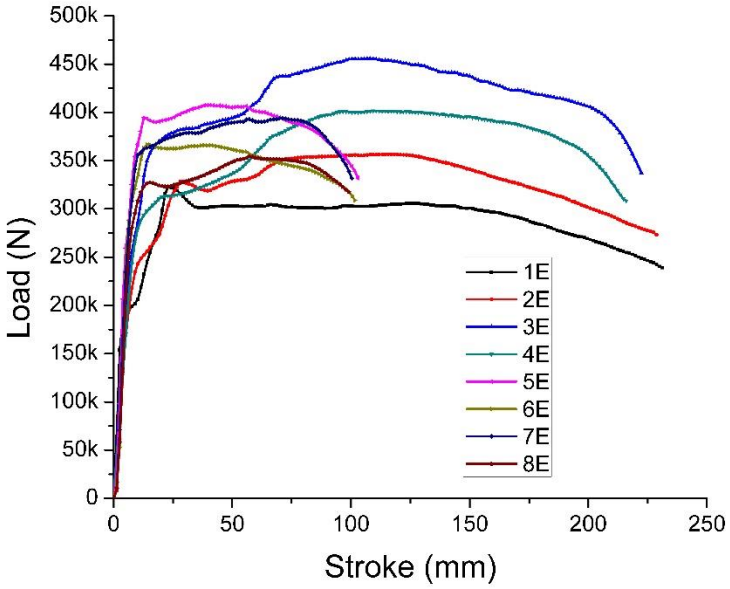

Figure 42: Press load for route 8E

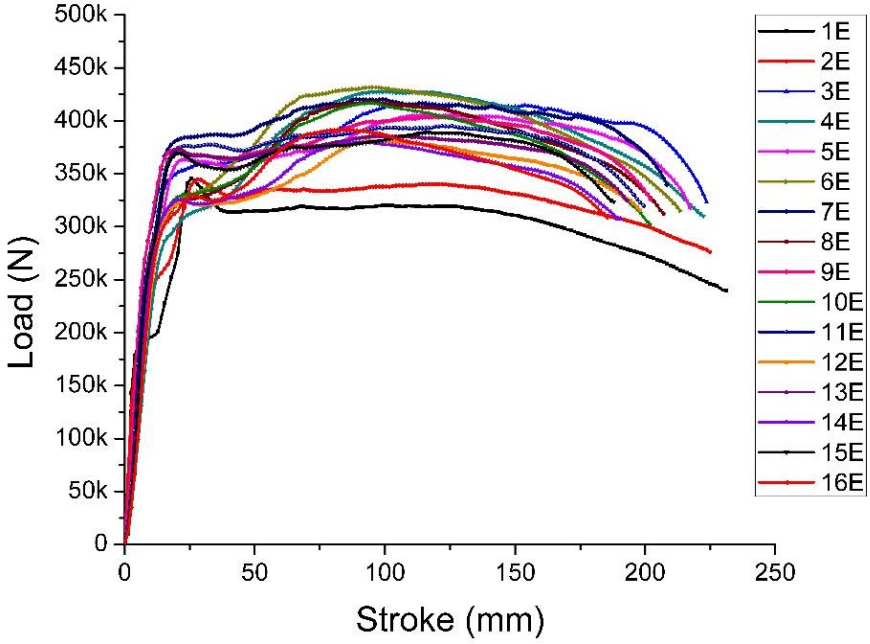

Figure 43: Press load for route 16E

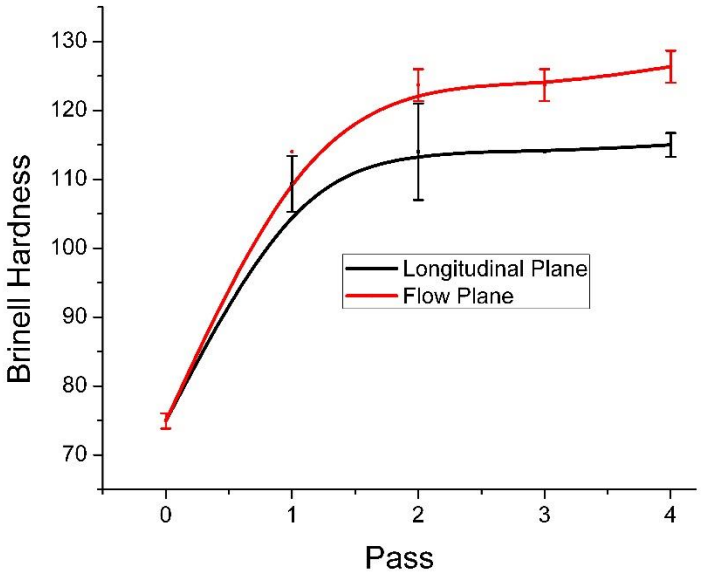

Figure 44: Brinell Hardness for route 4A

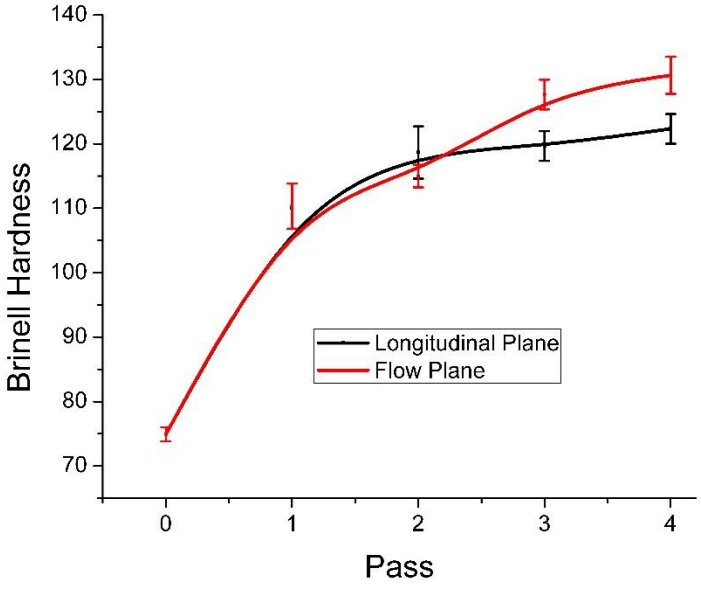

Figure 45: Brinell Hardness for route 4B

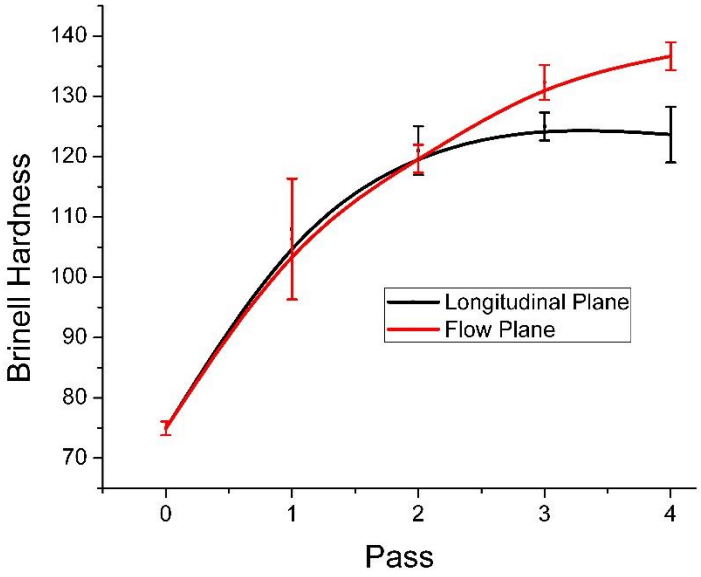

Figure 46: Brinell Hardness for route 4Bc

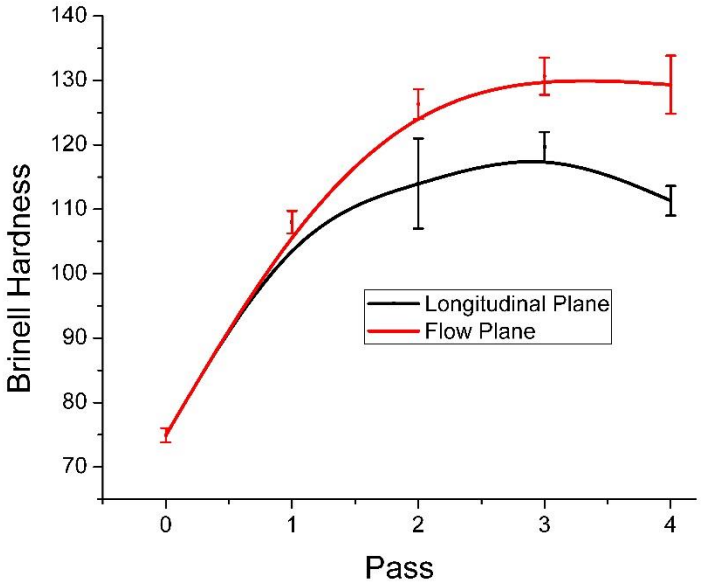

Figure 47: Brinell Hardness for route 4C

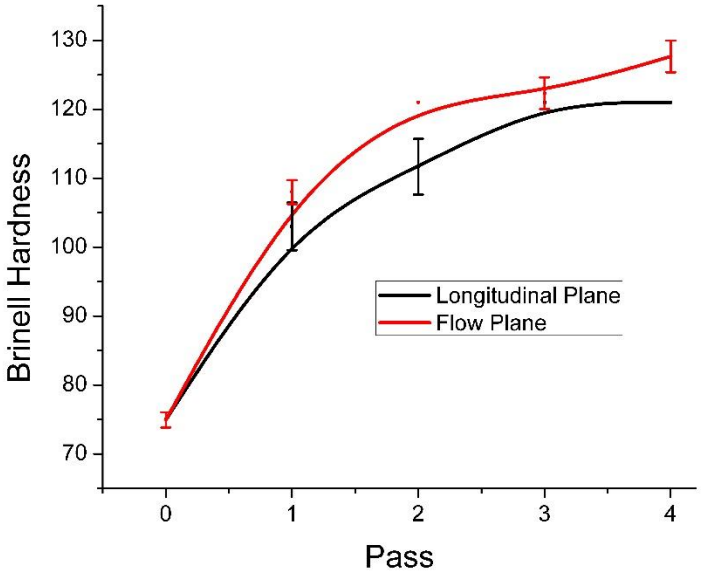

Figure 48: Brinell Hardness for route 4E

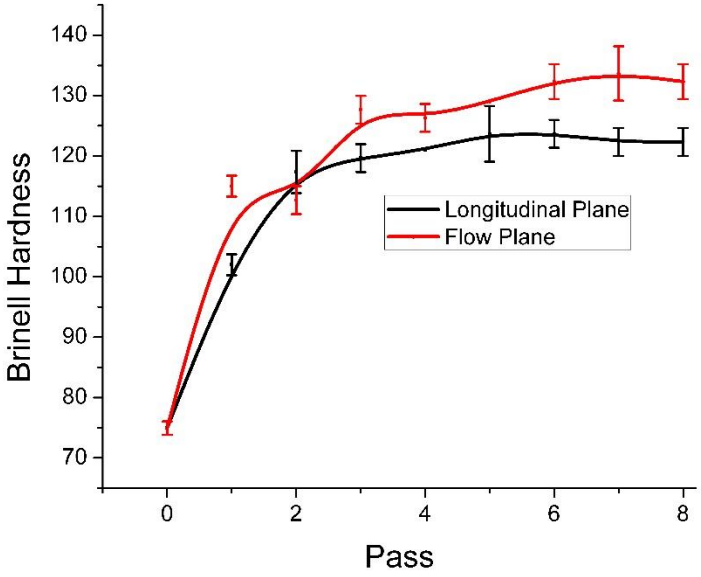

Figure 49: Brinell Hardness for route 8B

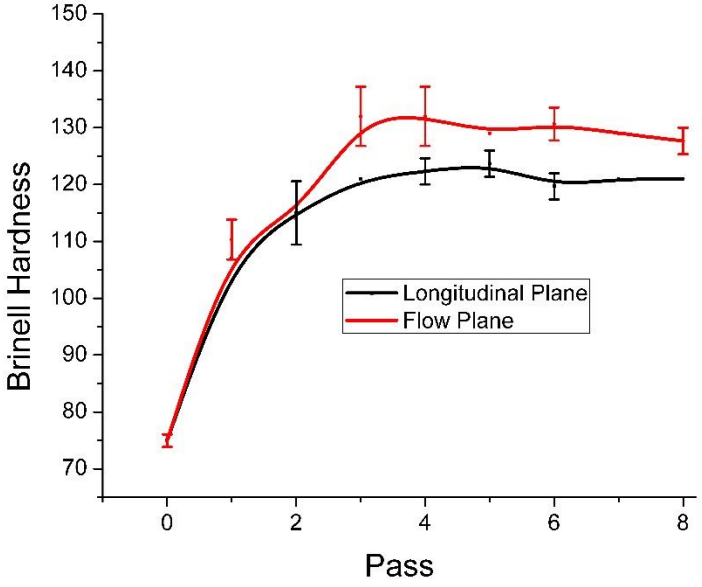

Figure 50: Brinell Hardness for route 8Bc

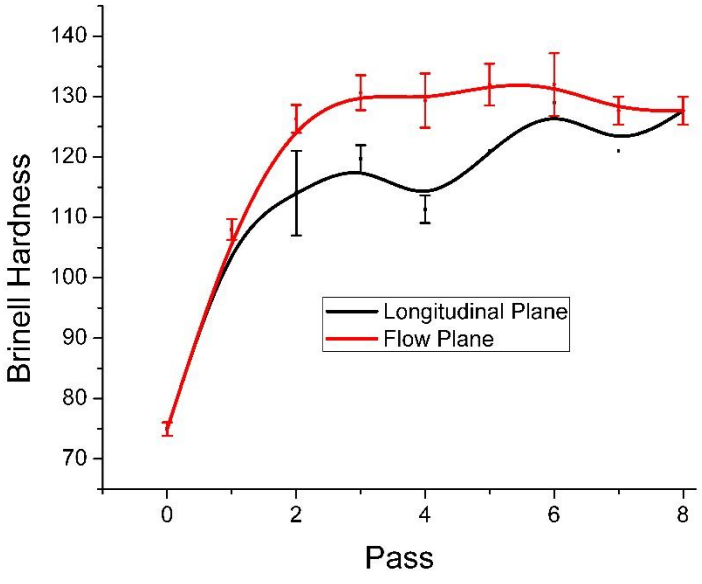

Figure 51: Brinell Hardness for route 8C

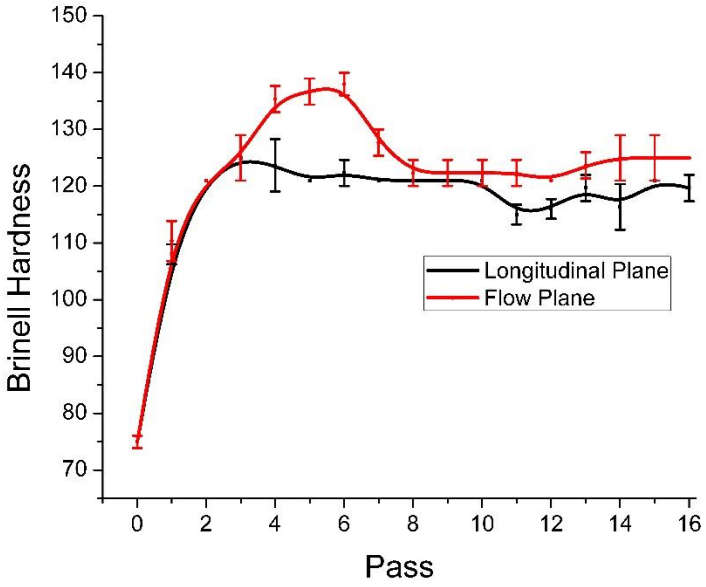

Figure 52: Brinell Hardness for route 16Bc

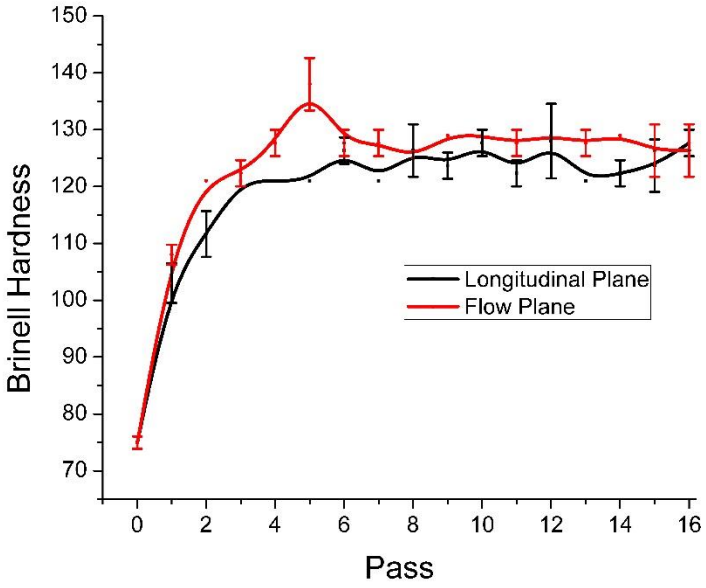

Figure 53: Brinell Hardness for route 16E

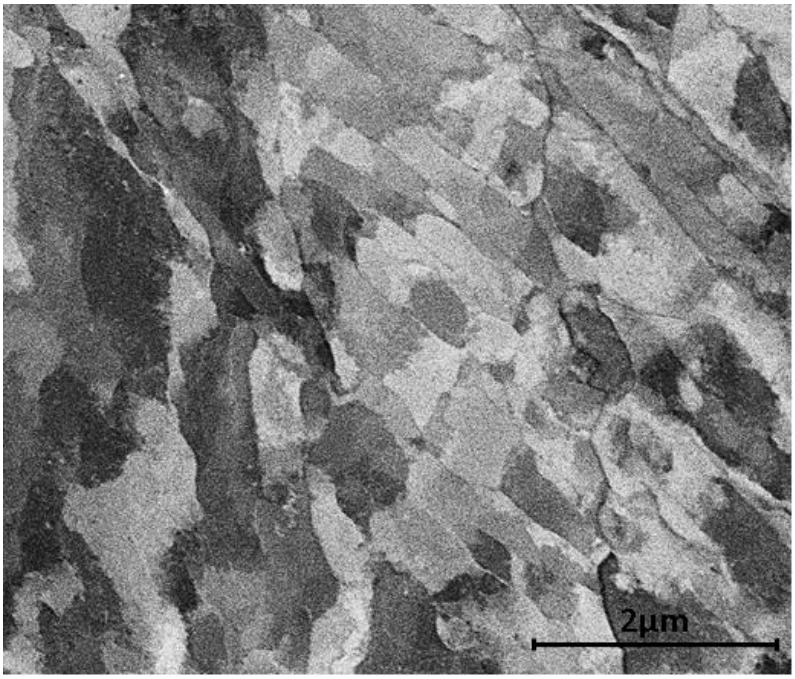

Figure 54: Microscopy of as-worked 1A sample

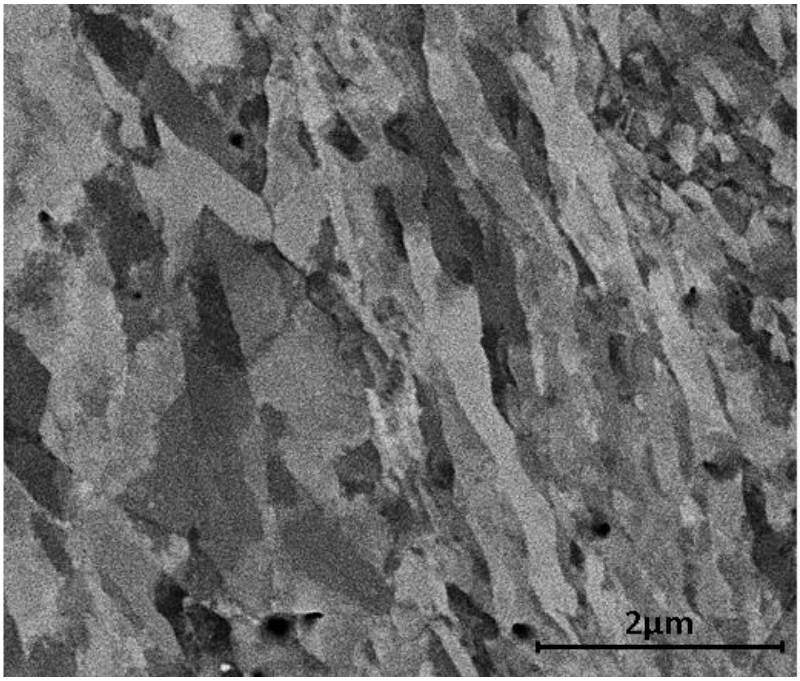

Figure 55: Microscopy of as-worked 2A sample

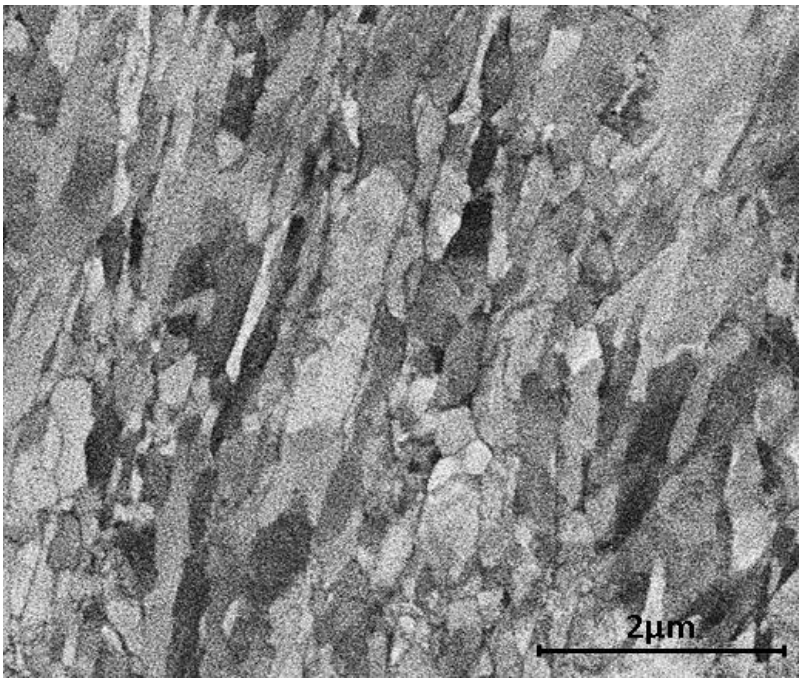

Figure 56: Microscopy of as-worked 4A sample

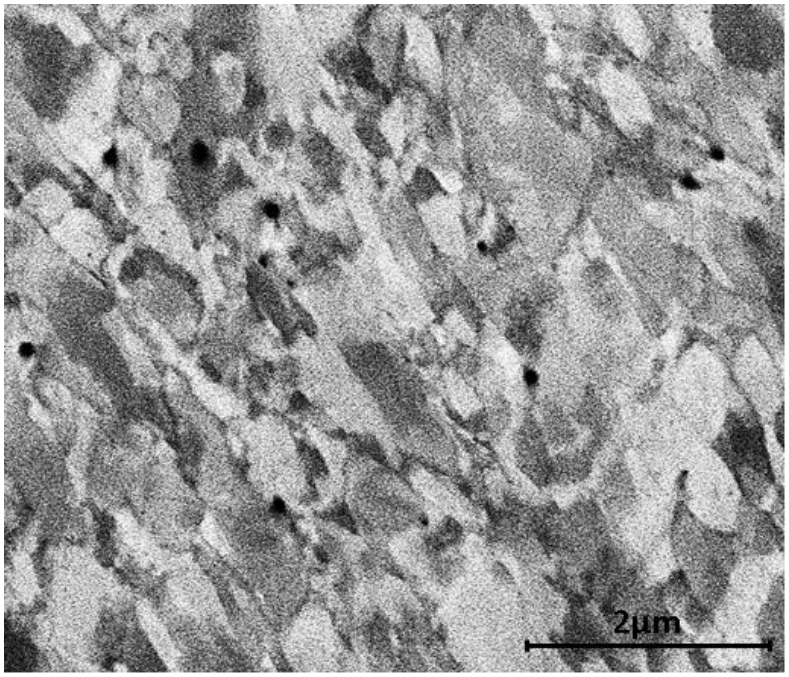

Figure 57: Microscopy of as-worked 4B sample

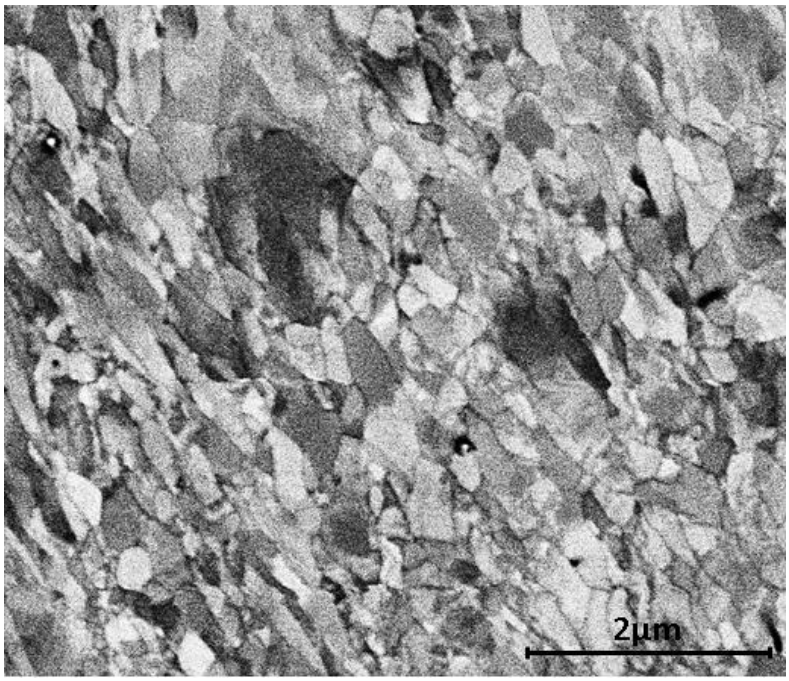

Figure 58: Microscopy of as-worked 4Bc sample

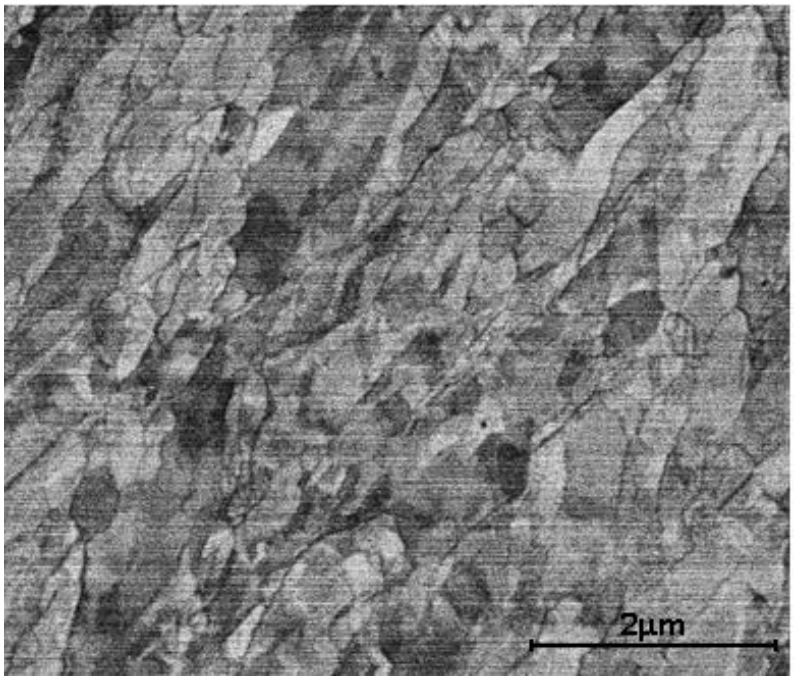

Figure 59: Microscopy of as-worked 4C sample

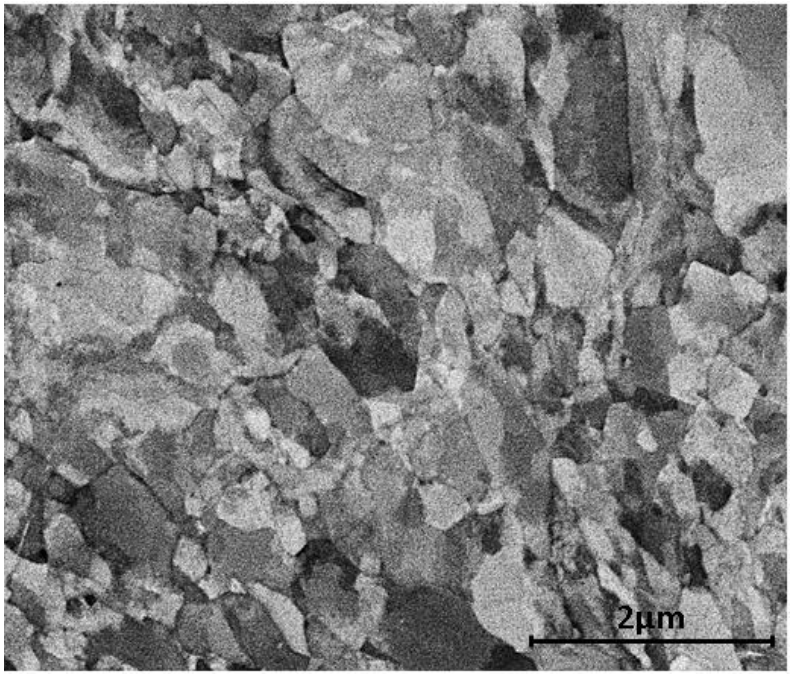

Figure 60: Microscopy of as-worked 4E sample

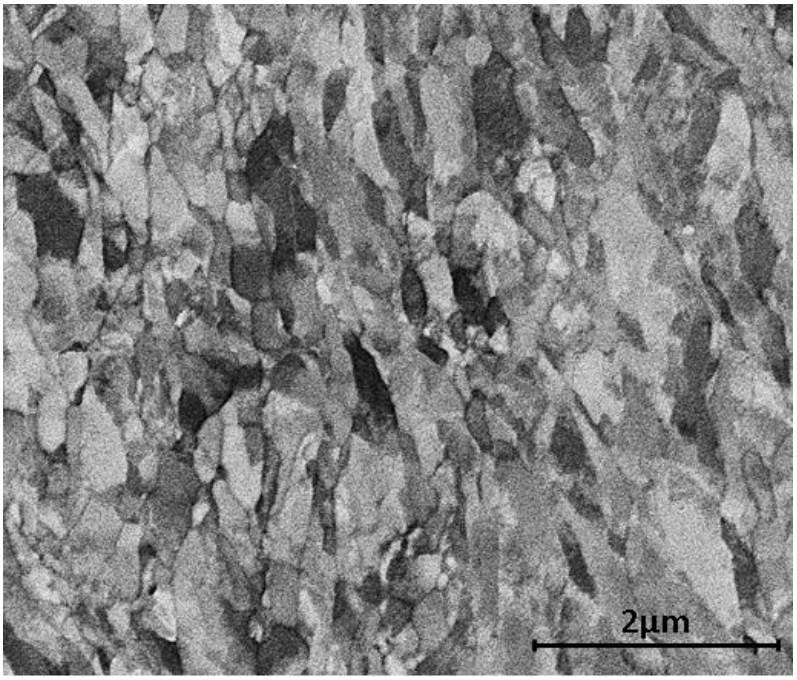

Figure 61: Microscopy of as-worked 8A sample

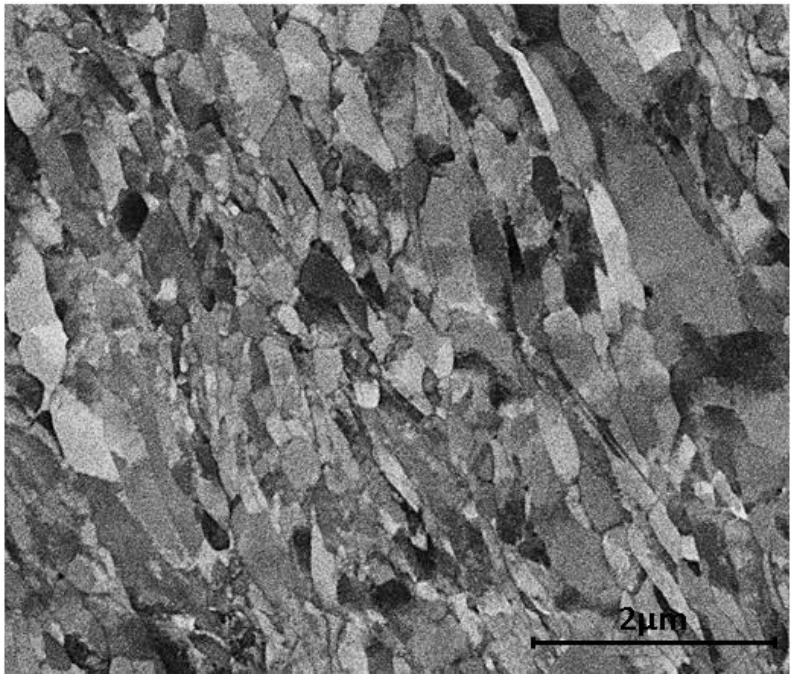

Figure 62: Microscopy of as-worked 8B sample

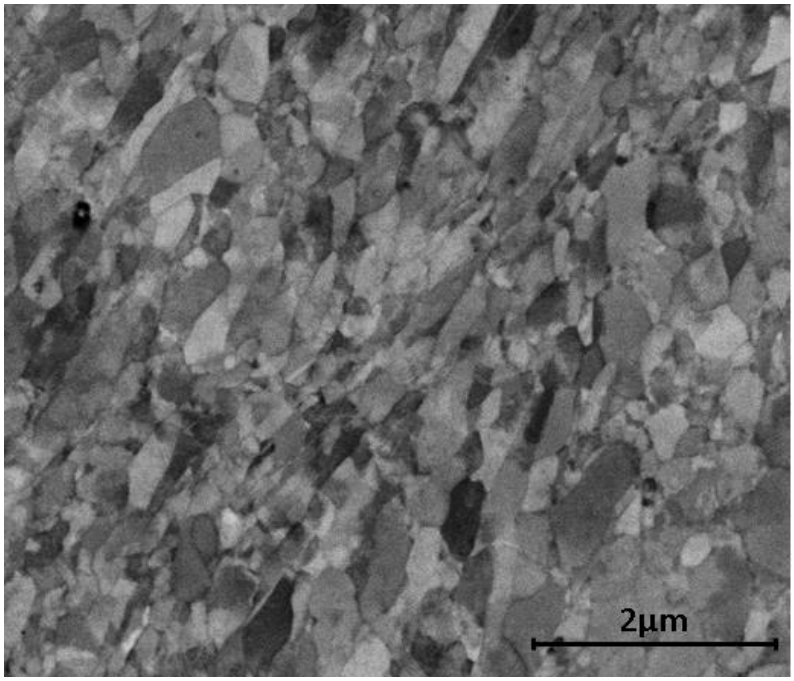

Figure 63: Microscopy of as-worked 8Bc sample

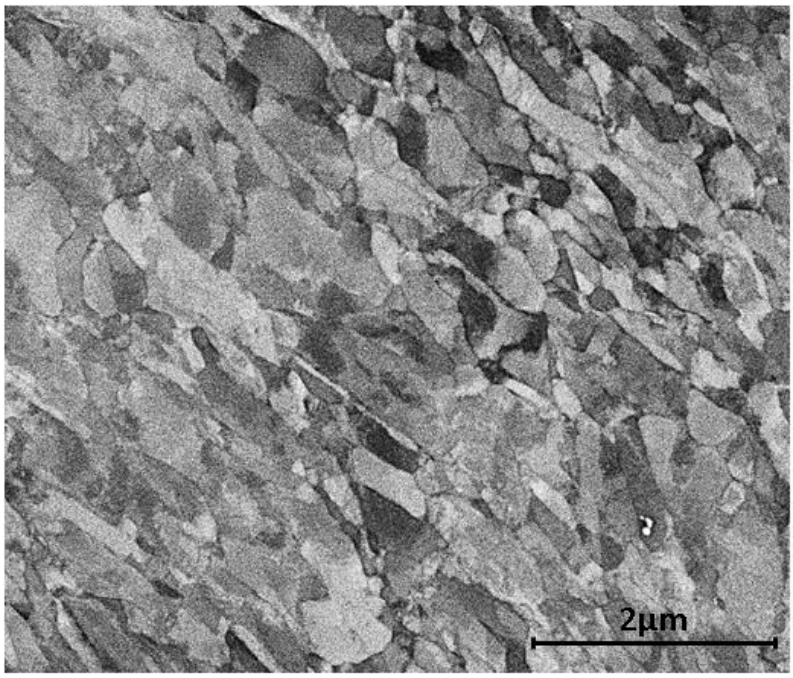

Figure 64: Microscopy of as-worked 8C sample

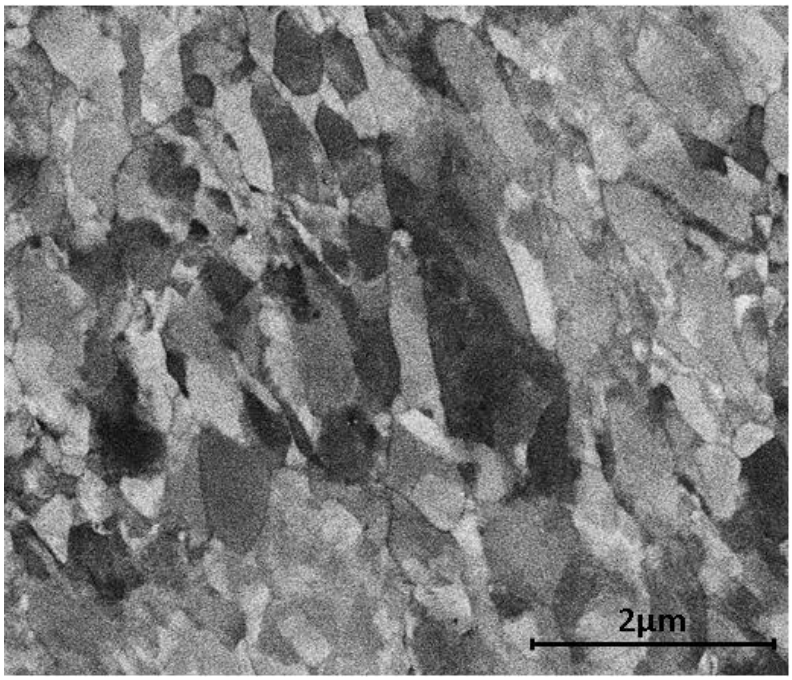

Figure 65: Microscopy of as-worked 8E sample

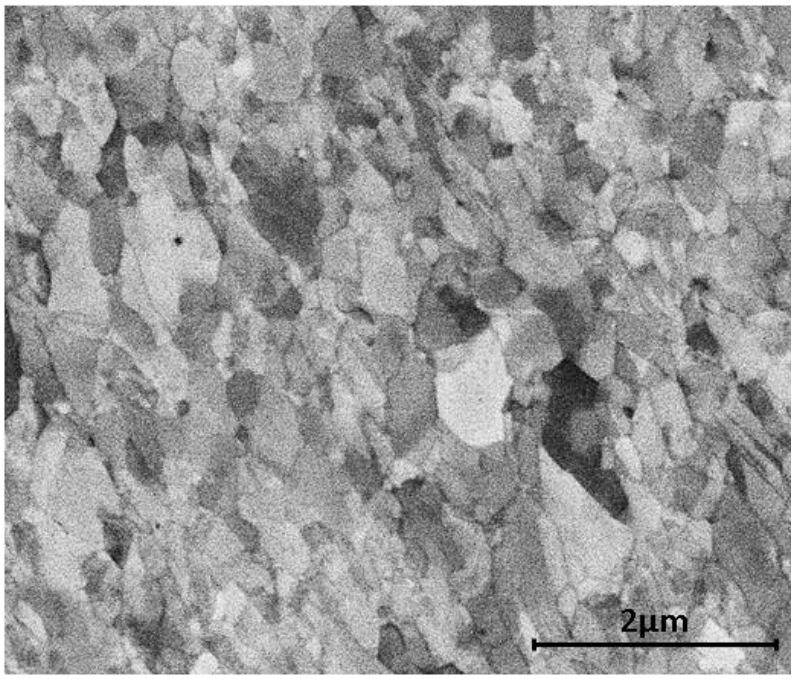

Figure 66: Microscopy of as-worked 16Bc sample

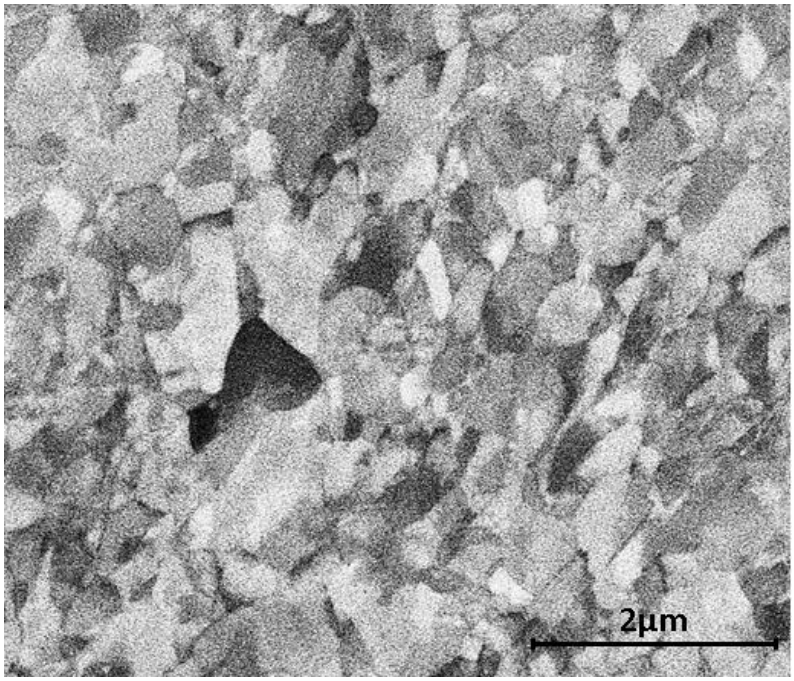

Figure 67: Microscopy of as-worked 16E sample

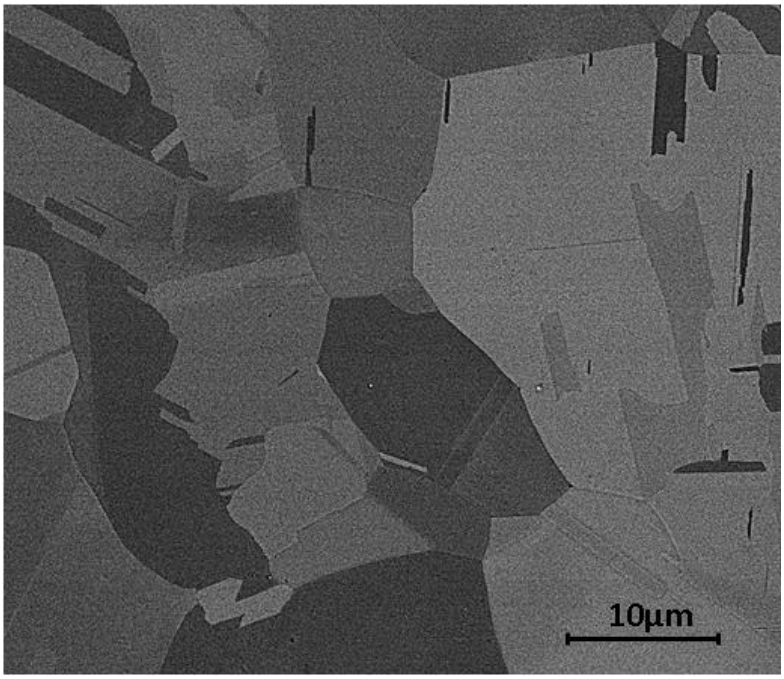

Figure 68: Microscopy of recrystallized 1A sample

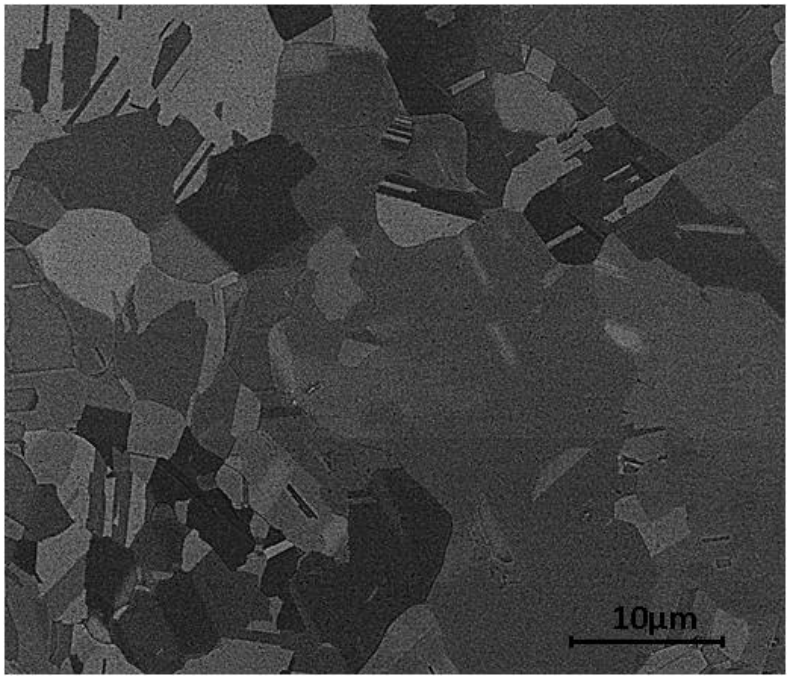

Figure 69: Microscopy of recrystallized 2A sample

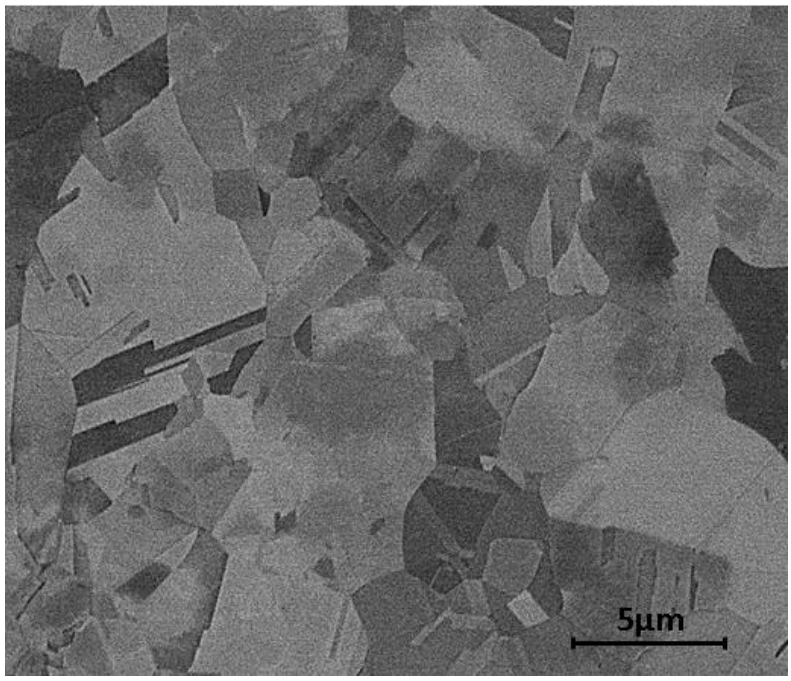

Figure 70: Microscopy of recrystallized 4A sample

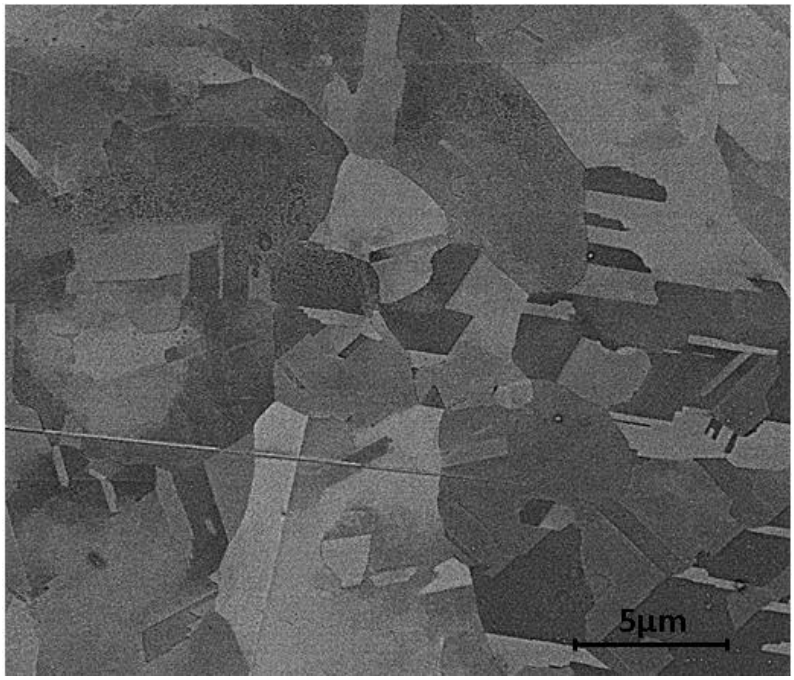

Figure 71: Microscopy of recrystallized 4B sample

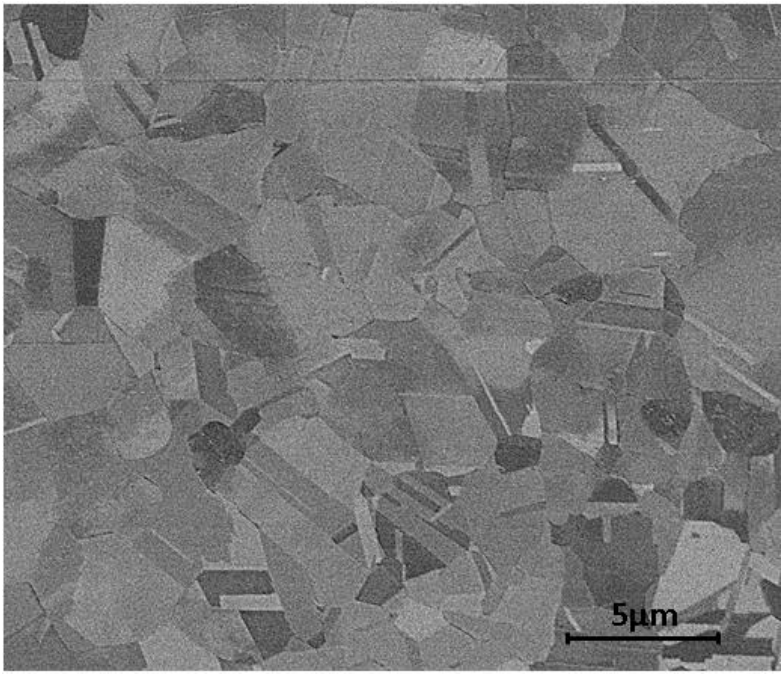

Figure 72: Microscopy of recrystallized 4Bc sample

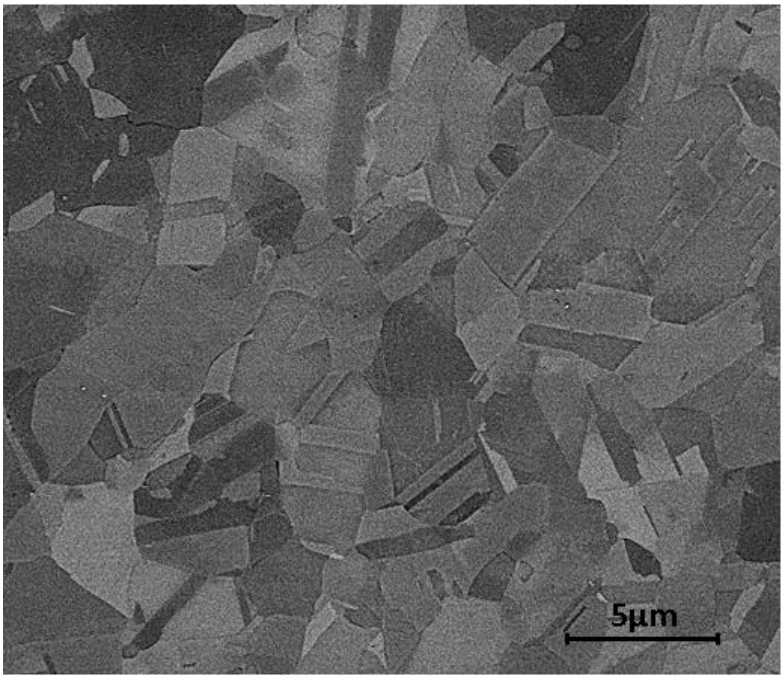

Figure 73: Microscopy of recrystallized 4C sample

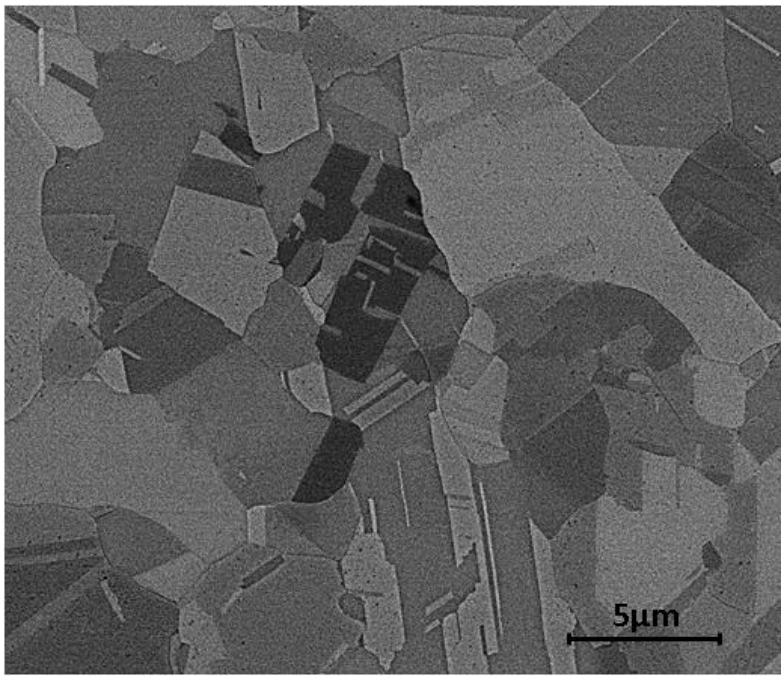

Figure 74: Microscopy of recrystallized 4E sample

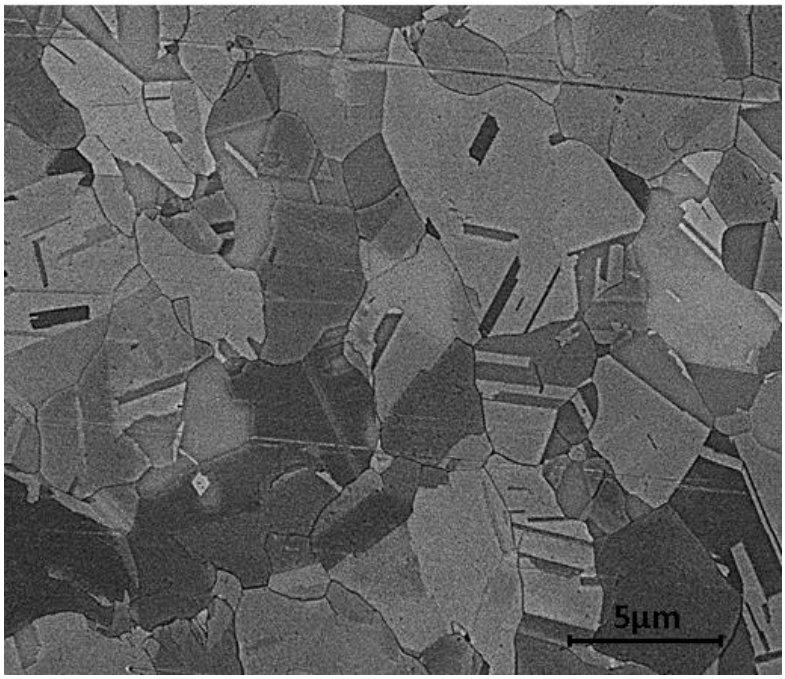

Figure 75: Microscopy of recrystallized 8A sample

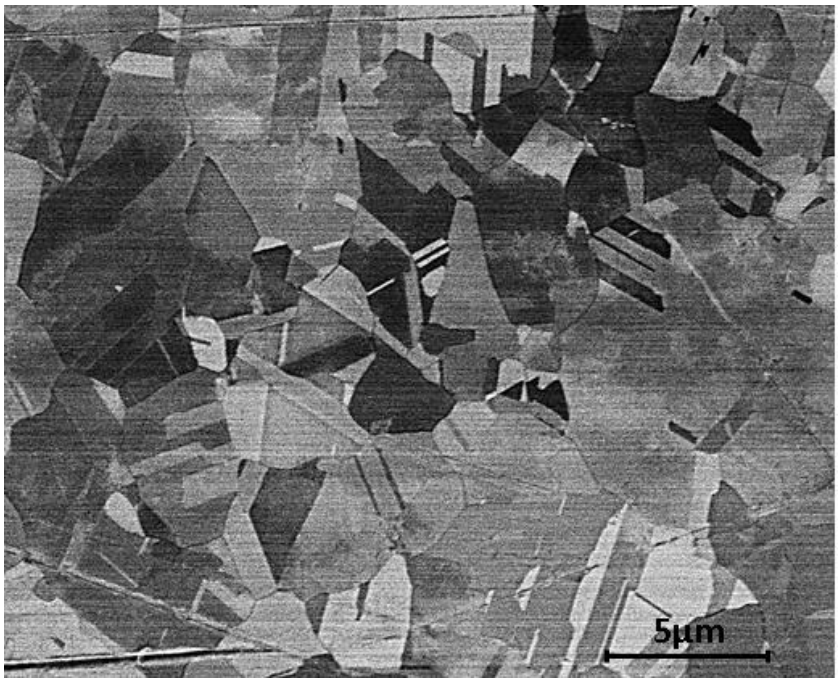

Figure 76: Microscopy of recrystallized 8B sample

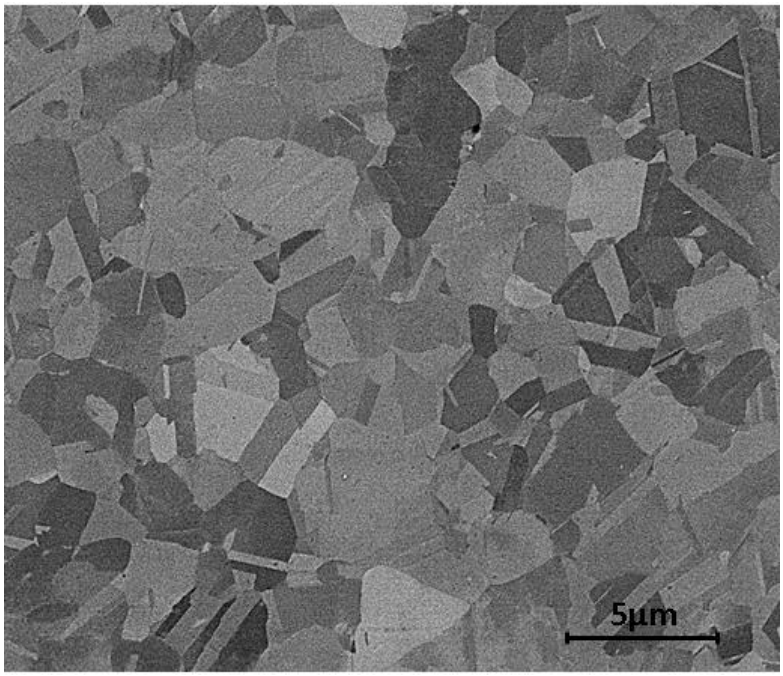

Figure 77: Microscopy of recrystallized 8Bc sample

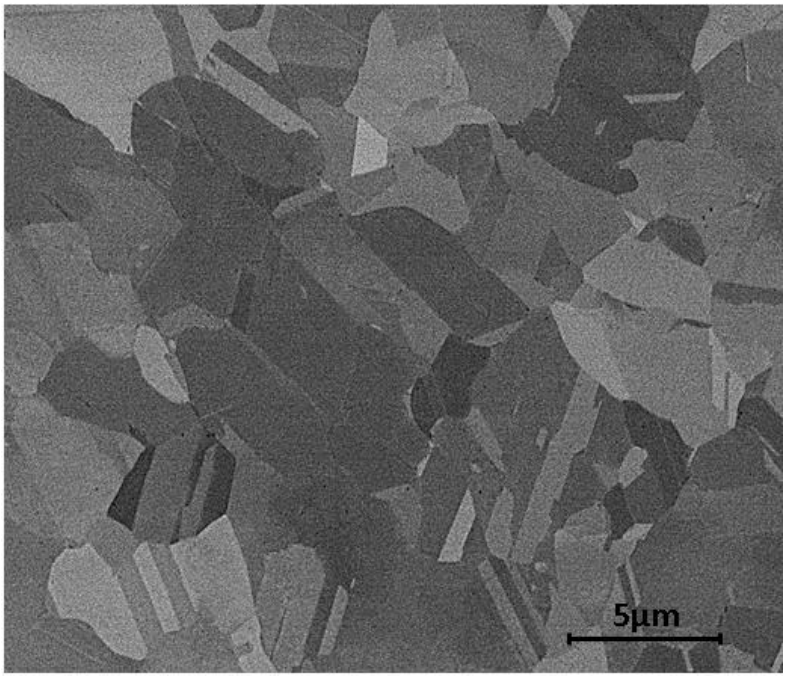

Figure 78: Microscopy of recrystallized 8C sample

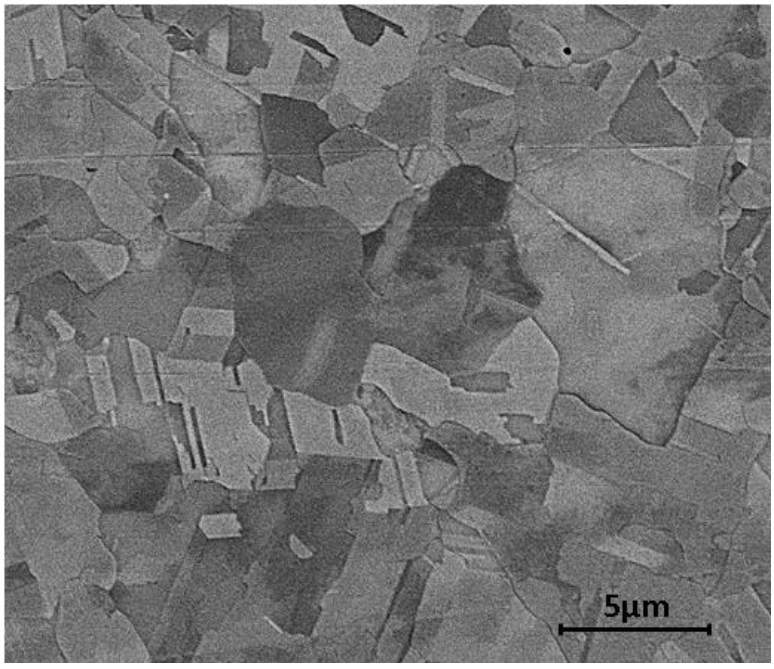

Figure 79: Microscopy of recrystallized 8E sample

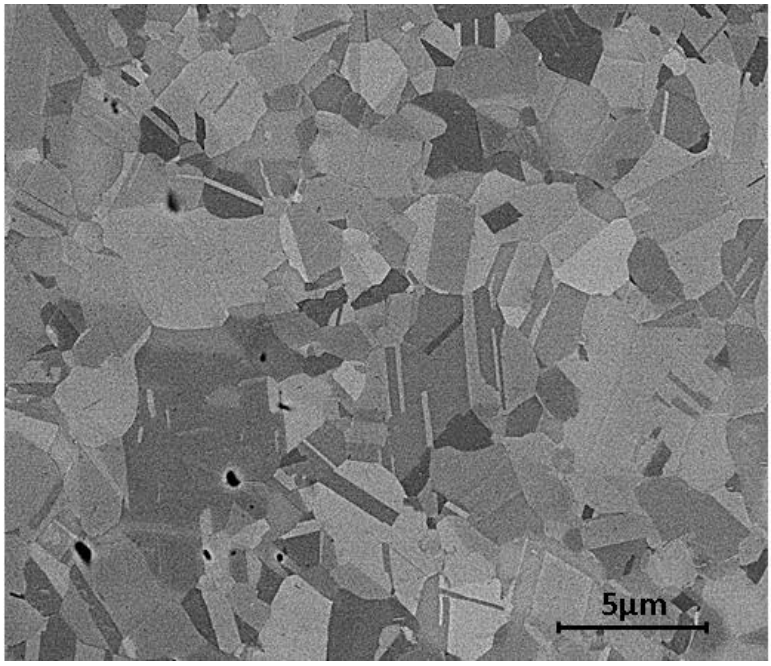

Figure 80: Microscopy of recrystallized 16Bc sample

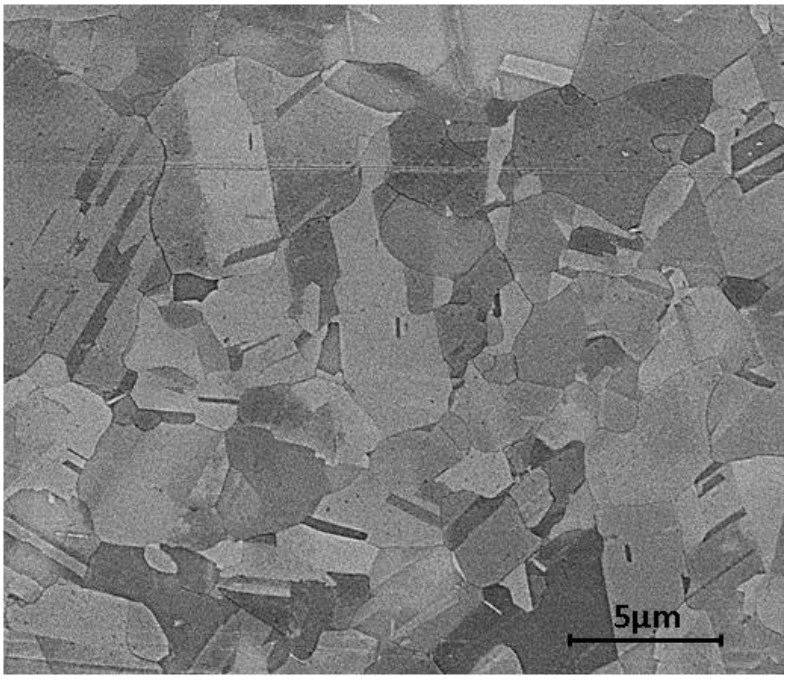

Figure 81: Microscopy of recrystallized 16E sample

APPENDIX B

One-way Analysis of As-Worked Grain Size By Route

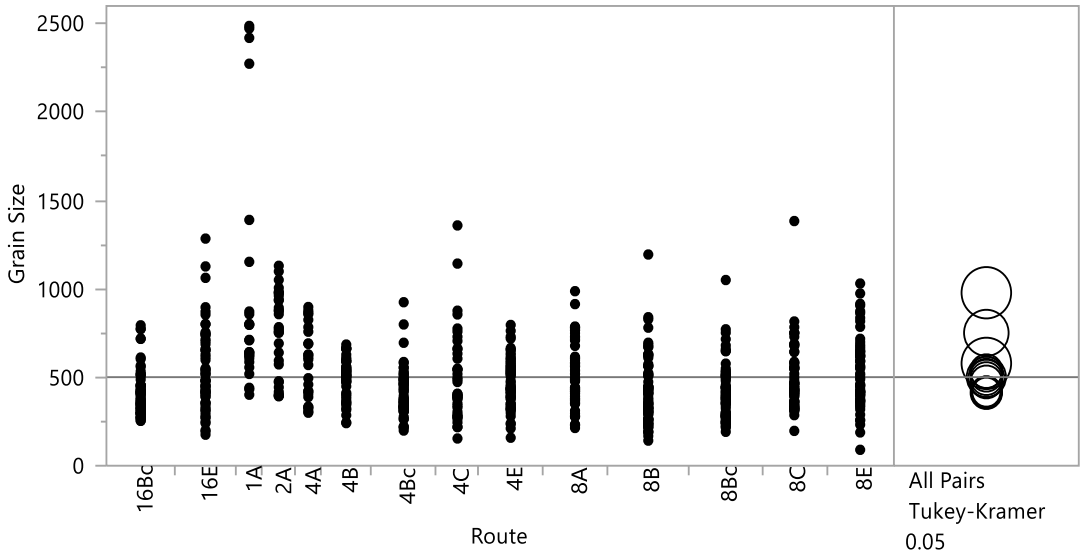

Missing Rows 2

Means Comparisons

Comparisons for all pairs using Tukey-Kramer HSD

Confidence Quantile

q*	Alpha
3.36503	0.05

HSD Threshold Matrix

Abs(Dif)-HSD

	1A	2A	4A	16E	8E	8A	4C	4B	8C	4E	8B	16Bc	8Bc	4Bc
1A	-205.5	31.48	193.92	269.46	279.48	293.53	291.24	304.81	312.95	331.85	394.92	392.02	393.51	393.14
2A	31.48	-184.5	-22.68	54.84	65.05	79.01	75.82	89.75	98.43	117.33	180.85	177.62	179.22	178.65
4A	193.92	-22.68	-205.5	-129.9	-119.9	-105.9	-108.2	-94.63	-86.49	-67.59	-4.51	-7.42	-5.93	-6.30
16E	269.46	54.84	-129.9	-134.9	-124.1	-110.4	-116.1	-101.2	-91.06	-72.16	-7.37	-11.53	-9.61	-10.76
8E	279.48	65.05	-119.9	-124.1	-128.4	-114.8	-120.8	-105.7	-95.37	-76.47	-11.48	-15.79	-13.83	-15.05
8A	293.53	79.01	-105.9	-110.4	-114.8	-131.5	-137.4	-122.4	-112.1	-93.25	-28.35	-32.59	-30.65	-31.83
4C	291.24	75.82	-108.2	-116.1	-120.8	-137.4	-162.4	-148.1	-138.8	-119.9	-55.88	-59.49	-57.76	-58.57
4B	304.81	89.75	-94.63	-101.2	-105.7	-122.4	-148.1	-149.8	-140.2	-121.3	-56.93	-60.78	-58.97	-59.92
8C	312.95	98.43	-86.49	-91.06	-95.37	-112.1	-138.8	-140.2	-131.5	-112.6	-47.78	-52.01	-50.08	-51.26
4E	331.85	117.33	-67.59	-72.16	-76.47	-93.25	-119.9	-121.3	-112.6	-131.5	-66.67	-70.91	-68.97	-70.15
8B	394.92	180.85	-4.51	-7.37	-11.48	-28.35	-55.88	-56.93	-47.78	-66.67	-116.3	-120.9	-118.8	-120.2
16Bc	392.02	177.62	-7.42	-11.53	-15.79	-32.59	-59.49	-60.78	-52.01	-70.91	-120.9	-127.4	-125.4	-126.7
8Bc	393.51	179.22	-5.93	-9.61	-13.83	-30.65	-57.76	-58.97	-50.08	-68.97	-118.8	-125.4	-123.7	-125.0
4Bc	393.14	178.65	-6.30	-10.76	-15.05	-31.83	-58.57	-59.92	-51.26	-70.15	-120.2	-126.7	-125.0	-130.5

Positive values show pairs of means that are significantly different.

Connecting Letters Report

Level				Mean
1A	A			978.16000
2A		B		751.35890
4A		B	C	578.72060
16E			C	534.85741
8E			C	527.30519
8A			C	512.08197
4C			C	501.67151
4B			C	493.48465
8C			C	492.65379
4E			C	473.76106
8B			C	416.23908
16Bc			C	415.13805
8Bc			C	415.02982
4Bc			C	412.87759

Levels not connected by same letter are significantly different.

Ordered Differences Report

Level	- Level	Difference	Std Err Dif	Lower CL	Upper CL	p-Value
1A	4Bc	565.2824	51.15767	393.135	737.4294	<.0001*
1A	8Bc	563.1302	50.40648	393.511	732.7494	<.0001*
1A	16Bc	563.0220	50.81730	392.020	734.0236	<.0001*
1A	8B	561.9209	49.62703	394.925	728.9173	<.0001*
1A	4E	504.3989	51.27803	331.847	676.9509	<.0001*
1A	8C	485.5062	51.27803	312.954	658.0582	<.0001*
1A	4B	484.6754	53.45204	304.808	664.5430	<.0001*
1A	4C	476.4885	55.05207	291.237	661.7403	<.0001*
1A	8A	466.0780	51.27803	293.526	638.6300	<.0001*
1A	8E	450.8548	50.92746	279.482	622.2271	<.0001*
1A	16E	443.3026	51.66210	269.458	617.1470	<.0001*
1A	4A	399.4394	61.07479	193.921	604.9578	<.0001*
2A	4Bc	338.4813	47.49871	178.647	498.3158	<.0001*
2A	8Bc	336.3291	46.68868	179.220	493.4378	<.0001*
2A	16Bc	336.2209	47.13192	177.621	494.8211	<.0001*
2A	8B	335.1198	45.84607	180.847	489.3931	<.0001*
2A	4E	277.5978	47.62831	117.327	437.8684	<.0001*
2A	8C	258.7051	47.62831	98.435	418.9757	<.0001*
2A	4B	257.8743	49.96139	89.753	425.9957	<.0001*
2A	4C	249.6874	51.66963	75.818	423.5571	0.0001*
2A	8A	239.2769	47.62831	79.006	399.5475	<.0001*
1A	2A	226.8011	58.04438	31.480	422.1221	0.0077*
2A	8E	224.0537	47.25067	65.054	383.0535	0.0002*
2A	16E	216.5015	48.04157	54.840	378.1627	0.0006*
2A	4A	172.6383	58.04438	-22.683	367.9593	0.1500
4A	4Bc	165.8430	51.15767	-6.304	337.9900	0.0724
4A	8Bc	163.6908	50.40648	-5.928	333.3100	0.0713
4A	16Bc	163.5826	50.81730	-7.419	334.5842	0.0774

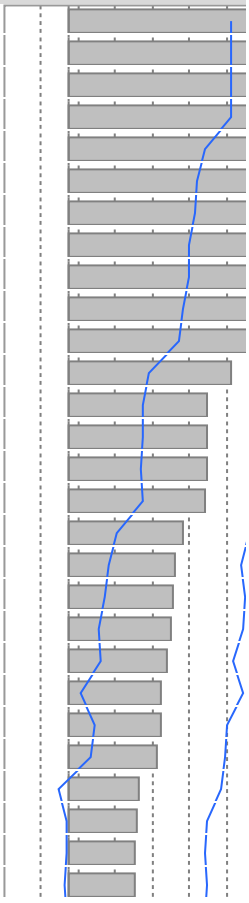

Level	- Level	Difference	Std Err Dif	Lower CL	Upper CL	p-Value
4A	8B	162.4815	49.62703	-4.515	329.4779	0.0659
16E	4Bc	121.9798	39.44553	-10.755	254.7151	0.1102
16E	8Bc	119.8276	38.46629	-9.613	249.2677	0.1036
16E	16Bc	119.7194	39.00308	-11.527	250.9658	0.1172
16E	8B	118.6183	37.43908	-7.365	244.6019	0.0894
8E	4Bc	114.4276	38.47835	-15.053	243.9083	0.1501
8E	8Bc	112.2754	37.47385	-13.825	238.3759	0.1419
8E	16Bc	112.1671	38.02465	-15.787	240.1211	0.1594
8E	8B	111.0661	36.41865	-11.484	233.6159	0.1235
4A	4E	104.9595	51.27803	-67.592	277.5115	0.7373
8A	4Bc	99.2044	38.94115	-31.834	230.2424	0.3767
8A	8Bc	97.0521	37.94890	-30.647	224.7513	0.3701
8A	16Bc	96.9439	38.49290	-32.586	226.4736	0.3965
8A	8B	95.8429	36.90729	-28.351	220.0370	0.3441
4C	4Bc	88.7939	43.79164	-58.566	236.1540	0.7499
4C	8Bc	86.6417	42.91170	-57.757	231.0408	0.7554
4C	16Bc	86.5335	43.39353	-59.487	232.5539	0.7712
4A	8C	86.0668	51.27803	-86.485	258.6188	0.9231
4C	8B	85.4324	41.99337	-55.876	226.7413	0.7455
4A	4B	85.2360	53.45204	-94.632	265.1036	0.9473
4B	4Bc	80.6071	41.76240	-59.925	221.1387	0.8094
8C	4Bc	79.7762	38.94115	-51.262	210.8143	0.7361
4B	8Bc	78.4548	40.83876	-58.969	215.8784	0.8146
4B	16Bc	78.3466	41.34475	-60.780	217.4729	0.8290
8C	8Bc	77.6240	37.94890	-50.075	205.3231	0.7382
8C	16Bc	77.5157	38.49290	-52.014	207.0454	0.7588
4B	8B	77.2456	39.87271	-56.927	211.4184	0.8053
4A	4C	77.0491	55.05207	-108.203	262.3009	0.9819
8C	8B	76.4147	36.90729	-47.779	200.6088	0.7215
4A	8A	66.6386	51.27803	-105.913	239.1906	0.9907
16E	4E	61.0964	39.60149	-72.164	194.3565	0.9593
4E	4Bc	60.8835	38.94115	-70.155	191.9215	0.9548
4E	8Bc	58.7312	37.94890	-68.968	186.4304	0.9583
4E	16Bc	58.6230	38.49290	-70.907	188.1527	0.9633
4E	8B	57.5220	36.90729	-66.672	181.7161	0.9559
8E	4E	53.5441	38.63822	-76.475	183.5628	0.9834
4A	8E	51.4154	50.92746	-119.957	222.7877	0.9992
4A	16E	43.8632	51.66210	-129.981	217.7076	0.9999
16E	8C	42.2036	39.60149	-91.057	175.4638	0.9987
16E	4B	41.3728	42.37881	-101.233	183.9786	0.9995
8A	4E	38.3209	39.09913	-93.249	169.8906	0.9994
8E	8C	34.6514	38.63822	-95.367	164.6701	0.9998
8E	4B	33.8205	41.48008	-105.761	173.4022	0.9999
16E	4C	33.1859	44.37987	-116.154	182.5254	1.0000
4C	4E	27.9105	43.93218	-119.923	175.7435	1.0000
8E	4C	25.6337	43.52249	-120.821	172.0881	1.0000
16E	8A	22.7754	39.60149	-110.485	156.0356	1.0000
4B	4E	19.7236	41.90975	-121.304	160.7511	1.0000
8A	8C	19.4282	39.09913	-112.141	150.9978	1.0000

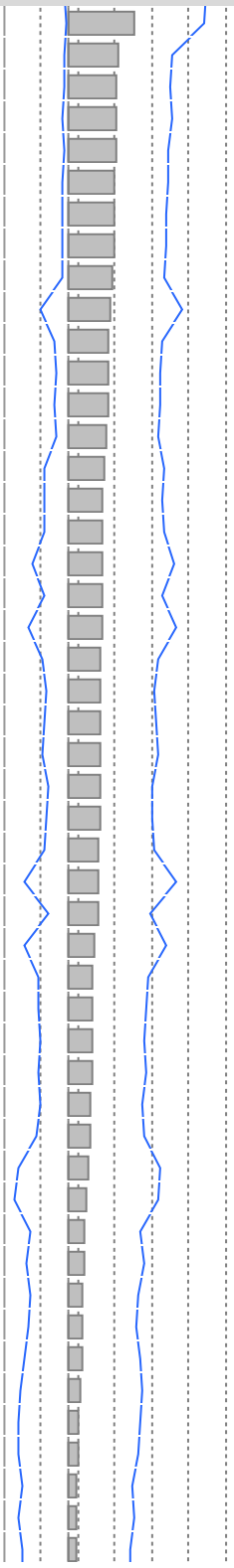

Level	- Level	Difference	Std Err Dif	Lower CL	Upper CL	p-Value
8C	4E	18.8927	39.09913	-112.677	150.4624	1.0000
8A	4B	18.5973	41.90975	-122.430	159.6248	1.0000
8E	8A	15.2232	38.63822	-114.795	145.2419	1.0000
8A	4C	10.4105	43.93218	-137.423	158.2435	1.0000
4C	8C	9.0177	43.93218	-138.815	156.8507	1.0000
4C	4B	8.1869	46.45128	-148.123	164.4967	1.0000
16E	8E	7.5522	39.14650	-124.177	139.2813	1.0000
8B	4Bc	3.3615	36.73989	-120.269	126.9923	1.0000
16Bc	4Bc	2.2605	38.33243	-126.729	131.2502	1.0000
8Bc	4Bc	2.1522	37.78612	-124.999	129.3036	1.0000
8B	8Bc	1.2093	35.68649	-118.877	121.2953	1.0000
8B	16Bc	1.1010	36.26445	-120.930	123.1319	1.0000
4B	8C	0.8309	41.90975	-140.197	141.8583	1.0000
16Bc	8Bc	0.1082	37.32400	-125.488	125.7045	1.0000

One-way Analysis of Recrystallized Grain Size By Route

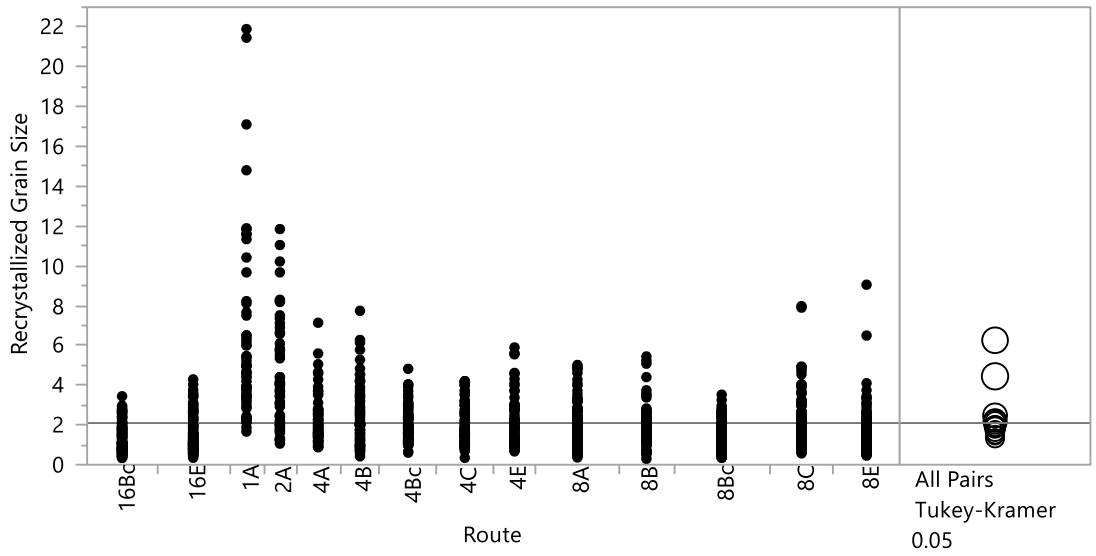

Means Comparisons

Comparisons for all pairs using Tukey-Kramer HSD

Confidence Quantile

q*	Alpha
3.35988	0.05

HSD Threshold Matrix

Abs(Dif)-HSD

	1A	2A	4B	4A	8C	4E	4Bc	4C	8B	8A	8E	16E	8Bc	16Bc
1A	-0.912	0.8874	2.8956	3.1729	3.2809	3.2537	3.4884	3.5044	3.5633	3.7040	3.805	3.962	4.104	4.147
2A	0.887	-0.9371	1.0705	1.3476	1.4546	1.4285	1.6623	1.6783	1.7373	1.8770	1.978	2.136	2.277	2.320
4B	2.895	1.0705	-0.8476	-0.5695	-0.4588	-0.4889	-0.2522	-0.2362	-0.1775	-0.0341	0.065	0.223	0.367	0.408

	1A	2A	4B	4A	8C	4E	4Bc	4C	8B	8A	8E	16E	8Bc	16Bc
4A	3.172	1.3476	-0.5695	-0.8059	-0.6935	-0.7255	-0.4874	-0.4714	-0.4129	-0.2676	-0.168	-0.010	0.134	0.173
8C	3.280	1.4546	-0.4588	-0.6935	-0.6688	-0.7077	-0.4647	-0.4488	-0.3908	-0.2389	-0.143	0.016	0.165	0.199
4E	3.253	1.4285	-0.4889	-0.7255	-0.7077	-0.8172	-0.5795	-0.5635	-0.5049	-0.3602	-0.261	-0.102	0.041	0.081
4Bc	3.488	1.6623	-0.2522	-0.4874	-0.4647	-0.5795	-0.7102	-0.6943	-0.6361	-0.4863	-0.389	-0.230	-0.082	-0.046
4C	3.504	1.6783	-0.2362	-0.4714	-0.4488	-0.5635	-0.6943	-0.7102	-0.6521	-0.5023	-0.405	-0.246	-0.098	-0.062
8B	3.563	1.7373	-0.1775	-0.4129	-0.3908	-0.5049	-0.6361	-0.6521	-0.7218	-0.5727	-0.475	-0.316	-0.169	-0.132
8A	3.704	1.8770	-0.0341	-0.2676	-0.2389	-0.3602	-0.4863	-0.5023	-0.5727	-0.5862	-0.493	-0.332	-0.180	-0.149
8E	3.805	1.9788	0.0658	-0.1687	-0.1435	-0.2610	-0.3898	-0.4058	-0.4758	-0.4931	-0.656	-0.496	-0.347	-0.313
16E	3.962	2.1362	0.2239	-0.0102	0.0164	-0.1026	-0.2303	-0.2463	-0.3165	-0.3323	-0.496	-0.628	-0.478	-0.445
8Bc	4.104	2.2777	0.3676	0.1346	0.1653	0.0419	-0.0827	-0.0987	-0.1692	-0.1805	-0.347	-0.478	-0.546	-0.516
16Bc	4.147	2.3207	0.4081	0.1739	0.1999	0.0815	-0.0466	-0.0626	-0.1328	-0.1491	-0.313	-0.445	-0.516	-0.639

Positive values show pairs of means that are significantly different.

Connecting Letters Report

Level						Mean
1A	A					6.2561930
2A		B				4.4441759
4B			C			2.4801818
4A			C	D	E	2.2226233
8C			C	D		2.1755142
4E			C	D	E	2.1365000
4Bc			C	D	E	F	1.9504096
4C			C	D	E	F	1.9344309
8B			C	D	E	F	1.8704231
8A			C	D	E	F	1.7855797
8E				D	E	F	1.6562864
16E					E	F	1.5100833
8Bc						F	1.3996132
16Bc						F	1.3213319

Levels not connected by same letter are significantly different.

Ordered Differences Report

Level	- Level	Difference	Std Err Dif	Lower CL	Upper CL	p-Value
1A	16Bc	4.934861	0.2344143	4.14726	5.722465	<.0001*
1A	8Bc	4.856580	0.2237269	4.10488	5.608275	<.0001*
1A	16E	4.746110	0.2331235	3.96284	5.529376	<.0001*
1A	8E	4.599907	0.2365113	3.80526	5.394556	<.0001*
1A	8A	4.470613	0.2281748	3.70397	5.237253	<.0001*
1A	8B	4.385770	0.2447936	3.56329	5.208247	<.0001*
1A	4C	4.321762	0.2432846	3.50436	5.139169	<.0001*
1A	4Bc	4.305783	0.2432846	3.48838	5.123190	<.0001*
1A	4E	4.119693	0.2577305	3.25375	4.985636	<.0001*
1A	8C	4.080679	0.2380295	3.28093	4.880429	<.0001*
1A	4A	4.033570	0.2561535	3.17293	4.894214	<.0001*
1A	4B	3.776011	0.2620418	2.89558	4.656440	<.0001*
2A	16Bc	3.122844	0.2387404	2.32071	3.924983	<.0001*
2A	8Bc	3.044563	0.2282558	2.27765	3.811474	<.0001*
2A	16E	2.934093	0.2374732	2.13621	3.731974	<.0001*
2A	8E	2.787890	0.2407998	1.97883	3.596948	<.0001*
2A	8A	2.658596	0.2326171	1.87703	3.440161	<.0001*
2A	8B	2.573753	0.2489395	1.73735	3.410159	<.0001*

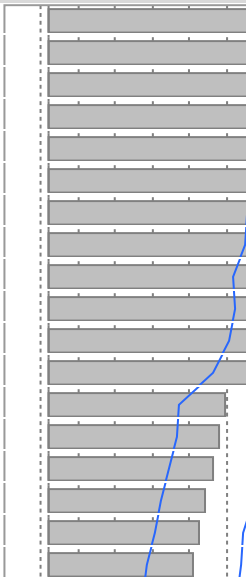

Level	- Level	Difference	Std Err Dif	Lower CL	Upper CL	p-Value
2A	4C	2.509745	0.2474557	1.67832	3.341166	<.0001*
2A	4Bc	2.493766	0.2474557	1.66235	3.325188	<.0001*
2A	4E	2.307676	0.2616715	1.42849	3.186860	<.0001*
2A	8C	2.268662	0.2422912	1.45459	3.082731	<.0001*
2A	4A	2.221553	0.2601183	1.34759	3.095519	<.0001*
2A	4B	1.963994	0.2659189	1.07054	2.857449	<.0001*
1A	2A	1.812017	0.2752039	0.88737	2.736669	<.0001*
4B	16Bc	1.158850	0.2234406	0.40812	1.909583	<.0001*
4B	8Bc	1.080569	0.2122014	0.36760	1.793539	<.0001*
4B	16E	0.970098	0.2220861	0.22392	1.716281	0.0011*
4A	16Bc	0.901291	0.2165050	0.17386	1.628722	0.0027*
8C	16Bc	0.854182	0.1947251	0.19993	1.508435	0.0010*
4B	8E	0.823895	0.2256397	0.06577	1.582017	0.0190*
4A	8Bc	0.823010	0.2048856	0.13462	1.511401	0.0048*
4E	16Bc	0.815168	0.2183685	0.08148	1.548860	0.0142*
8C	8Bc	0.775901	0.1817184	0.16535	1.386453	0.0017*
4E	8Bc	0.736887	0.2068538	0.04188	1.431891	0.0259*
4A	16E	0.712540	0.2151067	-0.01019	1.435273	0.0579
4B	8A	0.694602	0.2168857	-0.03411	1.423312	0.0802
8C	16E	0.665431	0.1931693	0.01641	1.314456	0.0382*
4Bc	16Bc	0.629078	0.2011149	-0.04664	1.304799	0.0990
4E	16E	0.626417	0.2169823	-0.10262	1.355451	0.1845
4C	16Bc	0.613099	0.2011149	-0.06262	1.288821	0.1228
4B	8B	0.609759	0.2343066	-0.17748	1.397001	0.3397
4A	8E	0.566337	0.2187737	-0.16872	1.301390	0.3486
4Bc	8Bc	0.550796	0.1885494	-0.08271	1.184300	0.1698
8B	16Bc	0.549091	0.2029378	-0.13276	1.230938	0.2766
4B	4C	0.545751	0.2327295	-0.23619	1.327694	0.5215
4C	8Bc	0.534818	0.1885494	-0.09869	1.168321	0.2076
4B	4Bc	0.529772	0.2327295	-0.25217	1.311715	0.5729
8C	8E	0.519228	0.1972446	-0.14349	1.181946	0.3206
4E	8E	0.480214	0.2206181	-0.26104	1.221464	0.6468
8B	8Bc	0.470810	0.1904926	-0.16922	1.110842	0.4288
8A	16Bc	0.464248	0.1825474	-0.14909	1.077585	0.3789
4Bc	16E	0.440326	0.1996088	-0.23034	1.110988	0.6253
4A	8A	0.437044	0.2097334	-0.26764	1.141723	0.7126
4C	16E	0.424348	0.1996088	-0.24631	1.095009	0.6833
8C	8A	0.389934	0.1871672	-0.23892	1.018794	0.7129
8A	8Bc	0.385967	0.1686039	-0.18052	0.952455	0.5633
8B	16E	0.360340	0.2014454	-0.31649	1.037172	0.8812
4A	8B	0.352200	0.2277022	-0.41285	1.117252	0.9587
4E	8A	0.350920	0.2116566	-0.36022	1.062061	0.9299
4B	4E	0.343682	0.2477916	-0.48887	1.176232	0.9834
8E	16Bc	0.334954	0.1928663	-0.31305	0.982962	0.9026
8C	8B	0.305091	0.2071032	-0.39075	1.000933	0.9722
4B	8C	0.304668	0.2272306	-0.45880	1.068135	0.9877
4Bc	8E	0.294123	0.2035552	-0.38980	0.978044	0.9764
4A	4C	0.288192	0.2260790	-0.47141	1.047791	0.9923
4C	8E	0.278144	0.2035552	-0.40578	0.962065	0.9854

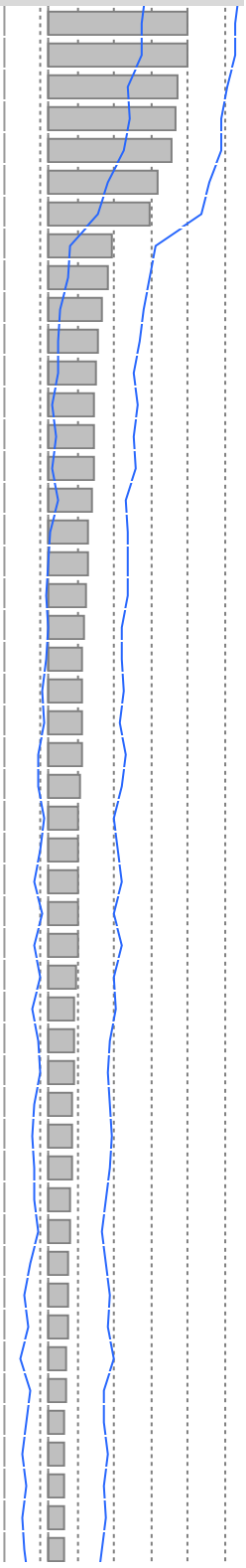

Level	- Level	Difference	Std Err Dif	Lower CL	Upper CL	p-Value	
8A	16E	0.275496	0.1808869	-0.33226	0.883254	0.9635	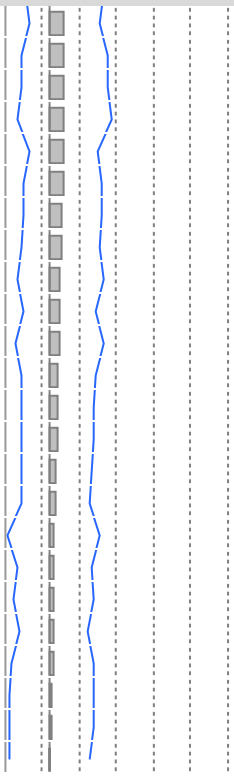
4A	4Bc	0.272214	0.2260790	-0.48738	1.031812	0.9955	
4E	8B	0.266077	0.2294748	-0.50493	1.037085	0.9969	
4B	4A	0.257559	0.2461509	-0.56948	1.084596	0.9989	
8E	8Bc	0.256673	0.1797251	-0.34718	0.860528	0.9786	
8C	4C	0.241083	0.2053173	-0.44876	0.930925	0.9965	
8C	4Bc	0.225105	0.2053173	-0.46474	0.914946	0.9982	
8B	8E	0.214137	0.2053565	-0.47584	0.904110	0.9990	
4E	4C	0.202069	0.2278643	-0.56353	0.967666	0.9998	
16E	16Bc	0.188751	0.1886965	-0.44525	0.822749	0.9993	
4E	4Bc	0.186090	0.2278643	-0.57951	0.951687	0.9999	
4Bc	8A	0.164830	0.1938063	-0.48634	0.815996	0.9999	
4C	8A	0.148851	0.1938063	-0.50231	0.800017	1.0000	
8E	16E	0.146203	0.1912953	-0.49653	0.788932	1.0000	
8A	8E	0.129293	0.1852326	-0.49307	0.751652	1.0000	
16E	8Bc	0.110470	0.1752429	-0.47832	0.699265	1.0000	
4A	4E	0.086123	0.2415561	-0.72548	0.897723	1.0000	
8B	8A	0.084843	0.1956973	-0.57268	0.742363	1.0000	
4Bc	8B	0.079986	0.2131222	-0.63608	0.796051	1.0000	
8Bc	16Bc	0.078281	0.1769564	-0.51627	0.672833	1.0000	
4C	8B	0.064008	0.2131222	-0.65206	0.780073	1.0000	
4A	8C	0.047109	0.2204142	-0.69346	0.787674	1.0000	
8C	4E	0.039014	0.2222450	-0.70770	0.785730	1.0000	
4Bc	4C	0.015979	0.2113871	-0.69426	0.726214	1.0000	